# UBX AS A NOVEL PROTEIN-BASED MATERIAL: STRUCTURAL INSIGHTS, FUNCTIONALIZATION VIA GENE FUSION AND BIOMEDICAL APPLICATIONS

A Dissertation

by

SHANG-PU TSAI

Submitted to the Office of Graduate and Professional Studies of
Texas A&M University
in partial fulfillment of the requirements for the degree of

DOCTOR OF PHILOSOPHY

| | |
|---|---|
| Chair of Committee, | Sarah E. Bondos |
| Co-Chair of Committee, | Kayla J. Bayless |
| Committee Members, | Emily Wilson |
| | J. Martin Scholtz |
| Head of Department, | Van Wilson |

May 2016

Major Subject: Medical Sciences

ABSTRACT

Compared to conventional synthetic polymers, protein-based materials have unique advantages, such as useful mechanical properties, biocompatibility and biodegradability. Protein-based materials have the potential to be customized for a variety of applications, for example, biosensor, tissue engineering scaffolds and drug delivery vehicles. All these applications require optimizing the mechanical properties and adding functional proteins. Current methods to produce and functionalize protein-based materials are often performed in harsh conditions, which is harmful for the functional molecules. Our laboratory discovered a protein-based biomaterial made from the *Drosophila* protein, Ultrabithorax (Ubx). Ubx protein rapidly self-assembles into material in mild aqueous buffers. This work explores the possible applications of Ubx materials, by extending the capacity to engineer the mechanical and functional properties of these materials.

Our first objective of this work was to investigate the structure and assembly of Ubx materials. We found the strength of Ubx materials is due to dityrosine bonds and located the amino acids that participate in these bonds. Tyrosine mutagenesis can decrease the strength of these materials, allowing the mechanical properties to be precisely tailored for a variety of applications.

Our second objective was to study how the physicochemical properties of appended proteins impact the production of monomer and assembly of Ubx materials. By fusing proteins with a variety of physicochemical properties to Ubx. We demonstrated that the appended proteins dictate the solubility and purification yield of the corresponding protein fusions. Surprisingly, all protein fusions self-assemble equally well to produce materials with similar morphologies. We concluded that a far wider range of proteins can

be successfully incorporated into elastomeric protein-based materials than originally anticipated.

Finally, we used Ubx materials as tissue engineering scaffolds. We found VEGF-Ubx materials trigger corresponding signaling and stimulate migration and attachment of endothelial cells, proving that Ubx material can deliver appended functional molecules to attaching cells *in vitro*.

In summary, this research explores a new way to control the mechanical properties of protein-based materials, reveals the great potential of Ubx materials as a system for functionalizing materials, and demonstrates the feasibility of using Ubx materials as bioactive tissue engineering scaffolds.

# ACKNOWLEDGEMENTS

I would like to thank my committee chair, Dr. Sarah Bondos, and my committee members, Dr. Bayless, Dr. Scholtz and Dr. Wilson, for their guidance and support throughout the course of this research.

Thanks also go to my friends and colleagues and the department faculty and staff for making my time at Texas A&M University a great experience.

Finally, thanks to my parents for their encouragement and to my wife for her patience and love.

TABLE OF CONTENTS

LIST OF FIGURES

Page

LIST OF TABLES

# CHAPTER I

# GENERAL INTRODUCTION AND LITERATURE REVIEW

## 1.1 Protein-based materials and their unique advantages

Protein-based materials are materials made from proteins or peptides. Natural protein-based materials have been widely used for different purposes in human history, for instance, silk from the silkworm, *Bombyx mori*, has been used as biomedical suture material for centuries (Altman et al., 2003, Scheibel, 2004). Protein-based materials have great potential to be used in a variety of biomedical applications. Many laboratories are focusing on their uses in tissue engineering and regenerative medicine, in which replacements for damaged or diseased organs or tissues are constructed, thes replacement requires scaffold that support cell growth in 3-dimensions. Compared to other conventional synthetic polymers that have been used for biomedical purposes, such as poly glycolic acid (PGA) (Moran et al., 2003, Asti et al., 2014), Poly lactic-co-glycolic acid (PLGA)(Makadia et al., 2011, Gentile et al., 2014) and polylactic acid/poly hydroxyester-ether (Garlotta et al., 2003, Shogren et al, 2003), protein-based materials have some unique advantages. To meet this requirement, spider silk fibers have superior strength that can provide structural support and burden the weight of cells and surrounding extra cellular matrix when used as a scaffold for hard tissue engineering (Gosline et al., 1999). Elastin is extensible and can tolerate repeating stretch /relax cycles and resist elastic fatigue (Faury 2001, Pasquali-Ronchetti et al., 1997), which is required for artificial tissues/organs like lung, skin and bladder. Both examples highlight the useful mechanical properties that can be provided by protein-based materials. Another

important property of protein-based materials is biocompatibility. For those materials designed to be implanted into or to interact with human bodies, biocompatibility, low level toxicity, immunogenicity and inflammation is essential and required (Crawford et al., 2008, Williams et al., 2009). Most useful synthetic polymers are too hydrophobic and not biocompatible. Extra modifications are needed to make these sorts of materials more biocompatible and suitable for implantation, which is time-consuming and costly (Mark et al. 2010). Although monomeric proteins can generate immune response in human bodies, some protein-based materials such as elastin, collagen and silk-based materials are proven to be biocompatible, when in the forms of polymers/materials (Altman et al., 2003, Rincon et al, 2006). Biodegradability is another attractive property of protein-based materials. For example, protein-based materials can delivery vector hydrophobic drugs into human bodies and undergo gradual hydrolysis to release the drugs to target sites (Kopecel, 2007, Lutolf, 2009, Geckil et al., 2010). In addition, an ideal tissue engineering scaffold will degrade over time and be replaced by extracellular matrix proteins produced by the cells. Degradation can be rely on nonspecific hydrolysis, as is often the case in swellen hydrogel, or on proteases, which recognize specific sites engineered into the protein sequence (Hu et al., 2012, Wang et al., 2009). This enzyme-catalyzed degradation is also programmable. Protein-based materials are also genetically engineerable (Bini et al., 2006, Huang et al., 2011). By modifying the amino acid sequence of the material-forming protein, the desired physicochemical properties or functions can be added to the materials. For example, the flgelliform spider silk protein contains repeating $(GPGGX)_n$ motifs, by mutating the X amino acid in the $(GPGGX)_n$ motif from hydrophilic to hydrophobic, the β turn content in this protein-based material

can be increased, resulting in higher elasticity of this material (Teule et al., 2007). Because of these unique properties, protein-based materials have the potential to be customized for a variety of applications, including drug delivery, tissue engineering, surgical sealants, medical imaging, biosensors, biofabrication, and biomineralization (Baneyx et al., 2007, Deming et al., 2007).

## 1.2 Common biomedical applications of protein-based materials

### 1.2.1 Tissue engineering scaffold

Autologous and allogenic grafts are the most common treatments of injured tissues or organs (Tsubouchi et al. 2008). However, the lack of donors severely limits this treatment. Tissue engineering and regenerative medicine offer a route to circumvent these conventional therapies. Constructing the artificial tissues or organs requires scaffolds that support cell growth in 3-dimensions and active factors that regulate cell behaviors, such as cell attachment, migration, proliferation and differentiation (George et al. 2010). Therefore, compatibility, proper mechanical properties and incorporating molecules with desired functions are the three basic requirements of scaffolds for tissue/organ engineering. The tunable mechanical properties, biocompatibility, biodegradability and engineerability make protein-based material an attractive choice as a tissue engineering scaffold. For example, natural polymers such as collagen, elastin, silk, keratin, chitosan and hyaluronic acid are widely used in tissue engineering (Mano et al. 2007, Chung et al. 2007).

### 1.2.2 Biosensors

A biosensor is an analytical device that combines a recognition element with a transducer (detection element) for the detection of a biological analyte (target) (Newman et al. 2006). The recognition process utilizes the affinity of the recognition element for the analyte, and the transducer transmits this interaction into a measurable signal (electrical, optical, etc.). At present, patient health status is primarily monitored with supercutaneous sensors. However, implantable or subcutaneous biosensors will provide significant advantage over conventional methods. For example, the major problem with conventional measuring systems is poor contact between the sensor and the human body, leading to weak and unstable signals (Turner, 2013, Yoo and Lee, 2010). In subcutaneous measuring systems, the sensor-to-body contact is more stable (Rogers and Boutelle, 2013, Hwang et al., 2012). In order to be implanted or injected in to human body, subcutaneous biosensors need to be biocompatible and biodegradable. Some protein-based materials are attractive for this purpose because they are biocompatible and their solubility in water can be programmed, over several orders of magnitude, through the control of crosslinking and crystallinity of material-forming proteins in the materials (Wang et al.2008).

### 1.2.3 Drug delivery

The delivery of therapeutics to target tissues/organs remains a critical problem in the treatment of several diseases. Conventional drug delivery systems often encounter problems of poor drug efficacy and non-specific delivery, which may cause systemic toxicity and undesirable side effects. In addition, some therapeutics are highly hydrophobic and poorly soluble in body fluids, leading to low drug concentration in the

target tissue/organ (Nerini et al. 2014). To solve these problems, controlled drug delivery systems are required. Protein-based materials are promising materials for the delivery of drugs and other active ingredients, mainly because of their biocompatibility, biodegradability and processability (Raucher et al. 2008, Mura et al. 2013, Ciofani et al. 2014). To fulfill the specific needs of drugs that target different tissues/organs, protein-based materials can form different morphologies (such as film, hydrogel or mesh) with desired hydrophobicity and biodegradability.

### 1.3 Common protein-based materials

The proteins or peptides that comprise protein-based materials can be purified from the native organisms that produce the natural protein-based materials, produced as recombinant proteins from other organisms (Kyle et al., 2009, Merle et al., 2002, Pakkanen et al., 2003), or chemically synthesized (Floss et al., 2010, Papapostolou et al., 2007). Depending on the source and production method, material-forming proteins/peptides can be classified into: i) naturally-derived proteins, ii) recombinant proteins generated in different organisms, and iii) self-assembling peptides.

#### 1.3.1 Naturally derived protein-based materials

Naturally derived protein-based materials have been widely discovered and used for different purposes for centuries. The most studied naturally derived protein-based materials are silk, elastin and collagen. Because of the useful properties of these materials, scientists have been putting extensive efforts on studying the assembly mechanism, mechanical properties and the structure of these materials. A general comparison of common naturally derived protein-based materials is summarized in Table

1.1 (Gomez et al., 2012). These studies have served as a guide for our characterization of Ubx materials, described in section 1.4.

**Table 1.1 Comparison of common natural protein-based materials.**
Modified from: Gomez et al. 2012.

| | **Silk** | **Elastin** | **Collagen** |
|---|---|---|---|
| Natural function | Web, cocoon | Tendon, connective tissue, extracellular matrix | Tendon, connective tissue, extracellular matrix |
| Structure | Stacked β-sheets, Random colis | Aggregate | Triple helix |
| Mechanical properties | Sequence dependent | Elastic, extensible | Inelastic, strong |
| Intermolecular forces | Van der Waal's, H-bond | Hydrophobic, cross-linking | Disulfide bond, H-bonds |

#### 1.3.1.1 Silk

Silk proteins and silk materials have been found in many organisms, the most common of which are silkworms and spiders (Kaplan, 1998). Silks are composed of many proteins, and their composition varies with the intened use. Consequently, different kinds of silk fibers have different mechanical properties (Vepari, 2007, Saravanan, 2006). Silk fiber is mainly composed of stacked β-sheet structures separated by glycine-rich regions. *In vivo,* silk protein undergoes a secondary structure as it transitions from a monomer to a fiber (van Beek et al., 1999). When stored in the silk-producing glands, the poly-Alanine regions of the spider fiber protein form α-helical structure while the poly-glycine regions form β-turns. During assembly, the spider fiber protein rapidly passes through the spinning duct, a low pH environment. The low pH environment forces the denaturation of

spider fiber protein, combined with the high flow rate and shearing force in the spinning duct, together, these forces drive the transition of the poly-Alanine regions from α-helical structure to stacked β-sheet structures (Hu et al., 2006). In this stacked β-sheet structures, H-bonds form between the β strands and the β-sheets are stabilized by the van der Waal's forces (Romer et al, 2008).

#### 1.3.1.2 Elastin

Elastin is a highly elastic protein in connective tissue and allows many tissues in the body to resume their original shape after stretching or contracting. It is found in all vertebrates above the jawless fish (Swatland et al., 1994). In humans, elastin is found in tendons, ligaments, skin, blood vessel, and elastic organs that undergo the stretch and relax cycle, for example lungs and bladders (Martyn and Greenwald, 2001, Faury, 2001). Elastic fiber is composed mainly of an amorphous component, the microfibril, which is extensively cross-linked elastin. Elastin protein is mainly composed of simple repetitive amino acid sequences that contains large amount of glycine, valine, alanine, and proline. The process of assembly and formation of elastin materials called coacervation (Cox et al., 1974). The precursor, tropoelastin is transcribed and translated from the elastin (ELN) gene and transported to the plasma membrane. Tropoelastin is then released and aggregates on the cell surface. Lysyl oxidase then oxidize the tropoelastin aggregates. This process cross-links the tropoelastin aggregates into microfibrils. Continuous deposition of the microfibrils then leads to the formation of mature elastic fibers/material (Wu et al., 1999). Because of its superior elasticity, elastin-derived materials are widely used in a variety of biomedical applications, for instance, vascular grafts (McClure et al.,

2010, Boland et al., 2004), heart valves (Schmidt et al., 2006), and skin substitutes (Powell et al., 1992).

#### 1.3.1.3 Collagen

Collagen is the most abundant protein in mammals (Gloria, 2002). Collagen is the main extracellular protein in the connective tissue (Frantz et al., 2010). Collagen is mostly found in tissues such as tendons, ligaments and skin. The collagen protein is composed of a triple helix formed by two identical α1-chains and an additional α2-chain. The composition of α2-chain is only slightly different from the α1 chain (Antipova et al., 2008). Collagen protein contains a high ratio of hydroxyproline (Paul, 2001). The most common motifs in the amino acid sequence of collagen are glycine-proline-X and glycine-X-hydroxyproline, where X is any amino acid other than glycine, proline or hydroxyproline. During assembly, procollagen precursor protein first forms the triple helix structure. Di-sulfide bonds form between each procollagen chains to stabilize the triple helix. The triple-helix is then exported outside the cells and undergoes cleavage by procollagen peptidase, to form the tropocollagen triple helices. Tropocollagen triple helices then spontaneously assemble into fibrils. H-bond and extensive cross-linking form to stabilize the fibril structure. The fibrils then continue assemble into higher hierarchical structures and form the collagen fiber (Khoshnioodi et al., 2006, Kyle et al., 2009). Collagen has a wide variety of biomedical applications. For example, Apligraf, the first FDA approved artificial skin, contains two types of cells-an outer layer of protective skin cells, and an inner layer of cells contained within collagen. This artificial skin mimics real skin and can be used to cover burn wounds (Zaulyanov and Kirsner, 2007).

### 1.3.2 Recombinant proteins generated in different organisms

Organisms that produce protein-based materials can be difficult to cultivated in large numbers. For example, most spider species are solitary and cannot live in large population. Therefore, producing enough natural material-forming proteins for industrial or biomedical applications has always been challenging. The development of recombinant DNA technology in past decades provides a solution for this obstacle. A variety of material-forming proteins have been genetically cloned and produced in other organisms, for example, *E.coli*, yeast and plants (Du et al., 2008, Kyle et al., 2009, Pakkanen et al., 2003). Using recombinat DNA techniques for producing material-forming proteins also enables the addition of desired functionalization and mechanical properties (Romer et al., 2007, Heim et al., 2010, Hardy et al., 2009). By gene fusion, ideally, proteins with desired functions can be produced as fusion proteins with the material forming protein and consequenly be incorporated into the material. However, not every protein can be fused to the material-forming protein without affecting the production and assembly of the material-forming protein. This fact is further discussed in Chapter III.

### 1.3.3 Engineered self-assembling proteins

The amino acid sequence of a protein drives its folding into a unique shape. The chemistry and topology of the resulting surface determines whether the protein remains a monomer, dimer or form larger oligomers. Based on this fact, some studies were conducted and aimed to analyze and isolate regions that drive self-assembly from the naturally derived material-forming proteins, for example, silk proteins and elastin

proteins (Woolfson et al., 2010, Daamen et al., 2007, Gosline et al., 2002, Herrero-Vanrell et al., 2005). These regions, when isolated, retain the ability to self-assemble into materials. In addition, these peptides can be chemically synthesized into homogenous product in large quantities (Lutolf et al., 2003, Deming et al., 2007), facilitating studies of the product materials. The simplified sequences also facilitate sequence engineering and allow easier monitoring when scientists try to modify or adjust the properties of the materials. Recombinant elastin-like protein (ELPs), derived from elastin, is one of the most studied self-assembling proteins (Li et al., 2003, Nicol et al., 1992). ELPs are composed of repetitive elastin peptide sequences, for example, VPGXG and VPVGP. These repetitive peptides are able to self-assemble into different hierarchical structures and form different materials, such as fibers, sheets and films (Urry, 1993). *In silico* de novo design of the self-assembling peptides has drawn more attention over the past decade (Woolfson et al., 2010). By computational simulation and chemically synthesis, these peptides are able to mimic the natural material-forming protein and self-assemble into materials with different structures (Kyle et al. 2009, Gelain et al., 2006, Galler et al., 2008, Beniash et al., 2005).

## 1.4 Challenges of current protein-based materials

### 1.4.1 Fine-tuning the mechanical properties of protein-based materials remains challenging

Protein-based materials can be used in a variety of biomedical applications, all of which require specific structure and mechanical properties. Current methods to modify the mechanical properties of protein-based materials are mainly focused on mutating the

amino acids in the repetitive motifs of silk proteins (Gosline et al., 1999, Tuele et al., 2012), elastin protein (Saumonneau et al., 2011, Miao et al., 2013) and collagen (Muiznieks and Keely, 2013). However, it is difficult to make mutations in these motifs to gain the desired mechanical properties without dramatically affecting the overall structure, morphology, biocompatibility, and biodegradability. Engineering covalent bonds such as disulfide bond (via cysteine) or dityrosine bond (via tyrosine) into protein-based material can potentially enhance the strength of the materials, however, current studies using this approach remain focusing on the repetitive motifs, the exact locations of the covalent bonds are unknown (Grip et al., 2009). Therefore, placing covalent bonds in a non-repetitive motif or domain may provide a useful tool for fine-tuning the mechanical properties of protein-based materials. In Chapter II, dityrosine bonds are identified in Ubx materials. The strength of these materials can be increased or decreased by tyrosine mutation.

### 1.4.2 Protein-based materials are difficult to functionalize in mild conditions

Current studies of protein-based materials, especially the functionalization of protein-based materials, expand our creativity and imagination on a variety of useful applications in different fields. However, the existing common approaches to incorporate functional molecules into protein-based materials, including chemical cross-linking and physical entrapment, both have problems and therefore limit the applications of protein-based materials. Chemical cross-linking requires the catalysis by chemical reagents, which creates toxic byproduct (Heck et al., 2013). Also, the reaction is usually performed in harsh conditions (low pH, extreme temperature and pressure), which are harmful for the

proteins, whose structures are held together by non-covalent bonds (Sperling et al., 2010). By physical entrapment, such as electrospinning (Khadka et al., 2012, Hardy et al., 2008), functional molecules and the material-forming proteins are together entrapped into materials (Hardy et al., 2008). However, this approach alters the mechanical properties of the protein-based materials, and the functional molecules may gradually diffuse out from the materials. The diffusion rate is dependent on the pore sizes of the materials, which also dictates mechanical properties of the materials. Gene fusion may provide an alternative solution. By gene fusion, the desired functional protein can be produced simultaneously, in addition, the functional protein is automatically linked to the material-forming proteins. However, most current protein-based materials still require denaturing environment for assembly (Gomez et al., 2011), which is still harmful for the functional proteins. Furthermore, the appended proteins are likely to interfere the assembly of material-forming proteins (Scherzinger et al., 1997), therefore only small, stable and simple (i.e. monomeric, neutrally charged) protein or peptide can be fused to current protein-based materials (Jansson et al., 2014, DiMarco and Heilshorn, 2011).

### 1.4.3 The difficulty of making a gradient of functional protein on protein-based materials

When utilizing protein-based materials as scaffold to create artificial tissues/organs, it is important to consider the nature of the cells and the interaction between cells and materials. Not all cell types are morphologically and functionally homogenous. For example, neuron cells need to develop polarity (Jun et al, 2009) to implement their functions. A neuron receives signals from neighboring cells through its dendrites. The

neuron then propagates an electrical signal down to the synapse, where neurotransmitters are released to propagate the signal to another neuron or effector cells (Rasband and Matthew, 2010). To guide the neuron stem cells to generate polarity on protein-based materials is challenging, because it requires a gradient or a heterogeneous distribution of functional molecules, such as BDNF and CTNF (Wittmer et al., 2011). By mixing proteins from two pumps that have different flow rate and passing the mixture through electrospinning apparatus, a gradient of functional molecules can be created, however, this method still faces the same limitation of conventional physical entrapment approach (Sundararaghavan and Burdick. 2011). Therefore, the development of an effective approach to generate a gradient of functional molecules on protein-based materials without sacrifice the desired mechanical properties is needed and important for next-generation protein-based materials.

### 1.5 Ubx material and its unique advantages as a protein-based material

Our laboratory discovered a novel protein-based biomaterial made from the *Drosophila* protein, Ultrabithorax (Ubx). Ultrabithorax (Ubx) protein is a transcription factor that regulates the development of the third thoracic and first abdominal segments of *Drosophila* (Figure 1.1) (Weatherbee et al., 1998). Our lab has discovered that the Ultrabithorax (Ubx) protein rapidly self-assembles into material in mild aqueous buffers such as phosphate buffer saline (Greer et al., 2009). By incubating the Ubx protein in a Teflon coated tray or adding a Ubx protein drop on a glass slide, Ubx materials form as a film at the air-liquid interface and can be pulled into different morphologies such as film, sheet, bundle or fiber (Greer et al., 2009) (Figure 1.2). The mechanical and

immunological properties of the materials determine their potential applications. Ubx materials are strong and remarkably extensible. By varying fiber diameter, the extensibility, the force required to rupture the meaterials and the mechanism of extension can be altered (Huang et al., 2010). In Chapter II, a method to alter the mechanical properties by changing the amino acid sequence is described. This approach allows a more accurate alteration of the mechanical properties and also enables engineering of he strength of the materials indepent of the area of their cross section. Both *in vivo* and *in vitro* assays showed that Ubx materials are cell compatible and not cytotoxic, suggesting Ubx materials can be used for biomedical applications (Patterson et al., 2013). In addition, Ubx materials do no activate macrophages or elicit immune response *in vivo* (Patterson et al., 2014) (Figure 1.3).

A major goal in material engineering is to functionalize the materials with bioactive compounds, especially, proteins. We found that when fused to Ubx protein and incorporated into materials, four tested appended proteins retain their function within Ubx material (Huang et al., 2011) (Figure 1.4). These four proteins are monomeric, stable, soluble, and have near neutral charge. Finally, Ubx materials can be patterned during assembly to create a gradient of functional proteins, which is useful as the tissue engineering scaffold of cells that possess polarity (Figure 1.5). Together, these unique features demonstrate that Ubx material may have great potential as a novel protein-based material. However, not every functional protein is likely to be incorporated into materials via gene fusion. Unstable or insoluble functional proteins could hamper expression of the fusion protein, or large/multimeric functional proteins may mis-position

the self-assembling protein, altering the mechanical properties of the materials or even preventing materials assembly. The impact of these properties on the assembly of Ubx materials is explored in Chapter III, and the activities of incorporated proteins are evaluated in Chapter IV and the appendix.

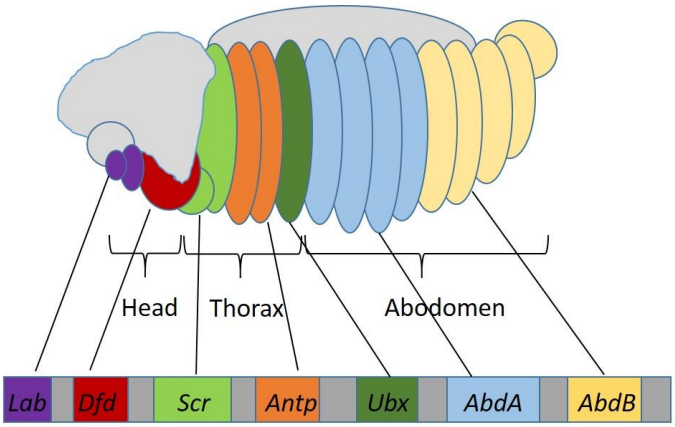


**Figure 1.1 Homeobox gene expression in *Drosophila melanogaster*.** The dark green-colored region in the fruit fly in this figure is the segment regulated by Ubx protein during morphological development.

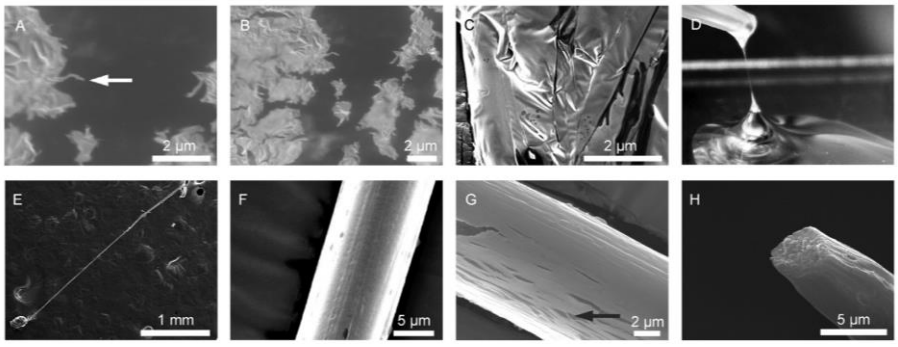


**Figure 1.2 Ubx protein self-assembles into polymer/materials.**
Basic materials formed in a hierarchical manner by Ubx. (A) A Ubx fiber, 50 nm in diameter (arrow). (B) Ubx film, formed from self-associating fibers. (C) Ubx sheet, generated by continuing to allow assembly after Ubx film has been formed. (D) A Ubx rope being pulled from a Ubx film. (E,F) Ubx rope at low and high magnification, respectively. (G) Ubx rope, fractured by the SEM beam, splinters into 50 nm fibers aligned along the main axis (arrow). (H) The free end of a severed rope shows a solid core. (Greer et al., 2009)

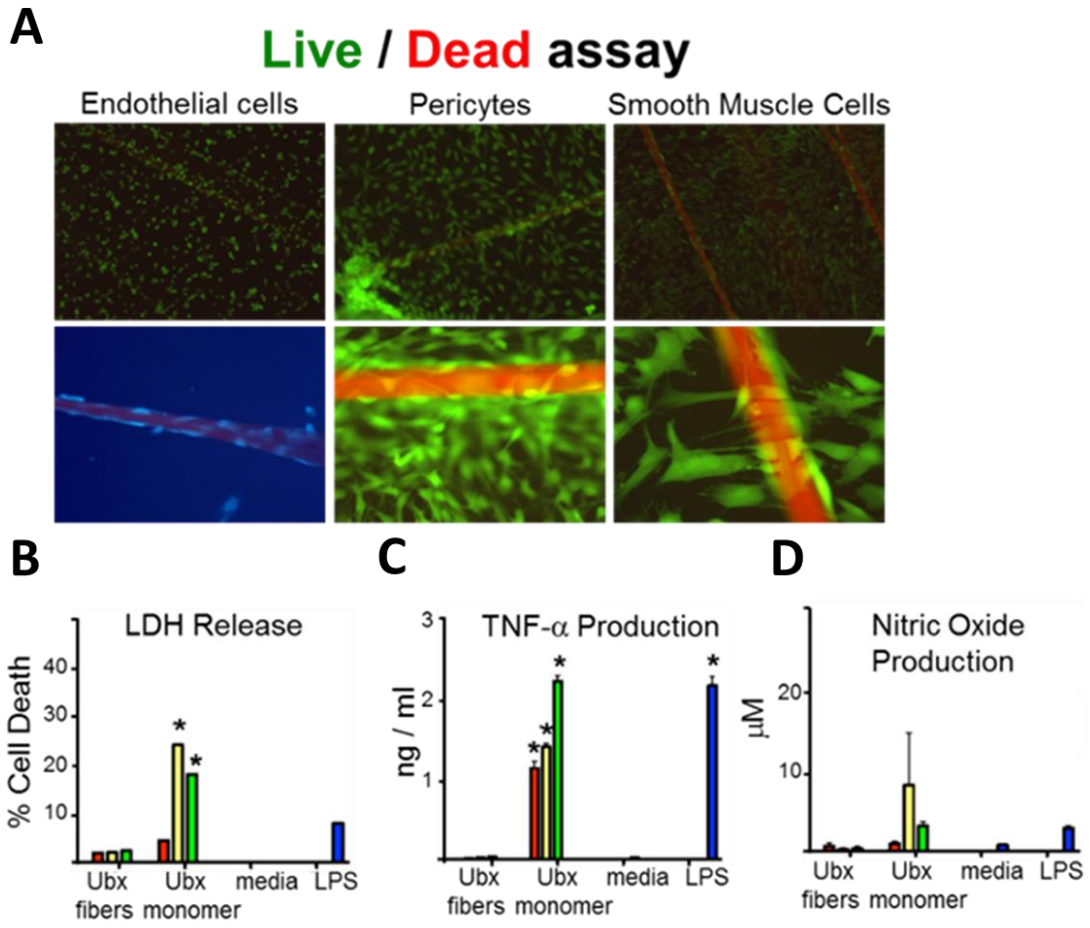


**Figure 1.3 Ubx are biocompatible and not cytotoxic.** (A) Endothelial cells, pericyte and smooth muscle cell interact with Ubx materials well and show no toxicity (B) LDH release. (C) TNF-a production. (D) Nitric oxide production. In each experiment, media was used as a negative control and lipopolysaccharide as a positive control. Ubx monomer and fiber concentrations were 0.45 lg/mL (red bar), 4.5 lg/mL (yellow bar), and 9 lg/mL (green bar). Lipopolysaccharides (LPS) served as a positive control, and media lacking any additives as a negative control. While Ubx monomers showed a positive response, Ubx fibers did not affect macrophages. (Patterson et al., 2013, Patterson et al., 2014)

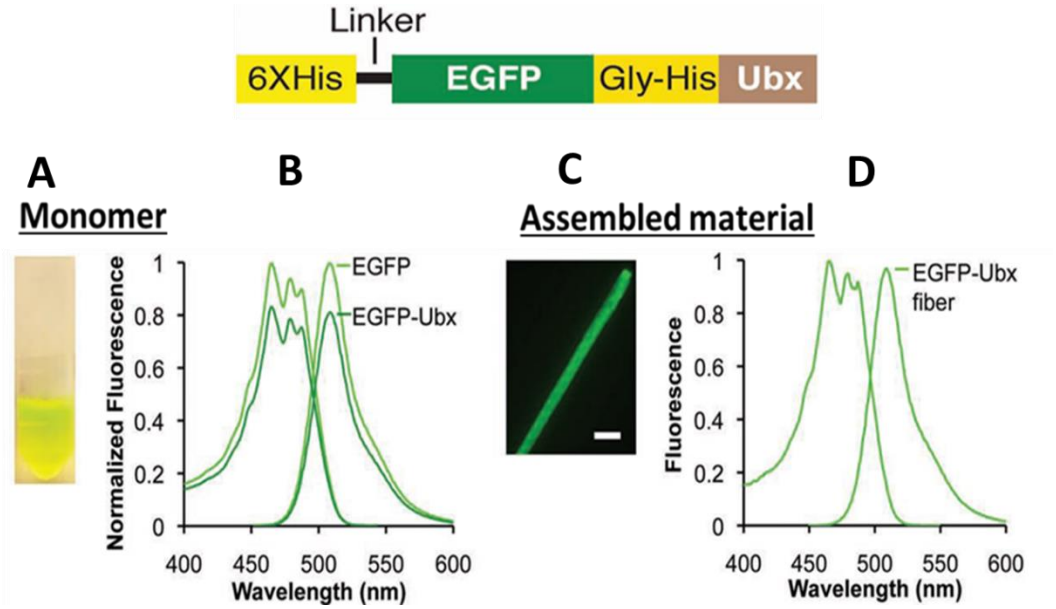


**Figure 1.4 Fused protein retains function within monomeric fusion and in Ubx material.** (A) EGFP-Ubx solution is green in color, (B) and its fluorescence excitation/emission spectra resemble those for EGFP. (C) EGFP-Ubx fibers retained the green fluorescence and (D) exhibit near identical excitation/emission spectra to EGFP-Ubx monomers. **(**Huang et al., 2011)

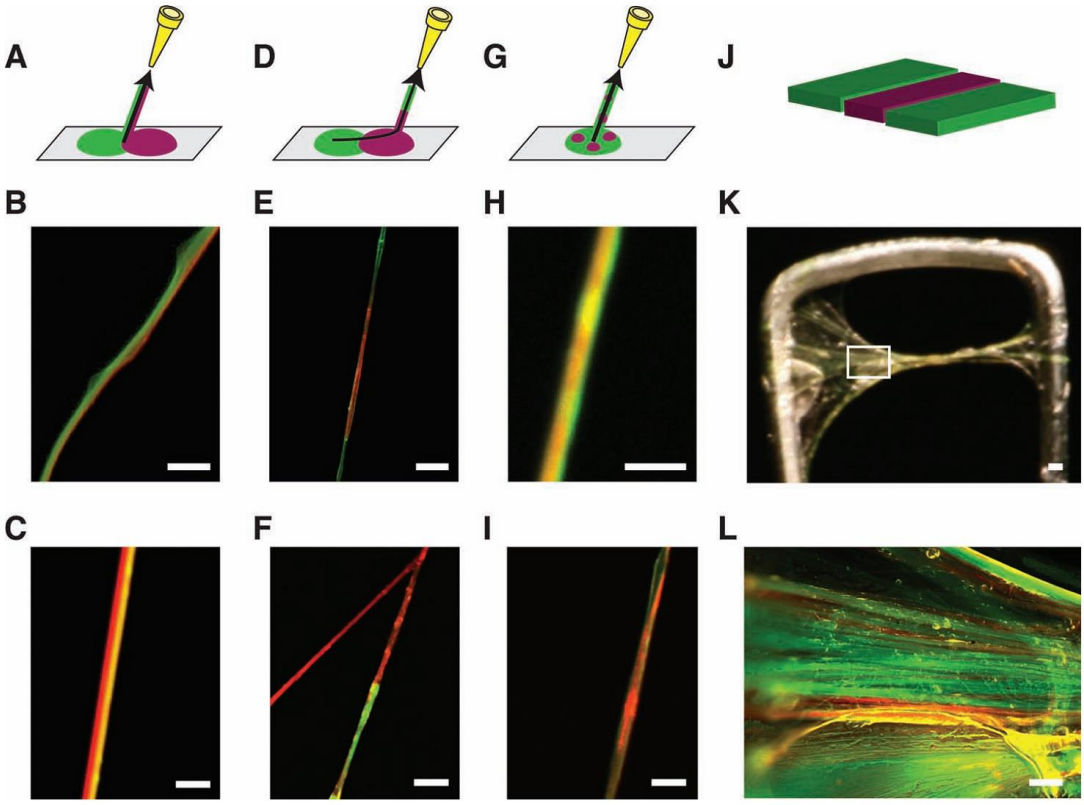


**Figure 1.5 Patterning of Ubx chimeric materials during materials assembly. (**A) Schematic and (B,C) fluorescence microscopy images of faced fibers produced along the boundary of side-by-side arranged solutions. (D) Schematic and (E-F) fluorescence microscopy images of striped fibers produced across the boundary of side-by-side solutions. G) Schematic and (H,I) fluorescence images of spotted fi bers produced from prearranged protein drops. (J) Schematic and (K) photograph of a film made from EGFP-Ubx and mCherry-Ubx chimeras. (L) Fluorescence microscopy image of a chimeric film containing EGFP-Ubx and mCherry-Ubx strands. All scale bars are 100 μm except for (K) (1 mm). (Huang et al., 2011)

# CHAPTER II

# IDENTIFICATION OF MULTIPLE DITYROSINE BONDS IN MATERIALS COMPOSED OF THE *DROSOPHILA* PROTEIN ULTRABITHORAX*

## 2.1 Introduction

Protein-based materials have the potential to be customized for a variety of applications, including drug delivery, tissue engineering, surgical sealants, medical imaging, biosensors, biofabrication, and biomineralization (Baneyx and Schwartz, 2007, Deming, 2007). However, realization of these innovations requires development of a variety of materials with different structural, mechanical, and functional properties (Maskarinec and Tirrel, 2005). For instance, macroscale materials in medical applications must be biodegradable (Velema and Kaplan, 2006, Grevellec et al., 2001), biocompatible (Rodriguez-Cabello et al., 2007, Ong et al., 2006), and have mechanical properties matching the tissues of interest (Chilkoti et al., 2006, Hollister et al., 2002); whereas materials destined for biofabrication must form rigid nanoscale three-dimensional structures (Lagziel-Simis et al., 2006, Gazit, 2007). The methods used to generate and process protein-based materials can have a substantial impact on both the mechanical and functional properties of the products (Huang et al., 2000, Qiu et al., 2009, Liivak et al., 1998, Leal-Egana and Scheibel, 2010, Engler et al., 22006, Georges et al., 2007).

*Reprinted with permission from "Identification of multiple dityrosine bonds in materials composed of the *Drosophila* protein Ultrabithorax" by Howell DW, Tsai SP, Churion K, Patterson J, Abbey C, Atkinson JT, Porterpan D, You YH, Meissner KE, Bayless KJ, Bondos SE, 2015. Advanced Functional Materials, 25, 5988-5998, Copyright 2015 by John Wiley & Sons.

Recombinant production of proteins provides a renewable supply of monomers for assembly whose sequences, and hence properties, can be easily engineered (Gomez, et al., 2012). Multiple approaches to rationally engineer or control the mechanical properties of materials formed from recombinant proteins have been explored, including chemical cross-linking, oxidation to form disulfide or dityrosine bonds, and incorporation of nanoparticles and metal films (Brooks et al., 2008, Grip et al., 2009, Teng et al., 2009, Lazaris et al., 2002, Kharlampieva, et al., 2010, Lee et al, 209, Ding et al., 2013, Souza et a., 2000).

Of these approaches, oxidation to form disulfide or dityrosine bonds is particularly attractive because these bonds do not always require additional steps for materials synthesis. The reversibility of disulfide bonds enables materials' strength and stability to be responsive to external conditions (Vaccaro and Waite, 2001, Meng et al., 2009). In contrast, dityrosine bonds are useful when the mechanical properties must be consistent in a variety of chemical environments, reflecting their inclusion in many natural and engineered materials, including resilin, silk, fibrinogen, keratin, elastin, and collagen (Nairn et al., 2008, Sando et al., 2010, Elvin et al., 2009, Chen et al., 2010, Mullerova et al., 1974, Qin et al., 2009, Ding et al., 2013, Fang and Li, 2012, Lin et al., 2015, Aparecido dos Santos-Pinto et al., 2014). In many cases, photocrosslinking is used to rapidly form dityrosine bonds throughout a material (Vashi et al., 2012, Fang et al, 2013). Dityrosine crosslinks have also been used to drive assembly of proteins or peptides that would not otherwise form materials, or to covalently link multiple proteins for materials assembly (Fang et al, 2013). However, the specific amino acids that form these bonds in protein-based materials have not been identified, information that is vital for engineering

the sequence to control bond formation, and hence the structure and mechanical properties of the resulting materials. Although in some materials, dityrosine bonds have been attributed to a single tyrosine residue in a repeated motif (Elvin et al., 2015, Waffenschmidt et al., 1993), each tyrosine motif is equally likely to participate in dityrosine bonds, resulting in monomer-to-monomer variation in the location of these bonds that would further complicate bond identification and sequence engineering.

In this study, we investigated the formation of dityrosine bonds in materials composed of Ultrabithorax (Ubx), a recombinant *Drosophila melanogaster* Hox transcription factor. *In vitro*, Ubx monomers coalesce in aqueous buffers near neutral pH to form globular aggregates, which further rearrange at the air-water interface to form nanoscale fibrils (Majithia et al., 2011). Fibrils associate laterally to generate macroscopic films, which are the building blocks for various macroscale Ubx architectures such as fibers, sheets, and bundles (Greer et al, 2009). Ubx materials have many useful properties, including cytocompatibility, biocompatibility, and nonimmunogenicity (Patterson et al., 2014, Patterson et al., 2015). Ubx materials can be functionalized i) with full-length proteins via gene fusion (Huang et al., 2011, Tsai et al., 2015), ii) with DNA by sequence-specific recognition (Churion et al.), and iii) with nanoparticles by non-covalent surface interactions (Majithia et al., 2011). Finally, Ubx materials are strong and remarkably extensible (Huang et al., 2010).

Ubx contains 15 tyrosines that are embedded in distinct regions of the amino acid sequence (Figure 2.1A). Therefore, Ubx has the potential to form unique, and thus

identifiable, dityrosine bonds in materials. In this study, we demonstrate that Ubx materials oxidize to form three dityrosine bonds, two of which are mutally exclusive, and we identify the participating tyrosine residues. In fibers pre-assembled in the absence of oxygen, exposure to oxygen rapidly triggers dityrosine formation, with biphasic bond formation kinetics. Because all Ubx monomers within the materials do not form both possible bonds, the dityrosine content can be increased by removing competing interactions. Dityrosine content directly correlates with the strength of the materials, suggesting these bonds are intermolecular and providing a mechanism to genetically tune the mechanical properties of the materials. These data illuminate the role of tyrosine residues in the formation and structure of Ubx materials, provide vital information for engineering the mechanical properties of Ubx fibers, and suggest approaches to insert specific dityrosine bonds into the sequence of other materials-forming proteins.

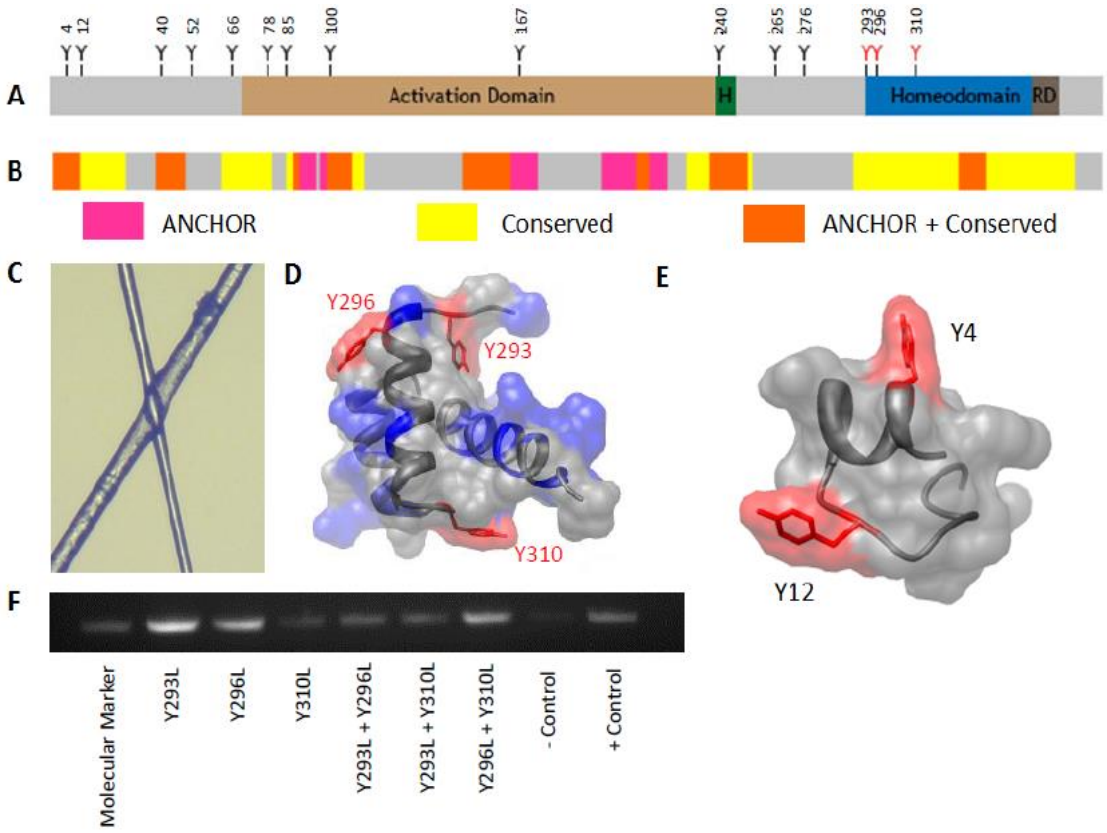


**Figure 2.1 Location and functionality of Ubx tyrosine mutants**. (A) Sequence schematic of Ubx, showing the location of tyrosine residues relative to functional domains and structural motifs. (B) ANCHOR schematic showing areas of disorder in Ubx. (C) Light microscopy of overlapping fibers shows that they are transparent and can diffract light. (D) The three tyrosines in the Ubx homeodomain all lie on the surface of the domain (pdb: 1B8I) (Passner et al., 1999). (E) Tyrosines 4 and 12 are not buried within this portion of Ubx. (F) DNA binding data showing that the homeodomain remains functional in tyrosine mutants.

## 2.2 Materials and methods

### 2.2.1 Production of Ubx materials

Protocols were used as established in the Bondos lab for expression, purification, and assembly of Ubx and Ubx fusion proteins into materials (Huang et al., 2011, Tsai et al., 2015). In brief, the *ubx* gene, cloned into pET-19b vector, was transformed into Rosetta (DE3) pLysS cells (Novagen). Single colonies were used to inoculate overnight liquid cultures. Protein expression was induced at mid-log phase with 1 mM IPTG for 4 hrs and cells were harvested by centrifugation and stored at -20 $^{0}$C. Frozen cell pellets were lysed and cell debris was removed by centrifugation for 30 min at 35,000 x g (17,000 rpm by JA25.5 rotor). Ubx protein was purified from the clarified cell lysate by Ni-NTA chromatography and, as previously described, fibers were pulled from films produced in a "buffer reservoir" (Huang et al., 2011) using a buffer containing 50 mM sodium phosphate buffer, 500 mM NaCl, 5% glucose w/v, pH 8.0. Fibers were wrapped around a 5 mm sterile plastic inoculation loop and stored in a sterile tissue culture dish until use.

### 2.2.2 Measuring fluorescent intensity in Ubx materials

The fluorescent intensity of both the auto-fluorescent and dityrosine antibody signal (N=2, sample=15, replicates=45) were measured using identical DAPI and FITC settings on the microscope and analyzed using Nikon Elements Imaging Software normalized to fiber width, which averaged approximately 15 µm. Z-stack images were captured using a 40X objective with a field depth of 1.1 µm and step sizes of 0.25 µm. Data in figures are displayed as average intensities +/- the standard deviation.

Quantitative measurement of dityrosine content based on fluorescence intensity requires tyrosine content to be the only variable. Since removal of specific tyrosine residues also prevents Ubx materials from being fluorescent, then there is clearly no other source of fluorescence that could interfere with our measurements. Since the materials can vary in size, the fluorescence intensity was always normalized to fiber diameter. This precaution allows us to quantitatively measure fluorescence, as previously demonstrated in measuring incorporation of different concentrations of Enhanced Green Fluorescent Protein-Ubx into Ubx materials (Tsai et al.,). Since the fluorescence intensity of the dityrosine signal is directly proportional to the fluorescence intensity of signal from anti-dityrosine antibodies (Figure 2.2), fluorescence intensity is a quantitative measure of dityrosine content.

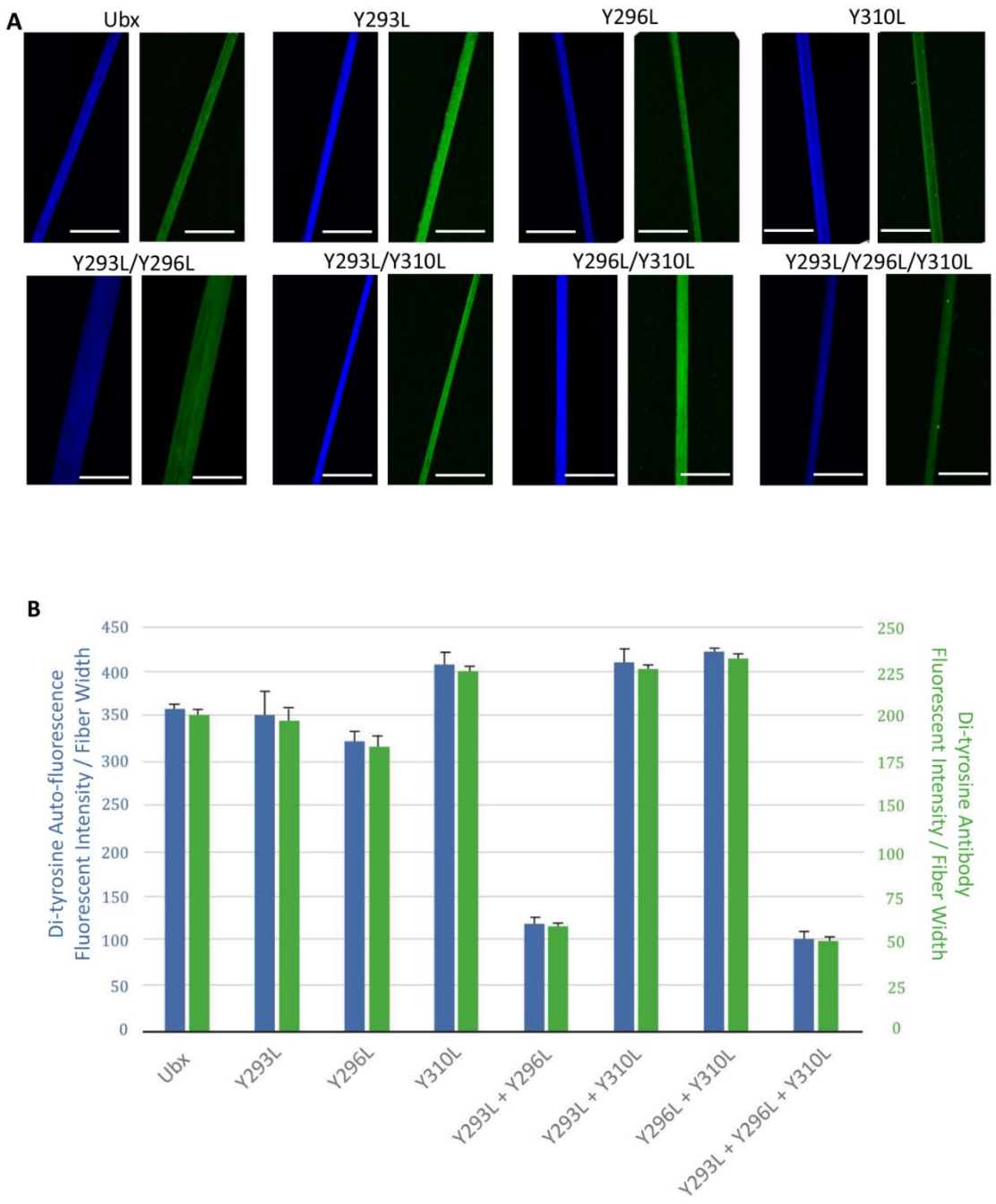


**Figure 2.2 A comparison of auto fluorescence and immunohistochemistry using antidityrosine antibodies for fibers composed of selected Ubx mutants.** Scale bar equals 30mm. (B) The auto-fluorescent intensity divided by fiber width corresponds to reactivity with dityrosine antibodies using immunohistochemistry.

### 2.2.3 Immunofluorescence

Ubx fibers wrapped around inoculation loops were allowed to dry at room temperature on the lab bench for 2 hrs. Loops were placed in sterile 4 well cell culture plates and incubated in 250 µL of blocking solution (0.1% Triton X-100, 1% BSA, 0.2% sodium azide, and 5% goat serum in PBS) at room temperature for 1 hr. Primary antibodies raised against dityrosine (Genox) were diluted 1:500 in blocking solution and incubated with Ubx fibers for 1 hr. After two washes for 10 min each in 0.1% Triton X-100 in PBS (250 µL), loops were incubated with goat anti-rabbit Alexa 488 conjugated secondary antibodies (Molecular Probes, diluted 1:300 in blocking solution) for 1 hr. Loops were washed twice (10 min per wash) in 0.1% Triton X-100 in PBS (250 µL), placed on a 22 mm x 55 mm coverslip, and imaged immediately using a 40X objective Nikon Eclipse Ti A1R inverted confocal microscope equipped with NIS Elements AR 4.10.01 software to analyze fluorescent intensity.

### 2.2.4 Measurement of absorption/emission spectra

A Ubx fiber was dissolved in commercially available 10 mM PBS buffer solution. The dispersed Ubx solution was transferred into a four sided quartz cuvette for the photoluminescence measurement. Steady state emission spectra were recorded using a QuantaMaster 40 spectrofluorometer (Photon Technology International, Canada). Light from the excitation source, a Xenon arc lamp, was dispersed by a 1200 line/mm grating blazed at 500 nm and focused on the sample. A 380 nm long-pass filter was placed in the emission path to remove excitation light. The Ubx solution was excited at 325 nm.

Emission was collected for 0.1 sec at each data point from 300 to 700 nm in steps of 1 nm.

### 2.2.5 Fiber assembly and imaging in low oxygen atmosphere

Ubx protein was purified as previously described; however, Ubx monomers were assembled into films and drawn into fibers in an argon-atmosphere glovebox (MBraun Labmaster, ~ 2 ppm $O_2$). Fibers were placed in a custom sealed imaging chamber (Figure 2.3) filled with $N_2$ gas to capture any $O_2$-independent auto-fluorescence. Ubx fibers were subsequently exposed to $O_2$ by removing the flow of $N_2$ gas and pushing room air into the chamber using a 50 mL syringe. The blue auto-fluorescence resulting from oxidation of Ubx fibers was analyzed over time using a Nikon Eclipse Ti A1R inverted confocal microscope equipped with NIS Elements AR 4.10.01 software.

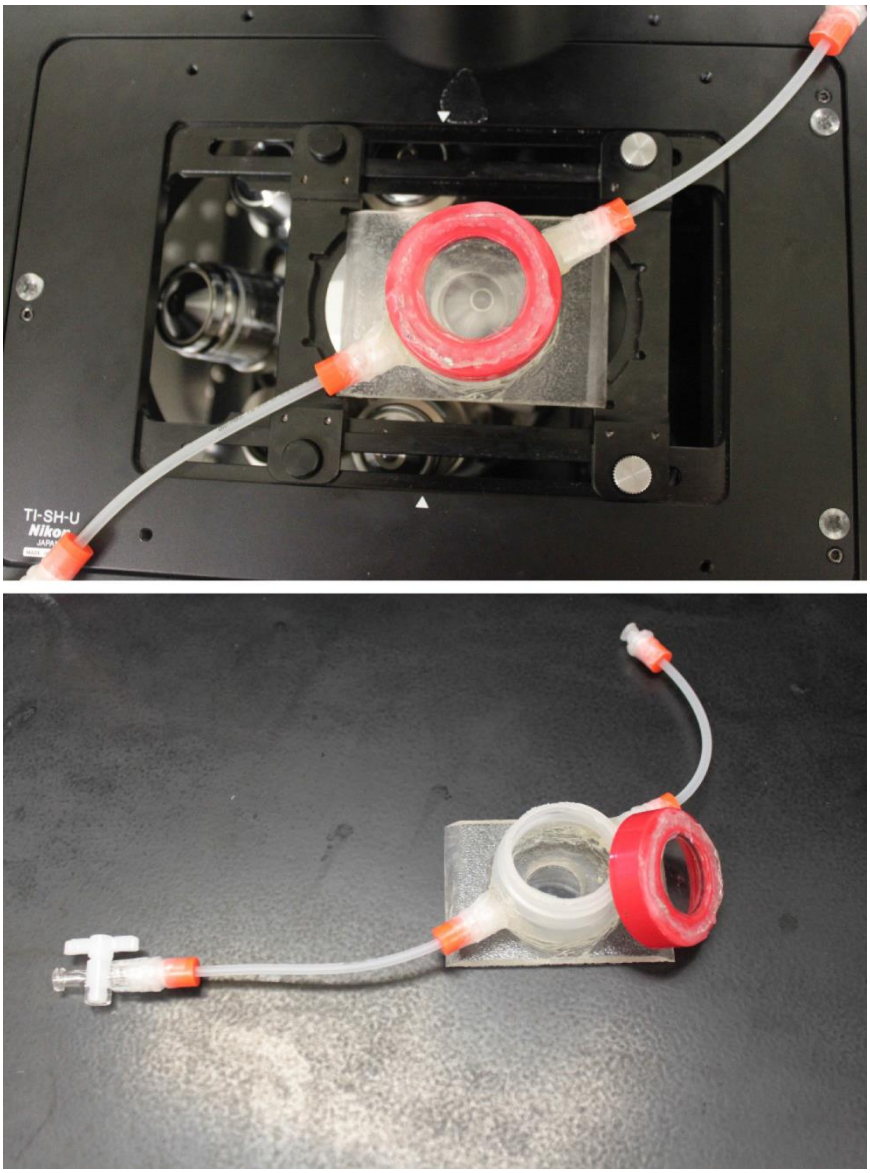


**Figure 2.3 Custom imaging chamber with a coverslip bottom and removable screw cap with viewing window.**

### 2.2.6 Mutagenesis of tyrosine

Tyrosines in the Ubx homeodomain region were mutated to leucine or serine using AccuPrime Pfx PCR kit (Invitrogen). (Figure 2.4) Primers (Table 2.1) for each mutation were designed using the OligoCalc (northwestern.edu/biotools/oligocalc) and mfold web servers (http://mfold.rna.albany.edu/?q=mfold). Mutated plasmids were transformed into DH5α competent cells (Zymo Research) and plated on LB agar with 50 μg/mL carbenicillin overnight at 37 ºC. Colonies were selected and grown in 5 ml cultures of LB for plasmid purification using QIAprep miniprep (Qiagen) kit. Plasmids were sequenced to confirm each mutation prior to use. Ubx mutants were expressed in *E. coli* and purified as described above for the wild-type protein.

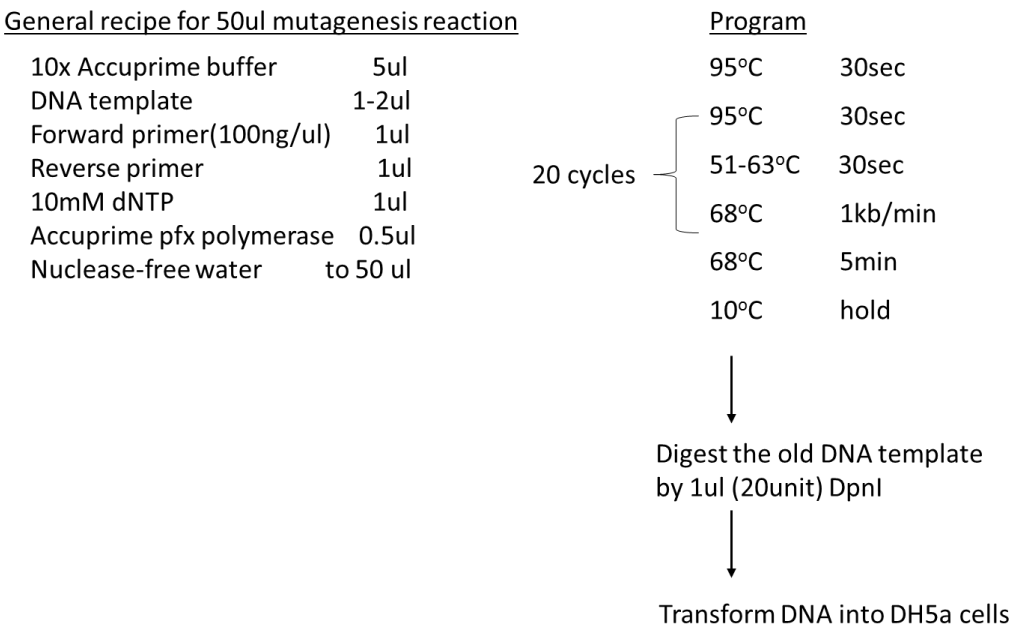


**Figure 2.4 General setup for site-directed mutagenesis reaction.**

**Table 2.1 DNA primers used for mutagenesis.**

| Mutation | Primer Sequence |
|---|---|
| Y4S | FWD: 5'- CATATGAACTCGTCCTTTGAACAGGCC-3' |
| | REV: 5'- GGCCTGTTCAAAGGACGAGTTCATATG -3' |
| Y12S | FWD: 5'- GCCTCCGGCTTTTCTGGCCATCCGCAC -3' |
| | REV: 5'- GTGCGGATGGCCAGAAAAGCCGGAGGC-3' |
| Y52S | FWD: 5'- GGCATGAGTCCCTCTGCCAACCACCATC-3' |
| | REV: 5'- GATGGTGGTTGGCAGAGGGACTCATGCC -3' |
| Y85S | FWD: 5'- GGAGCCGGAGCCTCCAAACAGGACTGC-3' |
| | REV: 5'- GCAGTCCTGTTTGGAGGCTCCGGCTCC-3' |
| Y100S | FWD: 5'- CGGTGAATGGCTCCAAAGACATTTGGAAC-3' |
| | REV: 5'- GTTCCAAATGTCTTTGGAGCCATTCACCG-3' |
| Y167S | FWD: 5'- GAGTGGGCGGCTCCTTGGACACGTC-3' |
| | REV: 5'- GACGTGTCCAAGGAGCCGCCCACTC-3' |
| Y240S | FWD: 5'- CAATCACACATTCTCCCCCTGGATGG -3' |
| | REV: 5'- CCATCCAGGGGGAGAATGTGTGATTG-3' |
| Y293L | FWD: 5'- GGCCGACAGACATTAACCCGCTACCAG-3' |
| | REV: 5'- CTGGTAGCGGGTTAATGTCTGTCGGCC-3' |
| Y296L | FWD: 5'-ACATACACCCGCTTACAGACGCTCGAG-3' |
| | REV: 5'- CTCGAGCGTCTGTAAGCGGGTGTATGT-3' |
| Y310L | FWD: 5'- CACACGAATCATTTGCTGACCCGCAGA-3' |
| | REV: 5'- TCTGCGGGTCAGCAAATGATTCGTGTG-3' |
| Y293S/ Y296S | FWD: 5'- GGCCGACAGACATCCACCCGCTCCCAGACGCTCGAG-3' |
| | REV: 5'- CTCGAGCGTCTGGGAGCGGGTGGATGTCTGTCGGCC-3' |

### 2.2.7 DNA binding assay

Ubx materials were produced using the drop method and DNA binding was measured as previously described (Churion et al.). Ubx was diluted in 250 µl of a solution containing 50 mM $NaH_2PO_4$ (pH 8.0), 300 mM NaCl, 10 mM β-mercaptoethanol, 5% glucose, and 200 mM imidazole, for a final protein concentration of 3 - 6 µM depending on the purification yield. Protein was carefully pipetted onto the surface of a siliconized glass slide, and covered with a screw cap from a 50 mL conical centrifuge tube (VWR International) and the slides were covered to prevent evaporation. After a 16 hr incubation at room temperature and humidity, a film, formed at the air-water interface, and was drawn into fibers using a sterile inoculating loop. Fibers were subsequently washed three times in PBS buffer and dried for 1-2 hrs at room temperature. The DNA stock was diluted to a final concentration of 10 µg/mL in phosphate buffered saline. Fiber loops were then placed in a well (24 well culture plate); subsequently, 200 µL of the diluted DNA was pipetted in each well and allowed to incubate at room temperature (parafilm wrapped) overnight. Fibers were washed three times in PBS buffer (3-5 minutes each) to remove excess DNA from the fiber. The Ubx fiber was removed from the inoculating loop with micro-scissors and transferred to a PCR tube containing the

following components: 1x PCR ThermoPol buffer (NEB), 50 μM each of dATP, dCTP, dGTP, dTTP, 0.5 μM of each primer, and 1 unit of Taq DNA polymerase (NEB) in a 50 μl reaction. The PCR reaction products were analyzed by electrophoresis through a 2% agarose gel, which was stained with ethidium bromide and visualized using a UV light source.

### 2.2.8 Fiber length measurements

Ubx protein was diluted to 1 mg in 590 mL of buffer in a shallow Teflon-coated tray (Nordic Ware), covered to prevent surface disruptions, and incubated 18 hrs at room temperature (approximately 25 $^{0}$C) and 40 - 60% humidity. To measure changes in fiber production, which depends on both fiber assembly and fiber strength, the length of fibers drawn from the resulting films were measured. A minimum of eight measurements, produced from a minimum of two purifications, were made for each Ubx variant.

## 2.3 Results and discussion

### 2.3.1. Ubx fibers are not amyloid

Elucidating the structure of protein-based materials is the first step toward understanding, and ultimately manipulating the mechanical properties of these materials. In contrast to amorphous protein aggregates which often appear as white flocculates, Ubx materials are transparent (Figure 2.1C) and can diffract light (Majithia et al., 2011), suggesting a more regular structure. Since Ubx does not form materials as part of its natural function, one possibility is that Ubx fibers are amyloid, thus accounting for their transparency and strength (Knowles and Buehler, 2011). However, X-ray diffraction and Thioflavin T binding studies of Ubx materials lack any indications of amyloid structure (data not shown). Furthermore, a large fraction of Ubx is extremely glycine-rich (Liu et al., 2008), and thus unlikely to form amyloid. The major structured region of Ubx is its DNA binding homeodomain, whose function is retained in the materials (Figure 2.1 A, D) (Churion et al.). Therefore, the helical structure of the homeodomain is likely intact as well. If both the unstructured and the structured regions of Ubx are unlikely to form amyloid, then amyloid structure cannot be responsible for the strength of Ubx materials.

### 2.3.2 Ubx materials contain dityrosine

Intermolecular covalent cross-links could also account for the strength of Ubx materials. Many natural macroscale materials rely on covalent crosslinks for strength (Elvin et al., 2009, Endrizzi et al., 2006, Kelley, 1968), and engineering covalent bonds into recombinant protein materials can dramatically improve both strength and assembly (Fang and Li, 2012). During fluorescent microscopy experiments, we observed that Ubx

materials autofluoresce when excited at 305 nanometers (nm) **(**Figure 2.5A**)**. The fluorescence emission spectrum (Figure 2.5B) corresponds with dityrosine, formed by oxidation of two tyrosine residues (Endrizzi et al., 2006, Marquez and Dunford, 1995, Aeschbach et al., 1976). The emission maximum of dityrosine typically ranges from 410 nm to 430 nm (Aeschbach et al., 1976, Harms, et al., 1997). For Ubx fibers, the emission peak is more red-shifted (438 nm). This difference may be due to proximity of the dityrosine bonds to positively charged amino acids, which can red-shift the emission spectra of aromatic amino acids by tens of nanometers (Vivian and Callis, 2001). Ubx has a predicted net charge of +9, and the Ubx homeodomain, which contains 3 tyrosines, has a predicted net charge of +11 (Figure 2.5D) (Majithia et al., 2009, Tsai et al., 2015). Anti-dityrosine antibodies specifically recognize Ubx fibers in immunohistochemistry experiments, thus confirming the presence of dityrosine in Ubx materials (Figure 2.5C). The secondary antibodies alone are unable to bind fibers in the absence of primary antibodies (Figure 2.5D), demonstrating the specificity of the interaction. Together, the fluorescence and immunohistochemistry data demonstrate that dityrosine is present in Ubx fibers.

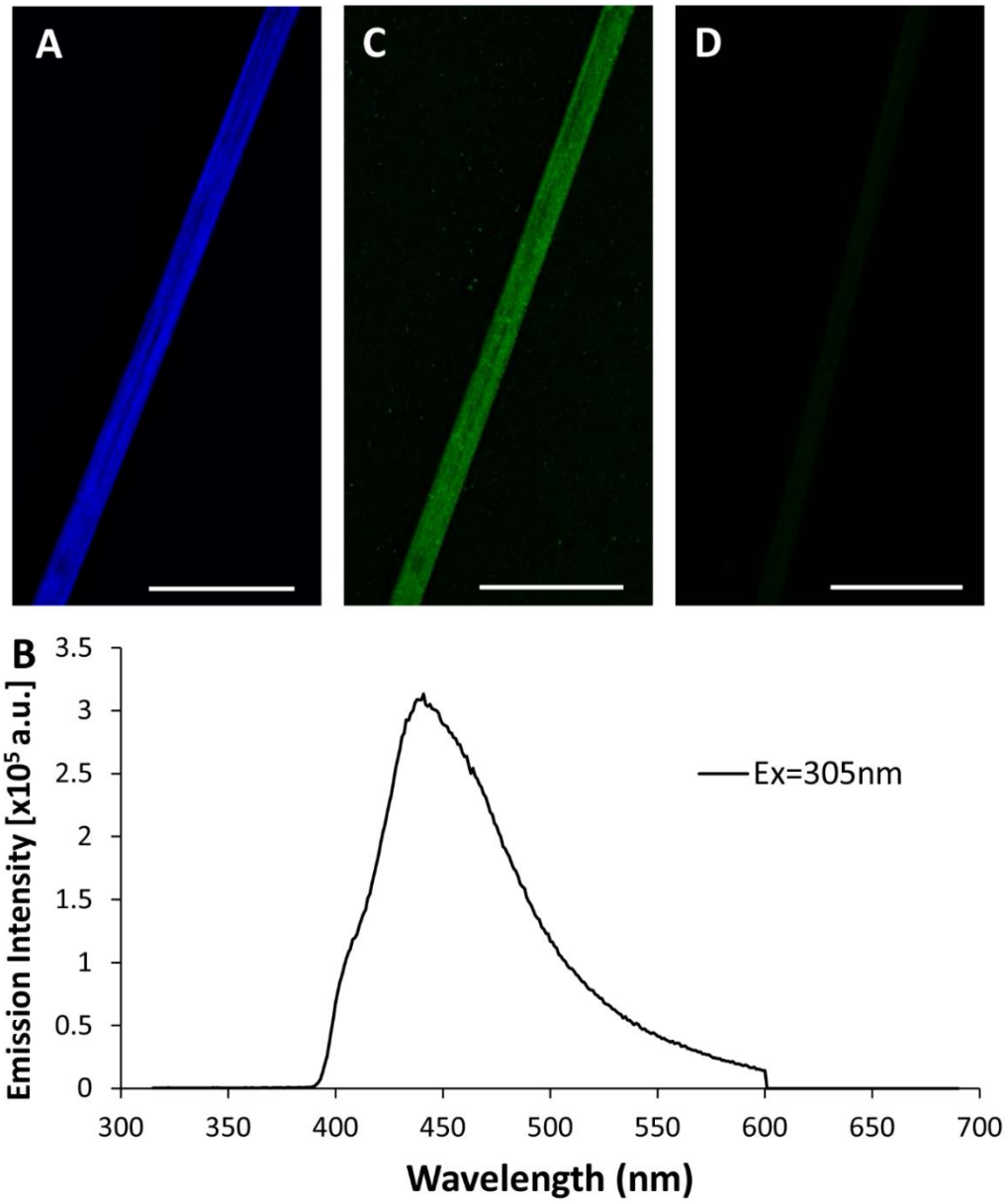


**Figure 2.5 Ubx materials contain dityrosine.** (A) Fibers autofluoresce blue. (B) The Ubx emission spectrum, with a peak at 438 nm when excited at 305 nm is similar to other dityrosine containing proteins. (C) Immunofluorescence of Ubx fiber demonstrating anti-dityrosine primary antibodies recognize a Ubx fiber. (D) A negative control experiment with the primary antibody omitted demonstrates that secondary antibodies do not adhere non-specificially to Ubx fibers. Scale bar equals 30 μm in all panels.

### 2.3.3 Measuring the kinetics of dityrosine bond formation

Because tyrosine must oxidize to form dityrosine bonds, the kinetics of dityrosine bond formation can be monitored by assembling Ubx in a low oxygen environment and then exposing the resulting fibers to oxygen. To this end, Ubx was allowed to assemble in an argon-atmosphere glovebox. Because films could be assembled and fibers could be drawn from films in this low oxygen environment, dityrosine bond formation is clearly not required for Ubx assembly. However, it is worth noting that these fibers were quite fragile and very difficult to handle.

Fibers were placed in a custom imaging chamber **(**Figure 2.3**)** under nitrogen gas flow to maintain a low oxygen environment during transfer of the chamber from the glove box to a microscope. Cover slips on the top and bottom of the chamber allowed fibers inside the chamber to be analyzed by fluorescence microscopy. In a nitrogen environment, the blue dityrosine signal was nearly undetectable **(**Figure 2.6A**)**. However, once the nitrogen gas in the chamber was replaced with air, the fibers gradually began to fluoresce blue (Figure 2.6B). Measurement of fluorescent intensity over time reveals two distinct transitions (Figure 2.6C): a fast initial transition followed by a slow transition.

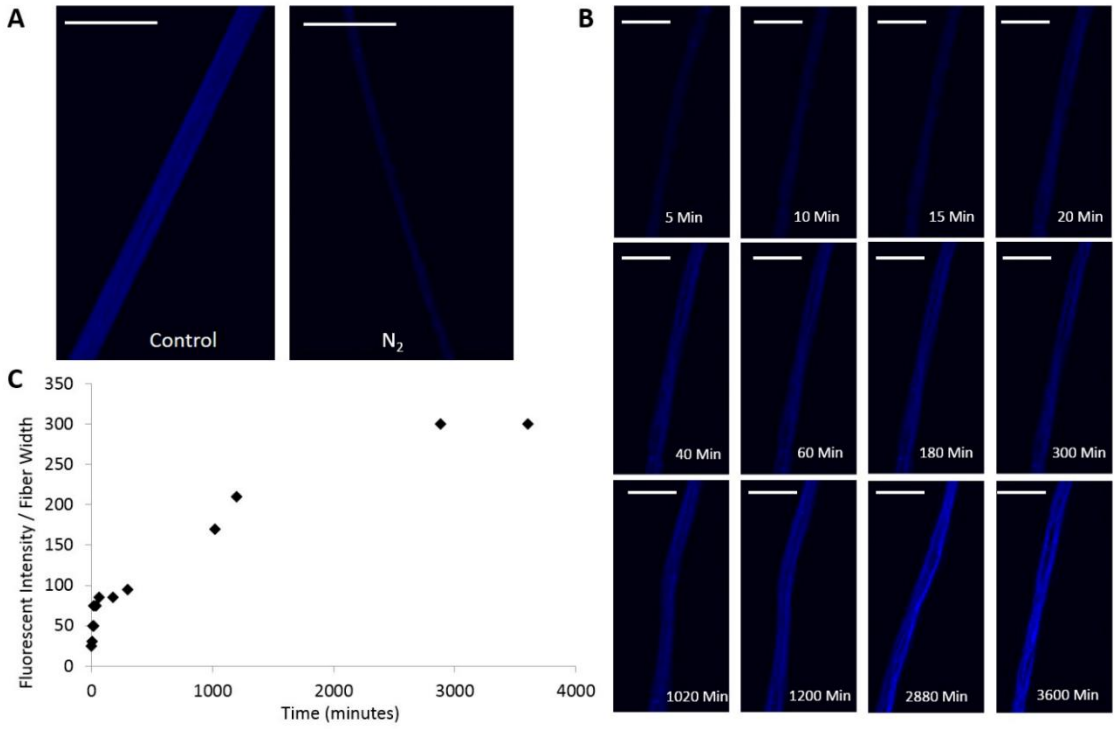


**Figure 2.6 The kinetics of dityrosine bond formation reveals two transitions.** (A) A fluorescent miscroscopy image of a Ubx fiber pulled and imaged in low oxygen environment $N_2$ compared to a fiber pulled in normal atmosphere (control). (B) Time-lapse images of a fiber pulled in low $O_2$ after exposure to normal atmosphere. (C) Graph of fluorescent intensity of the fiber shown in panel B over time showing 2 distinct transitions caused by dityrosine bond formation. Scale bar equals 30 µm in all panels.

### 2.3.4 Mutagenesis strategy

The presence of dityrosine provides an opportunity to manipulate the properties of Ubx materials by controlling dityrosine bond formation. To do so, the number of dityrosine bonds formed and the identity of the tyrosine residues that participate in these bonds must be determined. Because Ubx is produced as a recombinant protein in *E. coli*, we were able to use site-directed mutagenesis to identify participating tyrosines. This approach would be challenging to apply to many natural proteins that form materials. Because the amino acid sequence surrounding tyrosine residues impacts dityrosine bond formation (Harms et al., 1997), tyrosines located in repeating motifs in natural materials should have equal probabilities of participating in a dityrosine bond (Elvin et al., 2015, Waffenschmidt et al., 1993). In contrast, the unique sequences surrounding tyrosines in Ubx should lead to preferential interactions between specific tyrosines and thus consistent formation of the same dityrosine bonds. Furthermore, Ubx monomers rely on specific, long-range intramolecular interactions to regulate DNA binding (Liu et al., 2009). These interactions involve regions of the protein containing tyrosine. Therefore, any intermolecular dityrosine bonds based on these interactions should form between specific residues.

A complication of the site-directed mutagenesis approach stems from the fact that Ubx has 15 tyrosine residues. The identity of tyrosines contributing to a single bond may vary, and more than one dityrosine bond may be present in the materials, creating an enormous array of possible bond arrangements. We narrowed our initial search based on interactions formed by Ubx monomers in DNA binding. When bound to DNA, Ubx can

oligomerize in multiple orientations: side-to-side cooperative interactions when binding to linear DNA, and back-to-back interactions between clusters of cooperatively bound Ubx proteins to form the stem of a DNA loop (Beachy et al., 1993). Because Ubx fibers retain the ability to bind DNA (Figure 2.1F), it is possible that interactions used on a small scale to enable cooperative DNA binding and DNA loop formation *in vivo* may also be applied on a much larger scale to form Ubx materials *in vitro*: side-to-side interactions to form nanoscale fibrils, and back-to-back interactions to allow the fibrils to interact to form films and fibers. Therefore, our first criterion for selecting tyrosines for mutagenesis was that the tyrosine should be located in a region important for regulating DNA binding (Liu et al., 2009). Extending this logic, any tyrosine important for DNA binding is also expected to be evolutionarily conserved (Figure 2.1B), our second criterion. Next, for specific dityrosine bonds to form, the tyrosines would need to be embedded in regions of Ubx likely to participate in protein-protein interactions. The location of molecular recognition features, motifs capable of engaging in protein interactions, was predicted by the ANCHOR algorithm (Figure 2.1B) (Dosztanyi et al., 2008, Meszaros et al., 2009). It is important to note that this algorithm only identifies motifs located in intrinsically disordered regions; thus, it cannot provide information about the structured homeodomain. Finally, as demonstrated by the fragility of fibers drawn in a low-oxygen environment, dityrosine bonds significantly strengthen Ubx materials. Because fiber strength is one factor that determines the length of fibers that can be drawn from film, we reasoned that tyrosine residues, lost through truncation of the Ubx sequence, would shorten the average length of fibers produced by that Ubx variant. Fiber lengths were previously measured for a series of Ubx N-terminal and C-terminal

truncation mutants (Greer et al., 2009). This data provided the fourth criterion for selecting tyrosines for mutagenesis.

The ability of each of the 15 tyrosines in Ubx to meet these criteria is summarized in Table 2.2 Based on the logic described above, we hypothesized that tyrosines 4, 12, 100, 167, and 240 were most likely to be involved in dityrosine bonds. The three tyrosines on the surface of the homeodomain (HD) (293, 296, and 310; Figure 2.1A, D) were also selected because the homeodomain participates in long-range interactions with much of the rest of the protein (Liu et al., 2009), and because the dityrosine spectrum is red-shifted. Conversely, tyrosines 40, 52, 66, 78, 85, 265, and 276 were deemed less likely candidates. The goal of our mutagenesis study was to remove the ability to form crosslinks, while retaining as much of the chemical nature of tyrosine as possible to prevent mutagenesis-induced structural rearrangements. Tyrosines in intrinsically disordered regions outside the homeodomain were mutated to serine, because the transfer coefficient of serine best mimics that of tyrosine as a free amino acid, leading to their similar values on the Kyte-Doolittle hydropathy scale (Kyte and Doolittle et al., 1982). Tyrosines within the homeodomain were mutated to leucine, because leucine most closely resembles the hydropathy of tyrosine on the surface of a protein (Pace et al., 2014). These mutations do not alter the structure or function of the homeodomain, because fibers composed of homeodomain mutants can successfully bind DNA (Figure 2.1F). To confirm that hydrophobic patches created by the tyrosine to leucine mutants on the homeodomain surface were not causing a loss of fluorescence due to altered interactions with the rest of the protein, we also changed these three residues to serine. All Ubx variants carrying mutations in the homeodomain were able to form fibers, these

fibers all bound DNA (Figure 2.1F), and circular dichroism spectra of materials composed of wild-type Ubx and these mutants are similar (Figure 2.7), indicating the structure of the fibers was not significantly perturbed. Furthermore, for each position, the serine and leucine mutations had a similar impact on dityrosine fluorescence (Figure 2.8). Therefore, leucine mutations do not cause unanticipated effects on the structure of Ubx materials.

**Table 2.2 Criteria used to select tyrosines for mutagenesis studies.**

| Tyrosine | Regulating DNA binding[a] | Sequence conservation[b] | Anchor[c] | Fiber length[d] | Selected? |
|---|---|---|---|---|---|
| **4** | **Yes** | **Yes** | **Yes** | **Yes** | **Yes** |
| **12** | **Yes** | **Yes** | **No** | **Yes** | **Yes** |
| 40 | Yes | Yes | Yes | No | No |
| 52 | No | No | No | No | No |
| 66 | No | Yes | No | No | No |
| 78 | No | Yes | No | No | No |
| 85 | No | No | No | No | No |
| **100** | **Yes** | **Yes** | **Yes** | **Yes** | **Yes** |
| **167** | **Yes** | **No** | **Yes** | **Yes** | **Yes** |
| **240** | **Yes** | **Yes** | **Yes** | **N/A** | **Yes** |
| 265 | Yes | No | No | N/A | No |
| 276 | Yes | No | No | N/A | No |
| **293** | **Homeodomain** | **Yes** | **N/A** | **No** | **Yes** |
| **296** | **Homeodomain** | **Yes** | **N/A** | **No** | **Yes** |
| **310** | **Homeodomain** | **Yes** | **N/A** | **No** | **Yes** |

[a]Based on data published by Liu et al. 2009
[b]Based on the sequence alignment established by Liu et al. 2009
[c]The results of the Anchor prediction algorithm are shown in Figure 2.4B.
[d]The length of fibers produced by N- and C-terminal Ubx truncation mutants was previously reported (Greer et al., 2009).

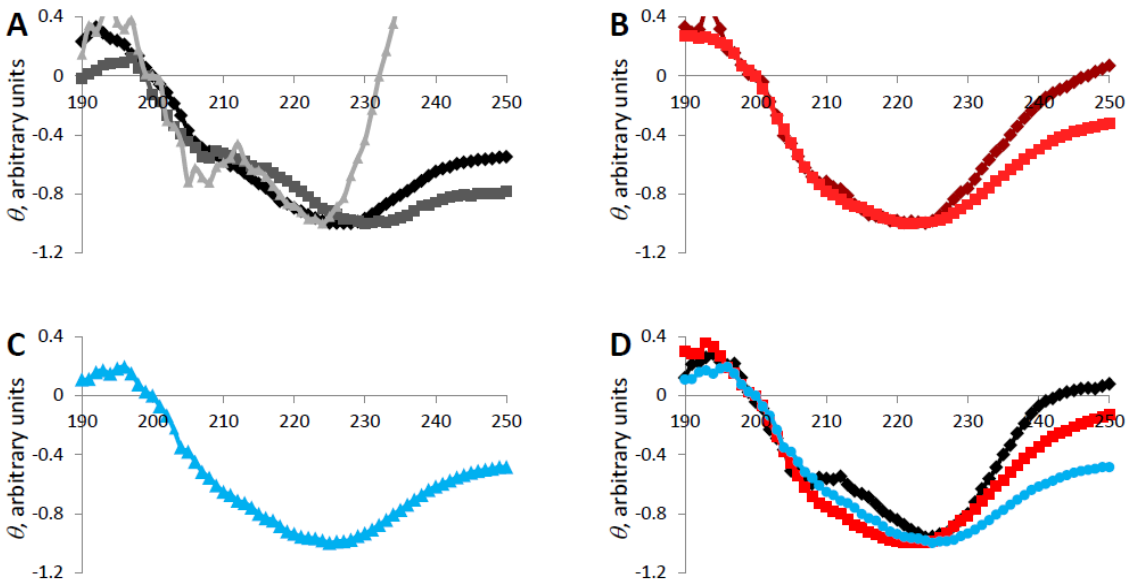


**Figure 2.7 Circular dichroism of films composed of wild-type and mutant Ubx.** Because the ellipticity depended both on the concentration of the sample in the beam, which we could not measure, and the dryness of the sample, which caused scattering, all data was normalized by setting the ellipticity at 200 nm to 0, and the minimum ellipticity to -1.0. This normalization allows comparison of the shape of the curves. (A) CD spectra for three wild-type Ubx films. The film corresponding to the light gray spectrum was thinner than the other films. (B) CD spectra for two films composed of the Y293L/Y296L double mutant. (C) A CD spectrum of a Y167S/Y240S Ubx film. (D) Average spectra for wild-type (black) and Y293L/Y296L (red) films superimposed on the Y167S/Y240S spectrum reveals little difference in the shape of the curves. In particular, the relative ellipticity at 208 nm and 22 nm is similar for these samples, suggesting a similar content of α-helices and β-sheets or β-turns in wild-type and mutant films.

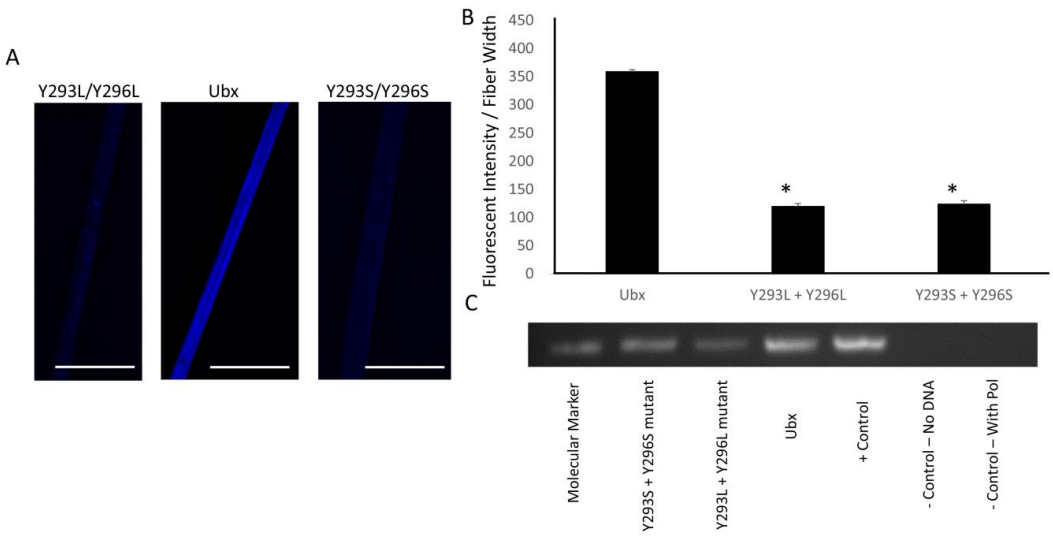


**Figure 2.8 Immunofluorescence of fibers composed of selected Ubx mutant proteins.** Scale bar equals 30 µm in all panels. (B) Graph of fluorescent intensity showing significant ($p < 0.01$ indicated by *) decrease in both L and S mutants relative to wild-type Ubx. (C) DNA binding assay comparing S and L mutation of Y293 and Y296.

### 2.3.5 Tyrosines that regulate DNA binding in Ubx monomers also participate in dityrosine bonds in Ubx fibers

To find tyrosines involved in dityrosine bonds, we tested whether single mutations of the selected tyrosines reduce Ubx fiber fluorescence. Of these eight mutants, the fluorescent intensities from Y12S, Y167S, Y240S, and Y296L mutants significantly decrease while the intensities from Y100S and Y310L mutants increase when compared to wild-type Ubx fiber fluorescence **(**Figure 2.9A; $p \leq 0.01$ indicated by *). The intensity of blue fluorescence corresponds very well with the fluorescent intensity from immunostaining using the anti-dityrosine primary antibody **(**Figure 2.10, $r^2 = 0.99$**)**, confirming that changes in fiber fluorescence directly correspond to alterations in dityrosine content. The Y167S and Y240S mutations both reduce the fluorescent intensity to a similar degree, suggesting that Y167 and Y240 participate in the same dityrosine bond.

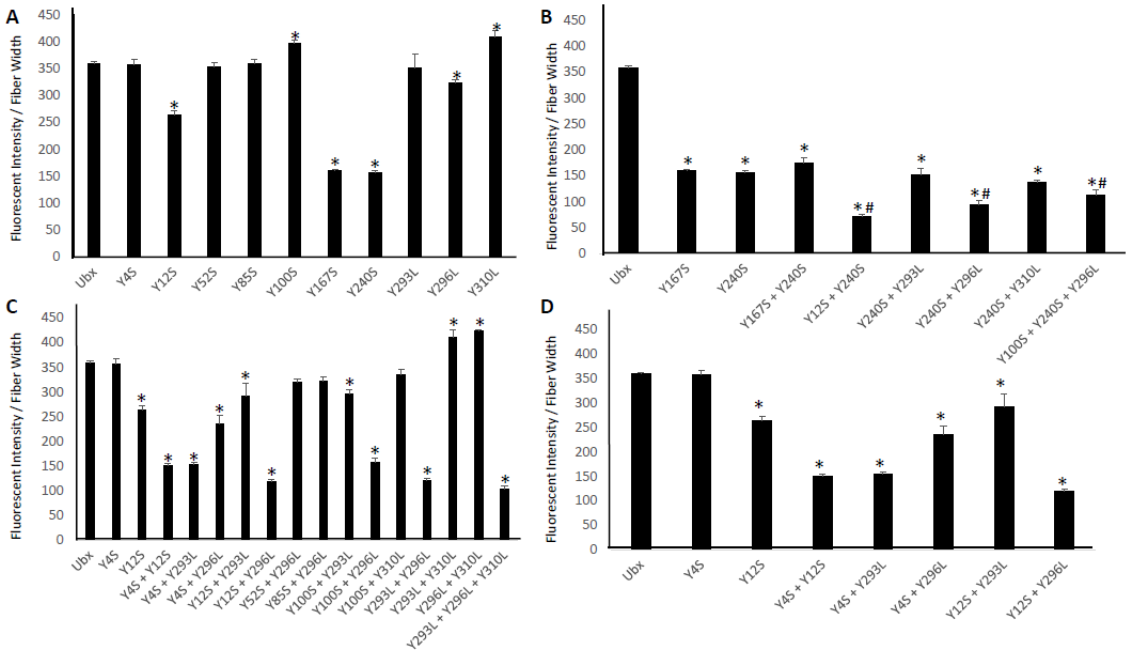


**Figure 2.9 Graph of fluorescent intensity divided by fiber width. (**A) Single mutations of the 8 tyrosines predicted to be involved show that only Y12S, Y167S, Y240S, Y296L, and Y310L show a significant difference ($p \leq 0.01$ indicated by *) in fluorescent intensity when compared to Ubx. (B) Comparison of mutants containing Y240S shows that Y240 binds Y167. Comparisons to Ubx are indicated by * ($p=0.005$) and to Y240 indicated by # ($p=0.04$) using t-tests. (C) Comparison of mutants containing combinations of N-terminal (Y4 and Y12), Y100, and homeodomain mutants. (D) A closer examination of N-terminal mutants with all three homeodomain mutants.

To test this hypothesis, we created a Y167S + Y240S double mutant. If these residues participate in different dityrosine bonds, the loss of fluorescent intensity should be additive. If Y167 and Y240 contribute to the same bond, then removing the second tyrosine should not cause an additional reduction in fluorescence. No further reduction in fluorescence was observed for the Y167S + Y240S double mutant (Figure 2.10B, 2.11, Table 2.3), suggesting that Y167 and Y240 form a single dityrosine bond **(**Figure 2.12). This assignment is supported by the fact that double mutants combining Y240S with other affected tyrosines (for instance, Y12S + Y240S and Y240S + Y296L) all fluoresce less than the isolated Y240S mutant, indicating that Y12 and Y296 participate in a different bond than Y240 (Figure 2.9B; $p \leq 0.04$ indicated by #). The Y167S + Y240S bond is responsible for a significant portion of the observed fluorescence in Ubx fibers (200/360 fluorescence units/μm). Finally, fibers composed of the Y293 mutant fluoresce to a similar extent as wild-type Ubx fibers. The fluorescent intensity of the Y240S + Y293L mutant fibers is similar to that of Y240S mutant fibers. Thus the Y240 mutant does not uncover any hidden contributions of Y293 to the Y167 + Y240 dityrosine bond.

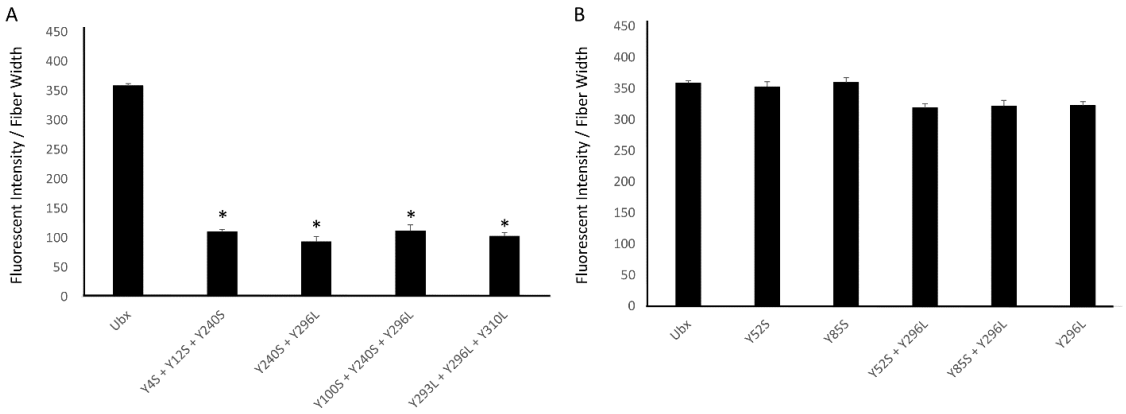


**Figure 2.10 More than one bonds in Ubx materials. (**A) The mutants Y4S + Y12S + Y240S, Y240S + Y296L, Y100S + Y240S + Y296L, and Y293L + Y296L + Y310L all show a loss of 250 fluorescent units per μm when compared to Ubx suggesting a loss of more than one tyrosine bond (p=0.005 indicated by *). (B) Mutation of tyrosines Y52 and Y85 which were not predicted to be involved in dityrosine bonds has no effect, either in wild-type Ubx or in the Y296 background.

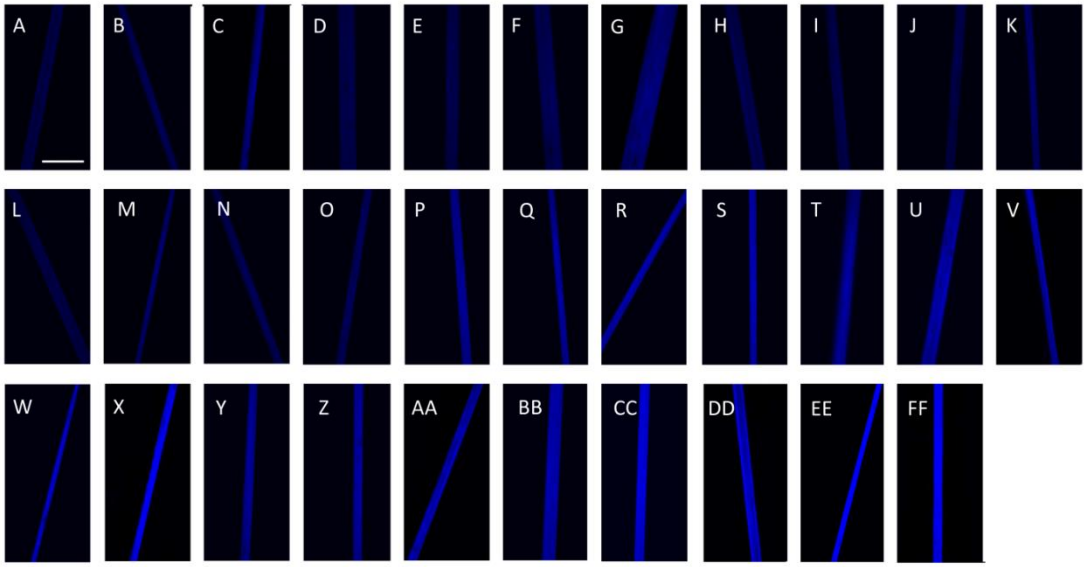


**Figure 2.11 Autofluorescence of all mutants**. (A) Y12S + Y240S, (B) Y240S + Y296L, (C) Y293L + Y296L + Y310L, (D) Y4S + Y12S + Y240L, (E) Y100S + Y240S + Y296L, (F) Y12S + Y296L, (G) Y293L + Y296L, (H) Y240S + Y310L, (I) Y4S + Y12S, (J) Y240S + Y293L, (K) Y4S + Y293L, (L) Y240S, (M) Y100S + Y296L, (N) Y167S, (O) Y167S + Y240S, (P) Y4S + Y296L, (Q) Y12S, ® Y12S + Y293L, (S) Y100S + Y293L, (T) Y52S + Y296L, (U) Y85S + Y296L, (V) Y296L, (W) Y100S + Y310L, (X) Y293L, (Y) Y52S, (Z) Y4S, (AA) Ubx, (BB) Y83S, (CC) Y100S, (DD) Y310L, (EE) Y293L + Y310L, (FF) Y296L + Y310L.

**Table 2.3 Fluorescence and physical parameter data for fibers composed of wild-type and mutant Ubx, arranged by increasing fluorescence.**

| ID | Mutant | DAPI Fluorescence | DAPI SE of the Mean | Avg. Width | Width SE of the Mean | Avg. Pull Length | Pull Length SE of the Mean |
|---|---|---|---|---|---|---|---|
| A | Y12S + Y240S | 71 | 9 | 11.6 | 0.67 | 1.3 | 0.2 |
| B | Y240S + Y296L | 94 | 9 | 12.9 | 0.54 | 1.6 | 0.2 |
| C | Y293L + Y296L + Y310L | 103 | 7 | 13.5 | 0.65 | 1.7 | 0.4 |
| D | Y4S + Y12S + Y240L | 110 | 4 | 10.1 | 0.08 | 1.6 | 0.5 |
| E | Y100S + Y240S + Y296L | 112 | 10 | 15.7 | 0.36 | 1.8 | 0.1 |
| F | Y12S + Y296L | 119 | 4 | 9.7 | 0.18 | 1.9 | 0.3 |
| G | Y293L + Y296L | 119 | 5 | 13.8 | 0.38 | 1.9 | 0.2 |
| H | Y240S + Y310L | 138 | 4 | 10.4 | 1.28 | 2.0 | 0.2 |
| I | Y4S + Y12S | 150 | 5 | 10.3 | 0.23 | 2.0 | 0.2 |
| J | Y240S + Y293L | 152 | 12 | 9.4 | 1.19 | 2.3 | 0.5 |
| K | Y4S + Y293L | 154 | 4 | 8.8 | 0.18 | 2.1 | 0.1 |
| L | Y240S | 157 | 4 | 7.5 | 0.12 | 2.2 | 0.2 |
| M | Y100S + Y296L | 158 | 8 | 10.9 | 1.54 | 2.3 | 0.4 |
| N | Y167S | 160 | 2 | 13.1 | 1.18 | 2.2 | 0.2 |
| O | Y167S + Y240S | 175 | 10 | 11.3 | 1.28 | 2.3 | 0.2 |
| P | Y4S + Y296L | 236 | 16 | 7.2 | 0.43 | 3.2 | 0.1 |
| Q | Y12S | 264 | 9 | 7.4 | 0.18 | 3.4 | 0.2 |
| R | Y12S + Y293L | 293 | 25 | 6.6 | 0.30 | 3.7 | 0.6 |
| S | Y100S + Y293L | 297 | 8 | 8.5 | 0.11 | 3.7 | 0.2 |
| T | Y52S + Y296L | 319 | 7 | 7.2 | 0.06 | 3.7 | 0.2 |
| U | Y85S + Y296L | 322 | 9 | 7.3 | 0.07 | 3.8 | 0.4 |
| V | Y296L | 323 | 6 | 8.6 | 0.08 | 3.8 | 0.5 |
| W | Y100S + Y310L | 335 | 11 | 6.6 | 0.63 | 4.0 | 0.6 |
| X | Y293L | 352 | 25 | 7.6 | 0.05 | 4.1 | 0.7 |
| Y | Y52S | 353 | 8 | 7.0 | 0.16 | 4.1 | 0.5 |
| Z | Y4S | 358 | 9 | 8.2 | 0.12 | 4.1 | 0.4 |
| AA | Ubx | 359 | 4 | 6.9 | 0.04 | 4.0 | 0.7 |
| BB | Y85S | 360 | 8 | 6.9 | 0.26 | 4.5 | 0.2 |
| CC | Y100S | 398 | 5 | 5.9 | 0.15 | 4.4 | 0.3 |
| DD | Y310L | 409 | 5 | 5.2 | 0.06 | 4.6 | 0.5 |
| EE | Y293L + Y310L | 411 | 15 | 6.0 | 0.04 | 4.7 | 0.5 |
| FF | Y296L + Y310L | 423 | 2 | 7.2 | 0.04 | 4.6 | 0.5 |

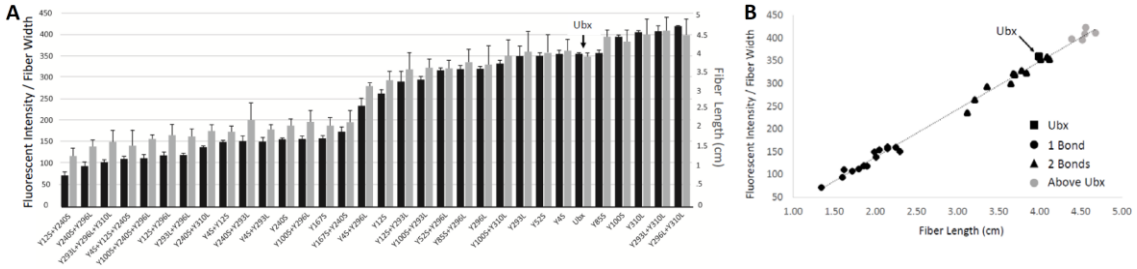


**Figure 2.12 Graph of mutants from smallest to largest fluorescent intensity.** (A) Normalized to fiber width (black bars) and fiber length (grey bars). (B) Scatter plot of fluorescent intensity compared to fiber length using linear regression with a coefficient of determination of 0.994.

Since all of the fluorescence cannot be attributed to the Y167/Y240 bond, at least one other bond is present. This additional bond(s) contributes less to the total fluorescence, indicating every monomer in the materials does not participate in this bond or bonds. This hypothesis is confirmed by the fact that Y12S and Y296L mutations decrease fluorescence while Y310L increases the fluorescence when compared to wild-type Ubx (Figure 2.9A). The impact of mutagenesis varies between these three residues; therefore, either i) there are multiple additional bonds, ii) there is one bond, but tyrosines that do not engage in the bond contribute to a chemical environment that regulates bond formation, iii) there is one bond formed by different tyrosine residues in different monomers, or iv) some combination of these possibilities.

Mutation of tyrosines 12, 296, and 310 also alter fiber fluorescence. These residues are located in two regions of Ubx: the N-terminus and the homeodomain, suggesting a dityrosine bond may form between these two regions. Indeed, the sequence conservation of both the N-terminus and the homeodomain in Hox proteins (Tour et al., 2005) suggests

these regions may interact. Furthermore, the N-terminus has a large impact on the DNA-binding affinity of the homeodomain. Finally, the ANCHOR algorithm identifies the N-terminus as a region likely to engage in protein interactions.

Any bond or bonds between the N-terminus and the homeodomain could also involve two other tyrosines: Y4 and Y293. For any of these tyrosines to participate in dityrosine bond formation, they must be exposed to the solvent. X-ray crystallography data of the Ubx homeodomain (Passner et al., 1999) reveals Y293, Y296, and Y310 are all located on the homeodomain surface (Figure 2.1D). Likewise, a model of the structure of the N-terminus suggests both Y4 and Y12 are also solvent exposed (Figure 2.1E). Although any of these surfaces could potentially pack against other regions of Ubx, the extreme flexibility of the intervening intrinsically disordered regions suggests that these residues are likely to be occasionally exposed.

To determine which, if any, of these residues participate in dityrosine bond formation, we created a series of double and triple mutants involving these five amino acids. First, we assessed the role of the three tyrosines on the surface of the homeodomain (Y293, Y296, Y310). We have already established that the Y296L and Y310L mutants alter fluorescence (Figure 2.9A). In addition, we find that the Y293L mutation, when combined with Y296L, causes an additional loss of fluorescence (Figure 2.9C, 2.11). The difference in fluorescence between wild type fibers and Y293L + Y296L fibers is similar to the difference between Y240 and wild type fibers, and thus is equivalent to the loss of one bond. This suggests that either Y293 or Y296 can contribute one tyrosine to a single

bond. This interpretation also explains why the Y293L mutation in isolation had no impact on fluorescence: Y296 provided an effective substitute.

Based on the logic described above, the other half of this bond may originate from the N-terminus of Ubx. Although the single Y4S mutation does not impact fiber fluorescence, Y4S in combination with Y12S significantly reduces fluorescence relative to Y12S fibers (Figure 2.9C). Thus, Y4 also impacts dityrosine content. The Y4 + Y12 scenario is similar to the one described above for Y293 + Y296: either Y4 or Y12 can participate in the dityrosine bond. Within a single fiber, different Ubx molecules may form a bond between the N-terminus and the homeodomain using different combinations of residues 4, 12, 293, and 296. However, the different chemical environments surrounding these residues should make some tyrosine pairs more likely to form a dityrosine bond. Comparison of pairs of double mutants should reveal if there are preferential interactions between 4 or 12 and 293 or 296. The Y4S + Y12S mutant removes all tyrosines from the N-terminus, and therefore prevents any possibility of forming a dityrosine bond with the homeodomain. The Y4S + Y293L double mutant had a similar level of fluorescence as Y4S + Y12S, suggesting neither possible N-terminus/homeodomain bond could form and thus Y4S does not bind Y293L. Therefore Y4 must bind Y296. Consistent with this conclusion, the fluorescence of Y4S + Y296L (one possible bond lost) was higher than Y4S + Y12S (both possible bonds lost), reflecting the fact that the Y12 and Y293 can still form a bond. Likewise, the Y12S + Y296 fibers fluoresce similar to Y4S + Y12S fibers, and with much less intensity than Y12S + Y293L fibers. Therefore Y12 binds Y293. Together, these results indicate that either a Y4/Y296 bond forms, or a Y12/Y293 bond

forms.

Interestingly, the fluorescence of many variants involving Y310 (Y310L, Y293L + Y310L, and Y296L + Y310L) fibers is increased relative to wild-type Ubx fibers. If Y310 quenched fluorescence of a dityrosine bond or induced a structure in which a dityrosine bond was quenched, then the same number of dityrosine bonds should be present in the wild type protein and the Y310 mutant. Consequently, immunofluorescence, using the anti-dityrosine antibody, should remain the same as for the fibers composed of wild-type Ubx. Instead, removal of Y310 *increases* immunofluorescence in proportion to the increase in dityrosine fluorescence. This increase in immunofluorescence was not only observed for fibers composed of wild-type versus Y310 Ubx, but also for other pairs of Ubx variants in which the only difference is the presence or absence of the Y310 mutation. Therefore, removal of Y310 must increase the average number of dityrosine bonds formed per molecule of Ubx. These results suggest that Y310 acts as a decoy, in which tyrosines can interact with Y310, but not form a dityrosine bond. Removal of Y310 prevents Y4 and Y12 from forming unproductive interactions and thus increases the percentage of monomers that participate in a dityrosine bond.

In the resulting model (Figure 2.12A), the N-terminus of Ubx (Y4 or Y12) interacts with the homeodomain (Y293, Y296, or Y310) but can only form a dityrosine bond with Y293 or Y296; while Y167/Y240 forms a second bond. Two separate bonds must form, because

mutation of tyrosines from at least two groups results in a greater loss of fluorescent

intensity than removing multiple amino acids attributed to a single bond **(**Figure 2.10A; $p<0.005$ indicated by *).

Finally, plotting all mutants in order of increasing fluorescence clearly reveals two distinct transitions, corresponding to the presence of 0, 1, or 2 dityrosine bonds **(**Figure 2.13A**)**. If this model is a complete description of the N-terminus/homeodomain interaction, then the fluorescence of Y4S + Y12S (150 units/μm) should equal that of Y293L + Y296L (100 units/μm). The discrepancy between these measurements may be due to differential contributions of Y100 to dityrosine bond formation. As a single mutant, Y100S increases fluorescence relative to wild-type Ubx, suggesting it is a decoy, like Y310, rather than a participant in dityrosine bonds. However, double mutants of Y100S with Y293L, Y296L, or Y310L all fluoresce less than the corresponding Y293L, Y296, or Y310L single mutants (Figure 2.9D). Thus, Y100 may contribute to a chemical environment that can either aid dityrosine bond formation or act as a decoy, depending on the Ubx variant. In this model, differential contributions of Y100 and Y310 account for the differences in the fluorescence of Y4S + Y12S and Y293L + Y296L fibers.

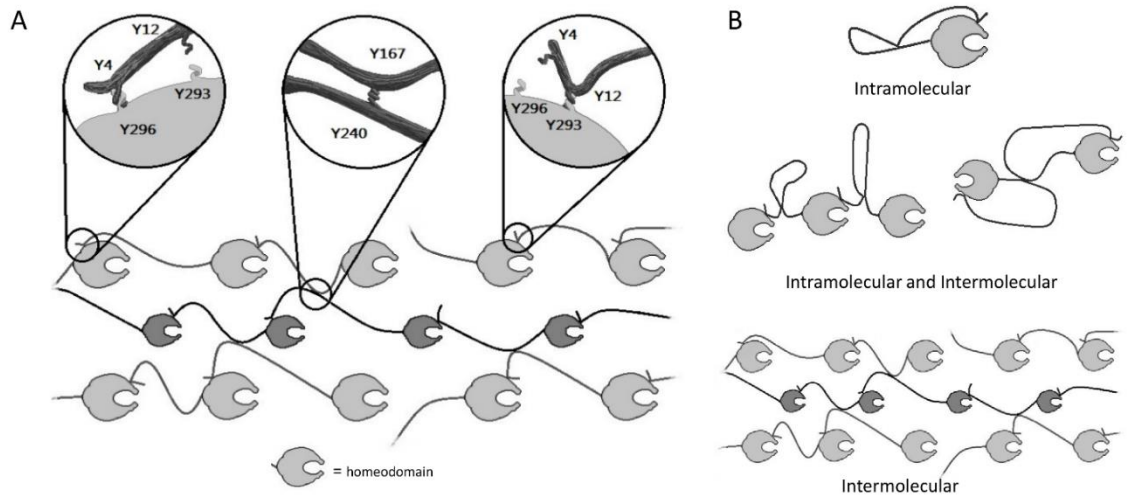


**Figure 2.13 Artistic representation of proposed dityrosine bonds.** (B) Artistic representation options for intramolecular or intermolecular bonds.

### 2.3.6 Regions that do not regulate DNA binding in Ubx monomers also do not participate in dityrosine bonds in Ubx fibers

The data presented thus far only tested the tyrosines we selected based on involvement in DNA binding, conservation, predicted ability to participate in protein interactions, and location in a region that impacts fiber length (Table 2.2). To determine whether tyrosines outside of our selected group can also contribute to bond formation, we created the Y52S and Y85S mutants. Neither single mutant had any effect on fiber fluorescence (Figure 2.10B). However, the contributions of Y4 and Y293 were only apparent when mutated in combination with other tyrosines. Therefore we mutated Y52S and Y85S in conjunction with Y296L, a mutation that was able to uncover the contributions of both Y4 and Y293. The fluorescence of Y52S + Y296L and Y85S + Y296L mutant fibers was similar to the single Y296L mutant (Figure 2.10B). Therefore, Y296L does not reveal a hidden contribution of either Y52 or Y85, and these residues do not contribute to dityrosine bonds.

### 2.3.7 Only two dityrosine bonds are formed by Ubx in materials

Both the mutant data and the kinetic data reveal two transitions, suggesting no more than two bonds are present (Figure 2.6, 2.12A). However, the mutants tested thus far do not eliminate absolutely all fluorescence from Ubx fibers. The remaining fluorescence could be due to random dityrosine bonds formed by the remaining amino acids, or it could be evidence of a third dityrosine bond. However, if our hypothesis is correct and Y167 and Y240 always participate in dityrosine bonds with each other, then one dityrosine bond contributes approximately 200 intensity units/μm, on our scale. Likewise, the Y4S +

Y12S mutations completely remove the other dityrosine bond, also resulting in a loss of approximately 200 intensity units per μm. The maximum intensity observed, close to 400 intensity units/μm, was observed for the Ubx variants Y100L, Y310L, Y293L+Y310L, and Y296L+Y310L. Therefore, if a single bond is worth 200 units/μm per and our maximum value for any of our mutants is 400 units/μm, then only 2 bonds can form. Thus any remaining fluorescence is likely due to random bond formation. Interestingly, the fluorescent intensity of fibers composed of wild-type Ubx is only 359 units/μm, suggesting that monomers in these fibers only form approximately 1 ¾ bonds on average.

### 2.3.8 Dityrosine bonds are intermolecular and contribute to the strength of the materials

Although mutagenesis can identify the amino acids that participate in dityrosine bonds, this approach does not establish whether these bonds are intramolecular, intermolecular, or a mix of both types of bonds (Figure 2.13B). Many natural macroscale materials rely on intermolecular covalent crosslinks for strength, including disulfide and dityrosine bonds (Elvin et al., 2009, Endrizzi et al., 2006, Kelly, 1968). Consequently, adding covalent bonds to protein materials can dramatically improve both strength and assembly (Asai et al., 2012).Therefore, if the dityrosine bonds in Ubx are intermolecular, they should impact the strength of the materials. The length to which a fiber can be pulled is dependent on protein assembly and the fibers' inherent strength (Greer et al., 2009). Since dramatic sequence changes, like fusing large, charged proteins to Ubx monomers do not impact assembly, tyrosine point mutations are also unlikely to impact materials assembly. Therefore, changes in fiber length are expected to reflect changes in fiber

strength. We observed that fibers formed in a low oxygen environment lack dityrosine bonds and are extremely short and fragile (data not shown). Plotting increasing values of both the normalized fluorescent intensity and the average fiber length reveals two transitions, corresponding to the formation of two bonds (Figure 2.12A). Comparison of fluorescent intensity with fiber length using linear regression (Figure 2.12B) revealed a striking correlation of 0.993. This correlation suggests that fiber strength directly depends on dityrosine bond formation, and thus the bonds are intermolecular. It is important to note that a subset of mutants – those that remove decoy tyrosines - increase Ubx fluorescence. These point mutations also increase fiber strength. Thus, point mutations can either increase or decrease the average number of dityrosine bonds formed per monomer and consequently increase or decrease the strength of the resulting fibers.

### 2.3.9 Ubx tyrosine motifs as transferable motifs for strengthening protein-based materials

We have demonstrated that bonds are only formed between specific tyrosine residues in Ubx materials. These residues are located in conserved regions of the protein sequence which are separated by intrinsically disordered (unstructured) regions of the Ubx protein (Liu et al., 2008). Therefore, it should be possible to add these conserved sequences to loops or unstructured regions of other self-assembling proteins, and thus add specific dityrosine bonds to increase the strength of those materials. As an example, the N-terminus-homeodomain bond yields less fluorescence than the Y167-Y240 bond due to competing interactions with the two decoy tyrosines, Y100 and Y310. Therefore, we reasoned that duplicating one of the tyrosines that can participate in this bond could allow

both decoy binding and dityrosine bond formation. We created the 2x296 Ubx mutant in which amino acids G289-Q297, which includes Y296, were duplicated. In this variant, both the original Y293 and the duplicated Y293 were mutated to leucine. Fibers formed by this mutant were significantly more fluorescent than wild-type fibers (Figure 2.14). Furthermore, the mutant protein created longer fibers, reflecting their increased strength. Therefore, the duplicated region was able to bind the decoy tyrosines and/or form a dityrosine bond, and thus can be considered active.

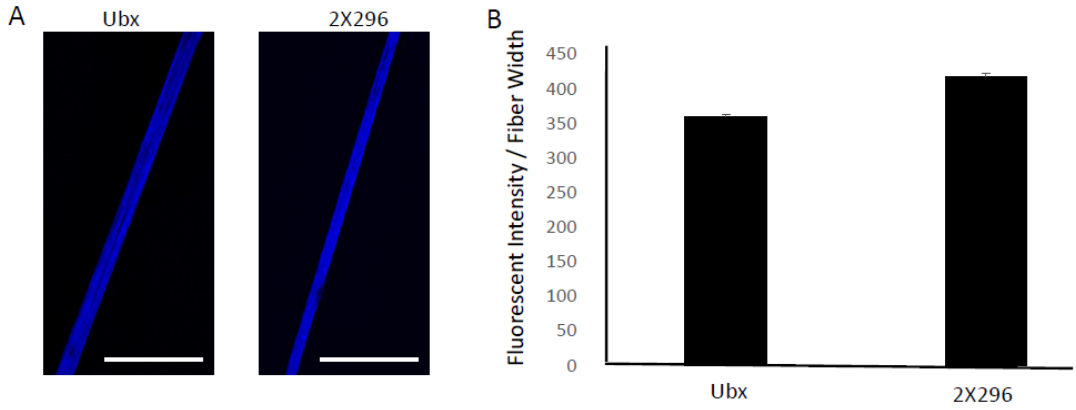


**Figure 2.14 Duplicating Y296 and its surrounding region in the 2x296 mutant increases the fluorescence of Ubx materials.**

Since adding an entire region of the Ubx protein might not be feasible for some self-assembling proteins, we have identified shorter sequences likely to replace the large insertion. The sequences surrounding tyrosines that form dityrosine bonds must contribute to interaction specificity, and thus would need to be transferred to the heterologous system. Based on Ubx sequence conservation, structure/disorder data (Liu et al., 2008), and the predicted propensity to engage in protein interactions (Figure 2.1), we recommend below sequences for transfer to other proteins to create dityrosine bonds. For proteins systems that can accommodate large insertions, the homeodomain (60 amino acids, RRRGR…LKKEI) and the N-terminus (MNSYFEQA) could be used. As an additional benefit, the solubility and stability of the homeodomain is expected to improve protein production when fused to a self-assembling protein (Tsai et al., 2015). For protein systems that can only tolerate small insertions or that self-assemble upon exposure to denaturing conditions, the conserved motifs surrounding residues 167 (VRPSACTPDSRVGGYLDTS) and 240 (FYPWMAIA) could be used. Thus the specific dityrosine-bond forming motifs in Ubx have the potential to be a useful tool for engineering the fluorescent and mechanical properties of other protein systems.

## 2.4 Conclusion

Although the extensibility of Ubx materials had previously been attributed to glycine-rich sequences resembling elastin (Greer et al., 2009, Huang et al, 2010), the molecular interactions responsible for the strength of Ubx materials were unknown. We have shown that Ubx materials auto-fluoresce blue as a result of two intermolecular dityrosine bonds that rapidly and spontaneously form as the materials oxidize. The bonds, located between

the N-terminus (Y4 or Y12) and the homeodomain (Y293 or Y296), and between Y167 and Y240 contribute to the strength of Ubx materials. Mutations that ablate one or both dityrosine bonds reduce fiber strength, whereas removing competing interactions or duplicating tyrosine-containing motifs both increase the strength of the materials.

# CHAPTER III

# THE EFFECT OF PROTEIN FUSIONS ON THE PRODUCTION AND MECHANICAL PROPERTIES OF PROTEIN-BASED MATERIALS*

## 3.1 Introduction

Proteins implement most of the vital molecular functions of living organisms, including providing structural support, generating energy, sensing biomolecules, and catalyzing, storing, and degrading important biomolecules. Proteins are particularly adept at highly specific molecular recognition, which can be adapted to bind virtually any ligand, ranging from small chemicals to specific types of cells. Such interactions are often regulated by the chemical environment, by binding additional ligands (allostery), or by post-translational modification of the protein.

Devices that capture proteins in materials have the potential to mimic these functions and be regulated by externally applied factors. However, this approach is technically challenging. The three-dimensional structures of proteins are maintained by non-covalent bonds, which are sensitive to the surrounding medium. Perturbations of this chemical environment can easily result in loss of protein function. Proteins are commonly incorporated into materials either by physically trapping them within the matrix of the materials during assembly or by covalently crosslinking them to the surface of the materials post-assembly.

---

*Reprinted with permission from "The Effect of Protein Fusions on the Production and Mechanical Properties of Protein-Based Materials" by Tsai SP, Howell DW, Huang Z, Hsiao HC, Lu Y, Matthews KS, Lou J, Bondos SE, 2015. Advanced Functional Materials, 25, 1442-1450, Copyright 2015 by John Wiley & Sons.

Both of these approaches can result in the loss of functional proteins. Physically trapped proteins can be inactivated by the harsh chemical environment often used to trigger materials assembly. Furthermore, the functional proteins are free to diffuse out of the materials (Woolfson and Mahmoud, 2010). Although crosslinking covalently tethers functional proteins to the materials, the crosslinking agent can also inactivate the appended protein or remain embedded in the materials, rendering them toxic to cells (Hershel et al., 2003). In addition, materials held together by non-covalent bonds may be too fragile for chemical modifications after assembly (Woolfson and Mahmoud, 2010). Finally, depending on the specificity of the cross-linking strategy, some portion of the functional protein may be oriented such that the materials' structure blocks ligand binding and hence function (Adak et al., 2014).

For materials composed of recombinant proteins, the use of protein fusions provides an attractive alternative. By fusing a gene encoding a functional protein to a gene encoding a self-assembling protein, a single polypeptide can be produced that contains the sequences of both proteins. This fusion protein should retain both the functional and self-assembly properties of the parent proteins. This method offers several advantages for incorporating functional proteins: (i) materials assembly and functionalization can be combined into a single step, (ii) stoichiometric levels of functionalization can be achieved, (iii) covalent attachment prevents loss of the functional protein due to diffusion, (iv) toxic by-products (remnants of chemical cross-linking) are not created, and (v) the functional proteins can be patterned within the materials (Woolfson and Mahmoud, 2010, Huang et al., 2011). In addition, all of the appended proteins have a

uniform orientation, although there are only two possible points of attachment – the N- and C-termini of the self-assembling protein. The gene fusion approach requires mild conditions for materials assembly that will not perturb the structure of the appended functional protein. Even so, full-length protein fusions have been successfully used to functionalize materials composed of many proteins, including elastin, silk, amyloid-forming proteins, and Ubx (Huang et al., 2011, Jansson et al., 2014, Huang et al., 2007, Kumar et al., 2006, Ngaoka et al., 2010, Sackewitz et al., 2008) .

Not every functional protein is likely to be a good candidate for incorporation into materials via gene fusion. For instance, unstable or insoluble functional proteins could hamper expression of the fusion protein, or large/multimeric functional proteins may mis-position the self-assembling protein, altering the mechanical properties of the materials or even preventing materials assembly. We have fused 24 proteins to the *Drosophila melanogaster* transcription factor Ultrabithorax (Ubx) to examine their impact on Ubx assembly and properties. Ubx self-assembles rapidly in gentle buffers to form films and fibers (Greer et al., 2009). Ubx materials are biocompatible, strong, and remarkably extensible. Furthermore, proteins fused to Ubx retain their activity once incorporated into materials (Huang et al., 2011, Huang et al., 2010, Patterson et al., 2014, Patterson et al., 2015). In this study, we find that inclusion in Ubx materials stabilizes the appended proteins. Because the fusions do not impact Ubx assembly, the concentration of functional protein in the materials can be predictably controlled by co-assembling the Ubx fusion protein with unmodified Ubx. The proteins appended to Ubx by gene fusion were selected to vary, as systematically as possible, the size, fold, quaternary structure,

stability, solubility, and charge density. We find that the appended protein had a large effect on the production of the fusion protein, with the solubility and quaternary structure of the appended protein best predicting successful expression and purification. In contrast, the ability to self-assemble into materials was dominated by Ubx, and the presence or identity of a fused protein had little impact on materials assembly. Although an appended protein can alter the mechanical properties of the materials, these properties still lie in a biologically relevant range. Finally, two proteins can be simultaneously fused to Ubx to create double fusions that still assemble into functionally active materials. These double fusions can be used to incorporate multiple activities at stoichiometric levels into the protein materials, or to improve the solubility or expression of a poorly performing single Ubx fusion.

## 3.2 Materials and methods

### 3.2.1 Construction of plasmids

pET19b-Ubx plasmid was used as the parent vector for all fusion proteins. In this plasmid, the gene encoding Ubx mRNA splicing isoform Ia (Figure 3.1) was inserted between the NdeI and BamHI sites of pET19b vector (Novagen), thus adding a 10xHis-tag and a hydrophilic linker (SSGGHDDDDK) to the amino-terminus of Ubx (Greer et al., 2009). DNA sequences encoding all protein fusion partners were inserted into the NdeI site of pET19b-Ubx, between the N-terminal His-tag and Ubx. General PCR and plasmid construction protocols are shown in Figure 3.2, 3.3. DNAs encoding the genes for SDF-1a and bFGF were cloned from a cDNA library derived from human cells and provided by Dr. Kayla Bayless (Texas A&M Health Science Center). The plasmids

expressing the isolated functional proteins were generated from plasmids that encode corresponding Ubx fusions by introducing a stop codon before the *ubx* gene using the following primers: Forward: 5'-CATATGAACTCGTAGTTTGAACAGGCCTCC-3' and Reverse: 5'-GGAGGCCTGTTCAAACTACGAGTTCATATG-3'. Table 3.1 lists the full length sequences of all fusions. Table 3.2 lists the sequence of Gly and Ser linkers which separate the fused protein from Ubx and provide sufficient flexibility for Ubx assembly and appended protein function. A general schematic of Ubx and Ubx fusions is shown in Figure 3.5A.

## Ultrabithorax (Ubx)

## DNA Sequence

ATGAACTCGTACTTTGAACAGGCCTCCGGCTTTTATGGCCATCCGCACCAGGCCACCGGAATGGCG
ATGGGCAGCGGTGGCCACCACGACCAGACGGCCAGTGCAGCGGCGGCCGCGTACAGGGGATTCC
CTCTCTCGCTGGGCATGAGTCCCTATGCCAACCACCATCTGCAGCGCACCACCCAGGACTCGCCCT
ACGATGCCAGCATCACGGCCGCCTGCAATAAGATATACGGCGATGGAGCCGGAGCCTACAAACAG
GACTGCCTGAACATCAAGGCGGATGCGGTGAATGGCTACAAAGACATTTGGAACACGGGCGGCTC
GAATGGCGGCGGGGGTGGCGGCGGAGGCGGTGGTGGCGGCGGAGCGGGCGGAACAGGTGGAG
CCGGCAATGCCAATGGCGGTAATGCGGCCAATGCAAACGGACAGAACAATCCGGCGGGCGGTATG
CCCGTTAGACCCTCCGCCTGCACCCCAGATTCCCGAGTGGGCGGCTACTTGGACACGTCGGGCGG
CAGTCCCGTTAGCCATCGCGGCGGCAGTGCCGGCGGTAATGTGAGTGTCAGCGGCGGCAACGGC
AACGCCGGAGGCGTACAGAGCGGCGTGGGCGTGGCCGGAGCGGGCACTGCCTGGAATGCCAATT
GCACCATCTCGGGCGCCGCTGCCCAAACGGCGGCCGCCAGCAGTTTACACCAGGCCAGCAATCAC
ACATTCTACCCCTGGATGGCTATCGCAGGTAAGATAAGATCTGATTTAACACAATACGGCGGCATAT
CAACAGACATGGGTAAGAGATACTCAGAATCTCTTGCGGGCTCACTTCTACCAGACTGGCTAGGTA
CAAATGGTCTGCGAAGACGCGGCCGACAGACATACACCCGCTACCAGACGCTCGAGCTGGAGAAG
GAGTTCCACACGAATCATTATCTGACCCGCAGACGGAGAATCGAGATGGCGCACGCGCTATGCCTG
ACGGAGCGGCAGATCAAGATCTGGTTCCAGAACCGGCGAATGAAGCTGAAGAAGGAGATCCAGGC
GATCAAGGAGCTGAACGAACAGGAGAAGCAGGCGCAGGCCCAGAAGGCGGCGGCGGCAGCGGCT
GCGGCGGCGGCGGTCCAAGGTGGACACTTAGATCAG

**Figure 3.1 DNA and protein sequences of Ubx.**

## Protein Sequence

MNSYFEQASG FYGHPHQATG MAMGSGGHHD QTASAAAAAY RGFPLSLGMS PYANHHLQRT TQDSPYDASI TAACNKIYGD GAGAYKQDCL NIKADAVNGY KDIWNTGGSN GGGGGGGGGG GGGAGGTGGA GNANGGNAAN ANGQNNPAGG MPVRPSACTP DSRVGGYLDT SGGSPVSHRG GSAGGNVSVS GGNGNAGGVQ SGVGVAGAGT AWNANCTISG AAAQTAAASS LHQASNHTFY PWMAIAGKIR SDLTQYGGIS TDMGKRYSES LAGSLLPDWL GTNGLRRRGR QTYTRYQTLE LEKEFHTNHY LTRRRRIEMA HALCLTERQI KIWFQNRRMK LKKEIQAIKE LNEQEKQAQA QKAAAAAAAA AAVQGGHLDQ

**Figure 3.1 Continued.**

| General recipe for 50ul PCR reaction | |
|---|---|
| 10x buffer | 5ul |
| DNA template | 1-5ul |
| Forward primer(100ng/ul) | 1ul |
| Reverse primer | 1ul |
| 10mM dNTP | 1ul |
| Taq polymerase | 0.5ul |
| Nuclease-free water | to 50 ul |

| Program | | |
|---|---|---|
| | 95°C | 30sec |
| 30 cycles | 95°C | 30sec |
| | 51-63°C | 30sec |
| | 68°C | 1kb/min |
| | 68°C | 5min |
| | 10°C | hold |

**Figure 3.2 General PCR reaction setup for constructing the fusions.**

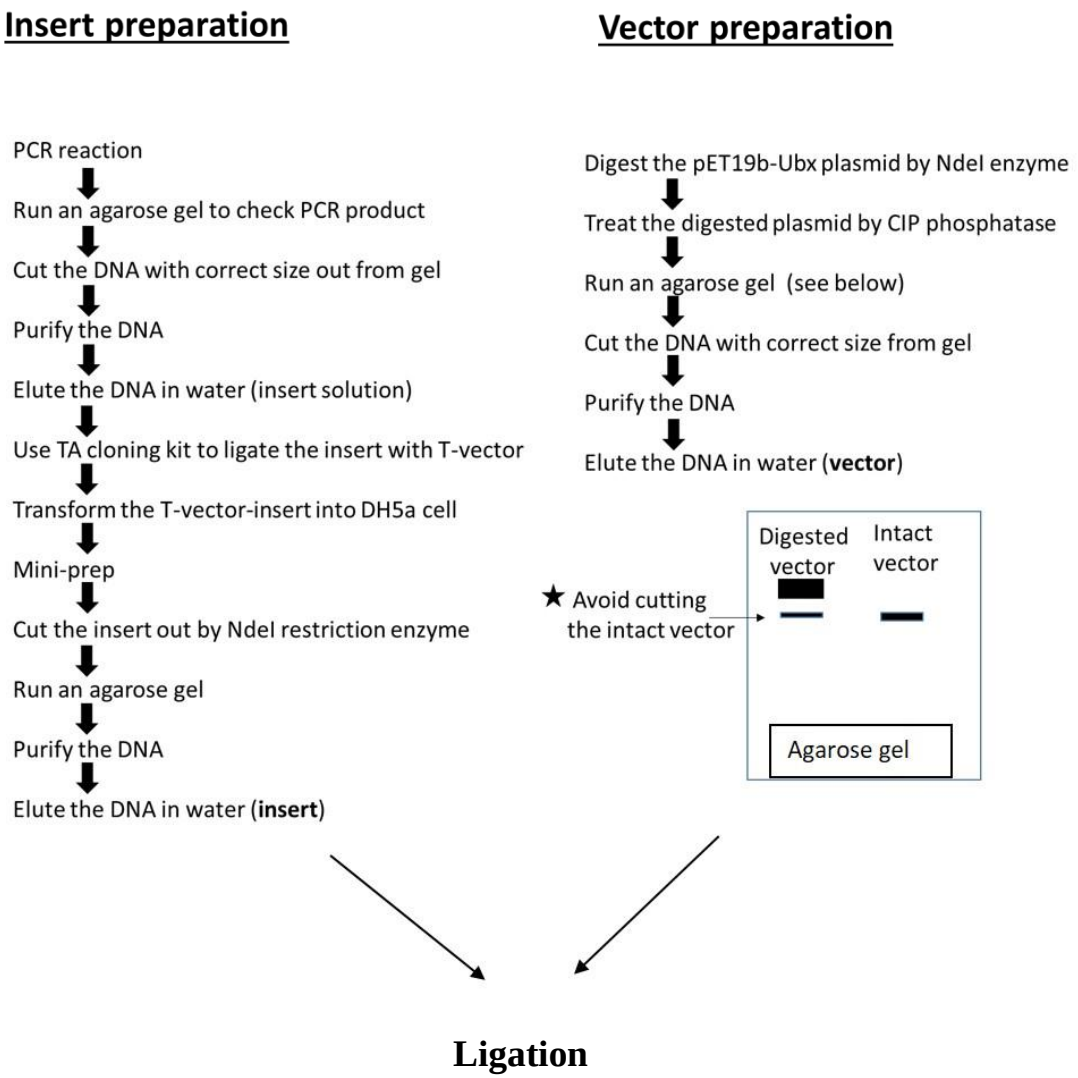


**Figure 3.3 Flow chart of constructing the Ubx fusions.**

**Table 3.1 Amino acid sequences of all fusions.**

| Protein name | Protein sequence |
|---|---|
| His-Ubx | MGHHHHHHHHHHSSGHIDDDDKHMNSYFEQASG FYGHPHQATG MAMGSGGHHD QTASAAAAAY RGFPLSLGMS PYANHHLQRT TQDSPYDASI TAACNKIYGD GAGAYKQDCL NIKADAVNGY KDIWNTGGSN GGGGGGGGGG GGGAGGTGGA GNANGGNAAN ANGQNNPAGG MPVRPSACTP DSRVGGYLDT SGGSPVSHRG GSAGGNVSVS GGNGNAGGVQ SGVGVAGAGT AWNANCTISG AAAQTAAASS LHQASNHTFY PWMAIAGKIR SDLTQYGGIS TDMGKRYSES LAGSLLPDWL GTNGLRRRGR QTYTRYQTLE LEKEFHTNHY LTRRRRIEMA HALCLTERQI KIWFQNRRMK LKKEIQAIKE LNEQEKQAQA QKAAAAAAAA AAVQGGHLDQ |
| RGD-Ubx | M G H H H H H H H H H H H S S G H I D D D D K G S R G D G S G S H MNSYFEQASG FYGHPHQATG MAMGSGGHHD QTASAAAAAY RGFPLSLGMS PYANHHLQRT TQDSPYDASI TAACNKIYGD GAGAYKQDCL NIKADAVNGY KDIWNTGGSN GGGGGGGGGG GGGAGGTGGA GNANGGNAAN ANGQNNPAGG MPVRPSACTP DSRVGGYLDT SGGSPVSHRG GSAGGNVSVS GGNGNAGGVQ SGVGVAGAGT AWNANCTISG AAAQTAAASS LHQASNHTFY PWMAIAGKIR SDLTQYGGIS TDMGKRYSES LAGSLLPDWL GTNGLRRRGR QTYTRYQTLE LEKEFHTNHY LTRRRRIEMA HALCLTERQI KIWFQNRRMK LKKEIQAIKE LNEQEKQAQA QKAAAAAAAA AAVQGGHLDQ |
| YKLKYY-Ubx | M G H H H H H H H H H H H S S G H I D D D D K G S Y K L K Y Y G S G S H MNSYFEQASGFYGHPHQATGMAMGSGGHHDQTASAAAAAYRGFPLSLGMSPYA NHHLQRTTQDSPYDASITAACNKIYGDGAGAYKQDCLNIKADAVNGYKDIWNTGGS NGGGGGGGGGGGGGAGGTGGAGNANGGNAANANGQNNPAGGMPVRPSACT PDSRVGGYLDTSGGSPVSHRGGSAGGNVSVSGGNGNAGGVQSGVGVAGAGTAW NANCTISGAAAQTAAASSLHQASNHTFYPWMAIAGKIRSDLTQYGGISTDMGKRYS ESLAGSLLPDWLGTNGLRRRGRQTYTRYQTLELEKEFHTNHYLTRRRRIEMAHALCLT ERQIKIWFQNRRMKLKKEIQAIKELNEQEKQAQAQKAAAAAAAAAAVQGGHLDQ |
| WRW-Ubx | **M** G H H H H H H H H H H H S S G H I D D D D K G S WRW G S G S H MNSYFEQASGFYGHPHQATGMAMGSGGHHDQTASAAAAAYRGFPLSLGMSPYA NHHLQRTTQDSPYDASITAACNKIYGDGAGAYKQDCLNIKADAVNGYKDIWNTGGS NGGGGGGGGGGGGGAGGTGGAGNANGGNAANANGQNNPAGGMPVRPSACT PDSRVGGYLDTSGGSPVSHRGGSAGGNVSVSGGNGNAGGVQSGVGVAGAGTAW NANCTISGAAAQTAAASSLHQASNHTFYPWMAIAGKIRSDLTQYGGISTDMGKRYS ESLAGSLLPDWLGTNGLRRRGRQTYTRYQTLELEKEFHTNHYLTRRRRIEMAHALCLT ERQIKIWFQNRRMKLKKEIQAIKELNEQEKQAQAQKAAAAAAAAAAVQGGHLDQ |
| GSGSGS-Ubx | M G H H H H H H H H H H H S S G H I D D D D K G S G S G S H MNSYFEQASGFYGHPHQATGMAMGSGGHHDQTASAAAAAYRGFPLSLGMSPYA NHHLQRTTQDSPYDASITAACNKIYGDGAGAYKQDCLNIKADAVNGYKDIWNTGGS NGGGGGGGGGGGGGAGGTGGAGNANGGNAANANGQNNPAGGMPVRPSACT PDSRVGGYLDTSGGSPVSHRGGSAGGNVSVSGGNGNAGGVQSGVGVAGAGTAW NANCTISGAAAQTAAASSLHQASNHTFYPWMAIAGKIRSDLTQYGGISTDMGKRYS ESLAGSLLPDWLGTNGLRRRGRQTYTRYQTLELEKEFHTNHYLTRRRRIEMAHALCLT ERQIKIWFQNRRMKLKKEIQAIKELNEQEKQAQAQKAAAAAAAAAAVQGGHLDQ |

**Table 3.1 Continued**

| Protein name | Protein sequence |
|---|---|
| EGFP-Ubx | MGHHHHHHHHHHSSGHIDDDDKHMVSKGEELFTGVVPILVELDGDVNGHK FSVSGEGEGDATYGKLTLKFICTTGKLPVPWPTLVTTLTYGVQCFSRYPDHMK QHDFFKSAMPEGYVQER TIFFKDDGNYKTRAEVKFEGD TLVNRIELKGIDFKEDGNILGHKLEYNYNSHNVYIMADK QKNGIKVNFKIRHNIEDGSVQLADHYQQNTPIGDGP VLLPDNHYLSTQSALSKDPNEKRDHMVLLEFVTAAGITLGMDELYKGHMNSY FEQASG FYGHPHQATG MAMGSGGHHD QTASAAAAAY RGFPLSLGMS PYANHHLQRT TQDSPYDASI TAACNKIYGD GAGAYKQDCL NIKADAVNGY KDIWNTGGSN GGGGGGGGGG GGGAGGTGGA GNANGGNAAN ANGQNNPAGG MPVRPSACTP DSRVGGYLDT SGGSPVSHRG GSAGGNVSVS GGNGNAGGVQ SGVGVAGAGT AWNANCTISG AAAQTAAASS LHQASNHTFY PWMAIAGKIR SDLTQYGGIS TDMGKRYSES LAGSLLPDWL GTNGLRRRGR QTYTRYQTLE LEKEFHTNHY LTRRRRIEMA HALCLTERQI KIWFQNRRMK LKKEIQAIKE LNEQEKQAQA QKAAAAAAAA AAVQGGHLDQ |
| mCherry-Ubx | MGHHHHHHHHHHSSGHIDDDDKHMVSKGEEDNMAIIKEFMRFKVHMEGS VNGHEFEIEGEGEGRPYEGTQTAKLKVTKGGPLPFAWDILSPQFMYGSKAYV KHPADIPDYLKLSFPEGFKWERVMNFEDGGVVTVTQDSSLQDGEFIYKVKLR GTNFPSDGPVMQKKTMGWEASSERMYPEDGALKGEIKQRLKLKDGGHYDA EVKTTYKAKKPVQLPGAYNVNIKLDITSHNEDYTIVEQYERAEGRHSTGGMDE LYKGHMNSYFEQASG FYGHPHQATG MAMGSGGHHD QTASAAAAAY RGFPLSLGMS PYANHHLQRT TQDSPYDASI TAACNKIYGD GAGAYKQDCL NIKADAVNGY KDIWNTGGSN GGGGGGGGGG GGGAGGTGGA GNANGGNAAN ANGQNNPAGG MPVRPSACTP DSRVGGYLDT SGGSPVSHRG GSAGGNVSVS GGNGNAGGVQ SGVGVAGAGT AWNANCTISG AAAQTAAASS LHQASNHTFY PWMAIAGKIR SDLTQYGGIS TDMGKRYSES LAGSLLPDWL GTNGLRRRGR QTYTRYQTLE LEKEFHTNHY LTRRRRIEMA HALCLTERQI KIWFQNRRMK LKKEIQAIKE LNEQEKQAQA QKAAAAAAAA AAVQGGHLDQ |
| AmCyan-Ubx | MGHHHHHHHHHHSSGHIDDDDKHMALSNKFIGDDMKMTYHMDGCVNG HYFTVKGEGSGKPYEGTQTSTFKVTMANGGPLAFSFDILSTVFMYGNRCFTA YPTSMPDYFKQAFPDGMSYERTFTYEDGGVATASWEISLKGNCF EHKST FHGVNFPADGPVMAKKTTGWDPSFEKMTVCDGILKGDVTAFLMLQGGGN YRCQFHTSYKTKKPVTMPPNHVVEHRIARTDLDKGGNSVQLTEHAVAHITSV VPFG HM NSYFEQASG FYGHPHQATGMAMGSGGHHD QTASAAAAAY RGFPLSLGMS PYANHHLQRT TQDSPYDASI TAACNKIYGD GAGAYKQDCL NIKADAVNGY KDIWNTGGSN GGGGGGGGGG GGGAGGTGGA GNANGGNAAN ANGQNNPAGG MPVRPSACTP DSRVGGYLDT SGGSPVSHRG GSAGGNVSVS GGNGNAGGVQ SGVGVAGAGT AWNANCTISG AAAQTAAASSLHQASNHTFY PWMAIAGKIR SDLTQYGGIS TDMGKRYSES LAGSLLPDWL GTNGLRRRGR QTYTRYQTLE LEKEFHTNHY LTRRRRIEMA HALCLTERQI KIWFQNRRMK LKKEIQAIKE LNEQEKQAQA QKAAAAAAAA AAVQGGHLDQ |

**Table 3.1 Continued**

| Protein name | Protein sequence |
|---|---|
| EBFP-Ubx | MGHHHHHHHHHHSSGHIDDDDKHMVSKGEELFTGVVPILVELDGDVNGHKFSV SGEGEGDATYGKLTLKFICTTGKLPVPWPTLVTTLTHGVQCFSRYPDHMKQHDFF KSAMPEGYVQERTIFFKDDGNYKTRAEVKFEGDTLVNRIELKGIDFKEDGNILGHKL EYNFNSHNVYIMADKQKNGIKVNFKIRHNIEDGSVQLADHYQQNTPIGDGPVLLP DNHYLSTQSALSKDPNEKRDHMVLLEFVTAAGITLGMDELYKGHM NSYFEQASG FYGHPHQATGMAMGSGGHHD QTASAAAAAY RGFPLSLGMS PYANHHLQRT TQDSPYDASI TAACNKIYGD GAGAYKQDCL NIKADAVNGY KDIWNTGGSN GGGGGGGGGG GGGAGGTGGA GNANGGNAAN ANGQNNPAGG MPVRPSACTP DSRVGGYLDT SGGSPVSHRG GSAGGNVSVS GGNGNAGGVQ SGVGVAGAGT AWNANCTISG AAAQTAAASSLHQASNHTFY PWMAIAGKIR SDLTQYGGIS TDMGKRYSES LAGSLLPDWL GTNGLRRRGR QTYTRYQTLE LEKEFHTNHY LTRRRRIEMA HALCLTERQI KIWFQNRRMK LKKEIQAIKE LNEQEKQAQA QKAAAAAAAA AAVQGGHLDQ |
| Osteopontin-Ubx | MGHHHHHHHHHHSSGHIDDDDKHMRIAVICFCLLGITCAIPVKQADSGSSEEKQL YNKYPDAVATWLNPDPSQKQNLLAPQNAVSSEETNDFKQETLPSKSNESHDHMD DMDDEDDDDHVDSQDSIDSNDSDDVDDTDDSHQSDESHHSDESDELVTDFPTD LPATEVFTPVVPTVDTYDGRGDSVVYGLRSKSKKFRRPDIQYPDATDEDITSHMES EELNGAYKAIPVAQDLNAPSDWDSRGKDSYETSQLDDQSAETHSHKQSRLYKRKA NDESNEHSDVIDSQELSKVSREFHSHEFHSHEDMLVVDPKSKEEDKHLKFRISHELD SASSEVNGHMNSYFEQASG FYGHPHQATG MAMGSGGHHD QTASAAAAAY RGFPLSLGMS PYANHHLQRT TQDSPYDASI TAACNKIYGD GAGAYKQDCL NIKADAVNGY KDIWNTGGSN GGGGGGGGGG GGGAGGTGGA GNANGGNAAN ANGQNNPAGG MPVRPSACTP DSRVGGYLDT SGGSPVSHRG GSAGGNVSVS GGNGNAGGVQ SGVGVAGAGT AWNANCTISG AAAQTAAASS LHQASNHTFY PWMAIAGKIR SDLTQYGGIS TDMGKRYSES LAGSLLPDWL GTNGLRRRGR QTYTRYQTLE LEKEFHTNHY LTRRRRIEMA HALCLTERQI KIWFQNRRMK LKKEIQAIKE LNEQEKQAQA QKAAAAAAAA AAVQGGHLDQ |
| VEGF165a-Ubx | MGHHHHHHHHHHSSGHIDDDDKHMS APMA EGGGQNHHEV VKFMDVYQRS YCHPIETLVDIFQEYPDEIE YIFKPSCVPL MRCGGCCNDE GLECVPTEES NITMQIMRIK PHQGQHIGEM SFLQHNKCEC RPKKDRARQE NPCGPCSERR KHLFVQDPQT CKCSCKNTDS RCKARQLELN ERTCRCDKPR RNHM NSYFEQASG FYGHPHQATGMAMGSGGHHD QTASAAAAAY RGFPLSLGMS PYANHHLQRT TQDSPYDASI TAACNKIYGD GAGAYKQDCL NIKADAVNGY KDIWNTGGSN GGGGGGGGGG GGGAGGTGGA GNANGGNAAN ANGQNNPAGG MPVRPSACTP DSRVGGYLDT SGGSPVSHRG GSAGGNVSVS GGNGNAGGVQ SGVGVAGAGT AWNANCTISG AAAQTAAASS LHQASNHTFY PWMAIAGKIR SDLTQYGGIS TDMGKRYSES LAGSLLPDWL GTNGLRRRGR QTYTRYQTLE LEKEFHTNHY LTRRRRIEMA HALCLTERQI KIWFQNRRMK LKKEIQAIKE LNEQEKQAQA QKAAAAAAAA AAVQGGHLDQ |

**Table 3.1 Continued**

| Protein name | Protein sequence |
|---|---|
| SDF-Ubx | MGHHHHHHHHHHSSGHIDDDDKHMKPVSLSYRCP CRFFESHVAR ANVKHLKILN T PNCAL QIVAR LKNNNRQVCI DPKLKWIQEY LEKALNKHM NSYFEQASG FYGHPHQATGMAMGSGGHHD QTASAAAAAY RGFPLSLGMS PYANHHLQRT TQDSPYDASI TAACNKIYGD GAGAYKQDCL NIKADAVNGY KDIWNTGGSN GGGGGGGGGG GGGAGGTGGA GNANGGNAAN ANGQNNPAGG MPVRPSACTP DSRVGGYLDT SGGSPVSHRG GSAGGNVSVS GGNGNAGGVQ SGVGVAGAGT AWNANCTISG AAAQTAAASS LHQASNHTFY PWMAIAGKIR SDLTQYGGIS TDMGKRYSES LAGSLLPDWL GTNGLRRRGR QTYTRYQTLE LEKEFHTNHY LTRRRRIEMA HALCLTERQI KIWFQNRRMK LKKEIQAIKE LNEQEKQAQA QKAAAAAAAA AAVQGGHLDQ |
| bFGF-Ubx | MGHHHHHHHHHHSSGHIDDDDKHMAAGSITTLP ALPEDGGSGA FPPGHFKDPK RLYCKNGGFF LRIHPDGRVD GVREKSDPHI KLQLQAEERG VVSIKGVCAN RYLAMKEDGR LLASKCVTDE CFFERLESN NYNTYRSRKYTSWYVALKRT GQYKLGSKTG PGQKAILFLP MSAKSHM NSYFEQASG FYGHPHQATGMAMGSGGHHD QTASAAAAAY RGFPLSLGMS PYANHHLQRT TQDSPYDASI TAACNKIYGD GAGAYKQDCL NIKADAVNGY KDIWNTGGSN GGGGGGGGGG GGGAGGTGGA GNANGGNAAN ANGQNNPAGG MPVRPSACTP DSRVGGYLDT SGGSPVSHRG GSAGGNVSVS GGNGNAGGVQ SGVGVAGAGT AWNANCTISG AAAQTAAASSLHQASNHTFY PWMAIAGKIR SDLTQYGGIS TDMGKRYSES LAGSLLPDWL GTNGLRRRGR QTYTRYQTLE LEKEFHTNHY LTRRRRIEMA HALCLTERQI KIWFQNRRMK LKKEIQAIKE LNEQEKQAQA QKAAAAAAAA AAVQGGHLDQ |
| Luciferase-Ubx | MGHHHHHHHHHHSSGHIDDDDKHMEDAKNIKKG PAPFYPLEDG TAGEQLHKAM KRYALVPGTI AFTDAHIEVN ITYAEYFEMS VRLAEAMKRY GLNTNHRIVV CSENSLQFFM PVLGALFIGV AVAPANDIYN ERELLNSMNI SQPTVVFVSK KGLQKILNVQ KKLPIIQKII IMDSKTDYQG FQSMYTFVTS HLPPGFNEYD FVPESFDRDK TIALIMNSSG STGLPKGVAL PHRTACVRFS HARDPIFGNQ IIPDTAILSV VPFHHGFGMF TTLGYLICGF RVVLMYRFEE ELFLRSLQDY KIQSALLVPT LFSFFAKSTL IDKYDLSNLH EIASGGAPLS KEVGEAVAKR FHLPGIRQGY GLTETTSAIL ITPEGDDKPG AVGKVVPFFE AKVVDLDTGK TLGVNQRGEL CVRGPMIMSG YVNNPEATNA LIDKDGWLHS GDIAYWDEDE HFFIVDRLKS LIKYKGYQVA PAELESILLQ HPNIFDAGVA GLPDDDAGEL PAAVVVLEHG KTMTEKEIVD YVASQVTTAK KLRGGVVFVD EVPKGLTGKL DARKIREILI KAKKGGKSKL GHM NSYFEQASG FYGHPHQATGMAMGSGGHHD QTASAAAAAY RGFPLSLGMS PYANHHLQRT TQDSPYDASI TAACNKIYGD GAGAYKQDCL NIKADAVNGY KDIWNTGGSN GGGGGGGGGG GGGAGGTGGA GNANGGNAAN ANGQNNPAGG MPVRPSACTP DSRVGGYLDT SGGSPVSHRG GSAGGNVSVS GGNGNAGGVQ SGVGVAGAGT AWNANCTISG AAAQTAAASSLHQASNHTFY PWMAIAGKIR SDLTQYGGIS TDMGKRYSES LAGSLLPDWL GTNGLRRRGR QTYTRYQTLE LEKEFHTNHY LTRRRRIEMA HALCLTERQI KIWFQNRRMK LKKEIQAIKE LNEQEKQAQA QKAAAAAAAA AAVQGGHLDQ |

**Table 3.1 Continued**

| Protein name | Protein sequence |
|---|---|
| Myoglobin-Ubx | MGHHHHHHHHHHSSGHIDDDDKHMVLSEGEWQLVLHVWAKVEADVAGHGQD ILIRLFKSH PETL EKFDRFKHLKTEAEMKASEDLKKHGVTVLTAL GAILKKKGHHEAELKPLAQSHATK HKIPIKYLEFISEAIIHVLHSRHPGNFGADA QGAMNKALELFRKDIAAKYKELGYQGGGH M NSYFEQASG FYGHPHQATGMAMGSGGHHD QTASAAAAAY RGFPLSLGMS PYANHHLQRT TQDSPYDASI TAACNKIYGD GAGAYKQDCL NIKADAVNGY KDIWNTGGSN GGGGGGGGGG GGGAGGTGGA GNANGGNAAN ANGQNNPAGG MPVRPSACTP DSRVGGYLDT SGGSPVSHRG GSAGGNVSVS GGNGNAGGVQ SGVGVAGAGT AWNANCTISG AAAQTAAASSLHQASNHTFY PWMAIAGKIR SDLTQYGGIS TDMGKRYSES LAGSLLPDWL GTNGLRRRGR QTYTRYQTLE LEKEFHTNHY LTRRRRIEMA HALCLTERQI KIWFQNRRMK LKKEIQAIKE LNEQEKQAQA QKAAAAAAAA AAVQGGHLDQ |
| Thioredoxin-Ubx | MGHHHHHHHHHHSSGGTMSDKIIHLTDDSFDTDVLKADGAILVDFWAEWCGPC KMIAPIL DEIADEYQGKLTVAKLNIDQNPGTAPKYGIRGIPTLLLFKNGE VAATKVGALSKGQLKEF LDANLAGTNIDDDDKHMSGSG M NSYFEQASG FYGHPHQATGMAMGSGGHHD QTASAAAAAY RGFPLSLGMS PYANHHLQRT TQDSPYDASI TAACNKIYGD GAGAYKQDCL NIKADAVNGY KDIWNTGGSN GGGGGGGGGG GGGAGGTGGA GNANGGNAAN ANGQNNPAGG MPVRPSACTP DSRVGGYLDT SGGSPVSHRG GSAGGNVSVS GGNGNAGGVQ SGVGVAGAGT AWNANCTISG AAAQTAAASS LHQASNHTFY PWMAIAGKIR SDLTQYGGIS TDMGKRYSES LAGSLLPDWL GTNGLRRRGR QTYTRYQTLE LEKEFHTNHY LTRRRRIEMA HALCLTERQI KIWFQNRRMK LKKEIQAIKE LNEQEKQAQA QKAAAAAAAA AAVQGGHLDQ |
| MBP-Ubx (Maltose binding protein) | MGHHHHHHHHHHSSGGTMKIEEGKLVIWINGDKGYNGLAEVGKKFEKDTGIKVT VEHPDK LEEKFPQVAATGDGPDIIFWAHDRFGGYAQSGLLAEITP DKAFQDKLYPFTWDAVRYNGK LIAYPIAVEALSLIYNKDLLPNPPKTWEE IPALDKELKAKGKSALMFNLQEPYFTWPLIA ADGGYAFKYENGKYDIKDVGV DNAGAKAGLTFLVDLIKNKHMNADTDYSIAEAAFNKGET AMTINGPWAW SNIDTSKVNYGVTVLPTFKGQPSKPFVGVLSAGINAASPNKELAKEFLEN YL LTDEGLEAVNKDKPLGAVALKSYEEELAKDPRIAATMENAQKGEIMPNIPQMSAF WYA VRTAVINAASGRQTVDEALKDAQTGTNIDDDDKHMSGSG MNSYFEQ ASG FYGHPHQATGMAMGSGGHHD QTASAAAAAY RGFPLSLGMS PYANHHLQRT TQDSPYDASI TAACNKIYGD GAGAYKQDCL NIKADAVNGY KDIWNTGGSN GGGGGGGGGG GGGAGGTGGA GNANGGNAAN ANGQNNPAGG MPVRPSACTP DSRVGGYLDT SGGSPVSHRG GSAGGNVSVS GGNGNAGGVQ SGVGVAGAGT AWNANCTISG AAAQTAAASS LHQASNHTFY PWMAIAGKIR SDLTQYGGIS TDMGKRYSES LAGSLLPDWL GTNGLRRRGR QTYTRYQTLE LEKEFHTNHY LTRRRRIEMA HALCLTERQI KIWFQNRRMK LKKEIQAIKE LNEQEKQAQA QKAAAAAAAA AAVQGGHLDQ |

**Table 3.1 Continued**

| Protein name | Protein sequence |
|---|---|
| GST-Ubx | MGHHHHHHHHHHSSGGTMSPILGYWKIKGLVQPTRLLLEYLEEKYEEHLYERDEGDK WRNKKFELGLEFPNLPYYIDGDVKLTQSMAIIRYIADKHNMLGGCPKERAEISMLEGAV LDIRYGVSRIAYSKDFETLKVDFLSKLPEMLKMFEDRLCHKTYLNGDHVTHPDFMLYDAL DVVLYMDPMCLDAFPKLVCFKKRIEAIPQIDKYLKSSKYIAWPLQGWQATFGGGDHPP KGTNIDDDDKHMSGSG MNSYFEQASG FYGHPHQATGMAMGSGGHHD QTASAAAAAY RGFPLSLGMS PYANHHLQRT TQDSPYDASI TAACNKIYGD GAGAYKQDCL NIKADAVNGY KDIWNTGGSN GGGGGGGGGG GGGAGGTGGA GNANGGNAAN ANGQNNPAGG MPVRPSACTP DSRVGGYLDT SGGSPVSHRG GSAGGNVSVS GGNGNAGGVQ SGVGVAGAGT AWNANCTISG AAAQTAAASS LHQASNHTFY PWMAIAGKIR SDLTQYGGIS TDMGKRYSES LAGSLLPDWL GTNGLRRRGR QTYTRYQTLE LEKEFHTNHY LTRRRRIEMA HALCLTERQI KIWFQNRRMK LKKEIQAIKE LNEQEKQAQA QKAAAAAAAA AAVQGGHLDQ |
| NusA-Ubx | MGHHHHHHHHHHSSGGTMNKEILAVVEAVSNEKALPREKIFEALESALATATKKKYEQ EIDVRVQIDRKSGDFDTFR RWLVVDEVTQPTKEITLEAARYEDESLNLG DYVEDQIESVTFDRITTQTAKQVIVQKVRE AERAMVVDQFREHEGEIITGVVKKV NRDNISLDLGNNAEAVILREDMLPRENFRPGDRVR GVLYSVRPEARGAQ LFVTRSKPEMLIELFRIEVPEIGEEVIEIKAAARDPGSRAKIAVKTNDKRIDPVGACVGMR GARVQAVSTELGGERIDIVLWDDNPAQFVINAMAPADVASIVVDE DKHTMDIAVEAGNLAQAIGRNGQNVRLASQLSGWELNVMTVDDLQAKHQAEAHAA IDTFTKYLDIDEDFATVLVEEGFSTLEELAYVPMKELLEIEGLDEPTVEALRERAKNALATI AQA QEESLGDNKPADDLLNLEGVDRDLAFKLAARGVCTLEDLAEQGIDDLAD IEGLTDEKAGA LIMAARNICWFGDEA GTNIDDDDKHMSGSG MNSYFEQASG FYGHPHQATGMAMGSGGHHD QTASAAAAAY RGFPLSLGMS PYANHHLQRT TQDSPYDASI TAACNKIYGD GAGAYKQDCL NIKADAVNGY KDIWNTGGSN GGGGGGGGGG GGGAGGTGGA GNANGGNAAN ANGQNNPAGG MPVRPSACTP DSRVGGYLDT SGGSPVSHRG GSAGGNVSVS GGNGNAGGVQ SGVGVAGAGT AWNANCTISG AAAQTAAASSLHQASNHTFY PWMAIAGKIR SDLTQYGGIS TDMGKRYSES LAGSLLPDWL GTNGLRRRGR QTYTRYQTLE LEKEFHTNHY LTRRRRIEMA HALCLTERQI KIWFQNRRMK LKKEIQAIKE LNEQEKQAQA QKAAAAAAAA AAVQGGHLDQ |
| SUMO-Ubx | MGHHHHHHHHHHSSGGTMSDSEVNQEAKPEVKPEVKPETHINLKVSDGSSEIFFKIKK TTPLRRLMEAFAKRQGKEM DSLRFLYDGIRIQADQTPEDLDMEDND IIEAHREQIGGGTNIDDDDKHMSGSG MNSYFEQASG FYGHPHQATGMAM GSGGHHD QTASAAAAAY RGFPLSLGMS PYANHHLQRT TQDSPYDASI TAACNKIYGD GAGAYKQDCL NIKADAVNGY KDIWNTGGSN GGGGGGGGGG GGGAGGTGGA GNANGGNAAN ANGQNNPAGG MPVRPSACTP DSRVGGYLDT SGGSPVSHRG GSAGGNVSVS GGNGNAGGVQ SGVGVAGAGT AWNANCTISG AAAQTAAASSLHQASNHTFY PWMAIAGKIR SDLTQYGGIS TDMGKRYSES LAGSLLPDWL GTNGLRRRGR QTYTRYQTLE LEKEFHTNHY LTRRRRIEMA HALCLTERQI KIWFQNRRMK LKKEIQAIKE LNEQEKQAQA QKAAAAAAAA AAVQGGHLDQ |

**Table 3.1 Continued**

| Protein name | Protein sequence |
|---|---|
| Tma-Ubx | MGHHHHHHHHHHSSGHIDDDDKHMSFFNKIILIGRLVRDPEERYTLSGTPVTTFTIA VDRVPRKNAPDDAQTTDFFRIVTFGRLAEFARTYLTKGRLVLVEGEMRMRRWETPT GEKRVSPEVVANVVR FMDRKPAETVSETEEELEIPEEDFSSDTFSEDEPPFGSGSHM NSYFEQASG FYGHPHQATGMAMGSGGHHD QTASAAAAAY RGFPLSLGMS PYANHHLQRT TQDSPYDASI TAACNKIYGD GAGAYKQDCL NIKADAVNGY KDIWNTGGSN GGGGGGGGGG GGGAGGTGGA GNANGGNAAN ANGQNNPAGG MPVRPSACTP DSRVGGYLDT SGGSPVSHRG GSAGGNVSVS GGNGNAGGVQ SGVGVAGAGT AWNANCTISG AAAQTAAASSLHQASNHTFY PWMAIAGKIR SDLTQYGGIS TDMGKRYSES LAGSLLPDWL GTNGLRRRGR QTYTRYQTLE LEKEFHTNHY LTRRRRIEMA HALCLTERQI KIWFQNRRMK LKKEIQAIKE LNEQEKQAQA QKAAAAAAAA AAVQGGHLDQ |
| Tne-Ubx | MGHHHHHHHHHHSSGHIDDDDKHMSFFNRIILIGRLVRDPEERYTLSGTPVTTFTIA VDRVPRKNAPDDAQTTDFFRVVTFGRLAEFARTYLTKGRLILVEGEMRMRRWETQT GEKRVS PEVVANVVRFMDRKPVEMPSEDIEEKLEIPEEDFTDDTFSEDEPPFHM NSYFEQASG FYGHPHQATGMAMGSGGHHD QTASAAAAAY RGFPLSLGMS PYANHHLQRT TQDSPYDASI TAACNKIYGD GAGAYKQDCL NIKADAVNGY KDIWNTGGSN GGGGGGGGGG GGGAGGTGGA GNANGGNAAN ANGQNNPAGG MPVRPSACTP DSRVGGYLDT SGGSPVSHRG GSAGGNVSVS GGNGNAGGVQ SGVGVAGAGT AWNANCTISG AAAQTAAASSLHQASNHTFY PWMAIAGKIR SDLTQYGGIS TDMGKRYSES LAGSLLPDWL GTNGLRRRGR QTYTRYQTLE LEKEFHTNHY LTRRRRIEMA HALCLTERQI KIWFQNRRMK LKKEIQAIKE LNEQEKQAQA QKAAAAAAAA AAVQGGHLDQ |
| LPYK-Ubx | MGHHHHHHHH HHSSGHIDDD DKHMEGPAGY LRRASVAQLT QELGTAFFQQ QQLPAAMADT FLEHLCLLDI DSEPVAARST SIIATIGPAS RSVERLKEMI KAGMNIARLN FSHGSHEYHA ESIANVREAV ESFAGSPLSY RPVAIALDTK GPEIRTGILQ GGPESEVELV KGSQVLVTVD PAFRTRGNAN TVWVDYPNIV RVVPVGGRIY IDDGLISLVV QKIGPEGLVT QVENGGVLGS RKGVNLPGAQ VDLPGLSEQD VRDLRFGVEH GVDIVFASFV RKASDVAAVR AALGPEGHGI KIISKIENHE GVKRFDEILE VSDGIMVARG DLGIEIPAEK VFLAQKMMIG RCNLAGKPVV CATQMLESMI TKARPTRAET SDVANAVLDG ADCIMLSGET AKGNFPVEAV KMQHAIAREA EAAVYHRQLF EELRRAAPLS RDPTEVTAIG AVEAAFKCCA AAIIVLTTTG RSAQLLSRYR PRAAVIAVTR SAQAARQVHL CRGVFPLLYR EPPEAIWADD VDRRVQFGIE SGKLRGFLRV GDLVIVVTGW RPGSGYTNIM RVLSISGGSG SHMNSYFEQA SGFYGHPHQA TGMAMGSGGH HDQTASAAAA AYRGFPLSLG MSPYANHHLQ RTTQDSPYDA SITAACNKIY GDGAGAYKQD CLNIKADAVN GYKDIWNTGG SNGGGGGGGG GGGGGAGGTG GAGNANGGNA ANANGQNNPA GGMPVRPSAC TPDSRVGGYL DTSGGSPVSH RGGSAGGNVS VSGGNGNAGG VQSGVGVAGA GTAWNANCTI SGAAAQTAAA SSLHQASNHT FYPWMAIAGK IRSDLTQYGG ISTDMGKRYS ESLAGSLLPD WLGTNGLRRR GRQTYTRYQT LELEKEFHTN HYLTRRRRIE MAHALCLTER QIKIWFQNRR MKLKKEIQAI KELNEQEKQA QAQKAAAAAA AAAAVQGGHL DQ |

**Table 3.1 Continued**

| Protein name | Protein sequence |
|---|---|
| PFK-Ubx | MGHHHHHHHH HHSSGHIDDD DKHMVKRIGV LTSGGDSPGM NAAIRSVVRK AIYHGVEVYG VYHGYAGLIA GNIKKLEVGD VGDIIHRGGT ILYTARCPEF KTEEGQKKGI EQLKKHGIEG LVVIGGDGSY QGAKKLTEHG FPCVGVPGTI DNDIPGTDFT IGFDTALNTV IDAIDKIRDT ATSHERTYVI EVMGRHAGDI ALWSGLAGGA ETILIPEADY DMNDVIARLK RGHERGKKHS IIIVAEGVGS GVDFGRQIQE ATGFETRVTV LGHVQRGGSP TAFDRVLASR LGARAVELLL EGKGGRCVGI QNNQLVDHDI AEALANKHTI DQRMYALSKE LSIGSGSHMN SYFEQASGFY GHPHQATGMA MGSGGHHDQT ASAAAAAYRG FPLSLGMSPY ANHHLQRTTQ DSPYDASITA ACNKIYGDGA GAYKQDCLNI KADAVNGYKD IWNTGGSNGG GGGGGGGGGG GAGGTGGAGN ANGGNAANAN GQNNPAGGMP VRPSACTPDS RVGGYLDTSG GSPVSHRGGS AGGNVSVSGG NGNAGGVQSG VGVAGAGTAW NANCTISGAA AQTAAASSLH QASNHTFYPW MAIAGKIRSD LTQYGGISTD MGKRYSESLA GSLLPDWLGT NGLRRRGRQT YTRYQTLELE KEFHTNHYLT RRRRIEMAHA LCLTERQIKI WFQNRRMKLK KEIQAIKELN EQEKQAQAQK AAAAAAAAAA VQGGHLDQ |
| NusA-NusA-Ubx | MGHHHHHHHHHHSSGGTMNKEILAVVEAVSNEKALPREKIFEALESALATATKKKYEQ EIDVRVQIDRKSGDFDTFR RWLVVDEVTQPTKEITLEAARYEDESLNLGDY VEDQIESVTFDRITTQTAKQVIVQKVRE AERAMVVDQFREHEGEIITGVVKKV NRDNISLDLGNNAEAVILREDMLPRENFRPGDRVR GVLYSVRPEARGAQ LFVTRSKPEMLIELFRIEVPEIGEEVIEIKAAARDPGSRAKIAVKT NDKRIDPVGAC VGMRGARVQAVSTELGGERIDIVLWDDNPAQFVINAMAPADVASIVVDE DKHTMDIAVEAGNLAQAIGRNGQNVRLASQLSGWELNVMTVDDLQAKHQAEAHAA IDTFT KYLDIDEDFATVLVEEGFSTLEELAYVPMKELLEIEGLDEPTVEAL RERAKNALATIAQA QEESLGDNKPADDLLNLEGVDRDLAFKLAAR GVCTLEDLAEQGIDDLADIEGLTDEKAGA LIMAARNICWFGDEA GTNIDDDDKHM MNKEILAVVEAVSNEKALPREKIFEALESALATATKKKYEQEIDVRVQIDRKSGDFDTFR RWLVVDEVTQPTKEITLEAARYEDESLNLGDYVEDQIESVTFDRITTQTAKQVIVQKVRE AERAMVVDQFREHEGEIITGVVKKVNRDNISLDLGNNAEAVILREDMLPRENFRPGDR VR GVLYSVRPEARGAQLFVTRSKPEMLIELFRIEVPEIGEEVIEIKAAARDPGSRAKIAVKT NDKRIDPVGACVGMRGARVQAVSTELGGERIDIVLWDD NPAQFVINAMAPADVASIVVDEDKHTMDIAVEAGNLAQAIGRNGQNVRLASQLSGW ELNVMTVDDLQAKHQAEAHAAIDTFT KYLDIDEDFATVLVEEGFSTLEELAYVP MKELLEIEGLDEPTVEALRERAKNALATIAQA QEESLGDNKPADDLLNLEGVDRDL AFKLAARGVCTLEDLAEQGIDDLADIEGLTDEKAGA LIMAARNICWFGDEA HMSGSG MNSYFEQASG FYGHPHQATGMAMGSGGHHD QTASAAAAAY RGFPLSLGMS PYANHHLQRT TQDSPYDASI TAACNKIYGD GAGAYKQDCL NIKADAVNGY KDIWNTGGSN GGGGGGGGGG GGGAGGTGGA GNANGGNAAN ANGQNNPAGG MPVRPSACTP DSRVGGYLDT SGGSPVSHRG GSAGGNVSVS GGNGNAGGVQ SGVGVAGAGT AWNANCTISG AAAQTAAASSLHQASNHTFY PWMAIAGKIR SDLTQYGGIS TDMGKRYSES LAGSLLPDWL GTNGLRRRGR QTYTRYQTLE LEKEFHTNHY LTRRRRIEMA HALCLTERQI KIWFQNRRMK LKKEIQAIKE LNEQEKQAQA QKAAAAAAAA AAVQGGHLDQ |

**Table 3.1 Continued**

| Protein name | Protein sequence |
|---|---|
| EGFP-VEGF-Ubx | MGHHHHHHHHHHSSGHIDDDDKLMVSKGEELFTGVVPILVELDGDVNGHKFSV SGEGEGD ATYGKLTLKFICTTGKLPVPWPTLVTTLTYGVQCFSRY PDHMKQHDFFKSAMPEGYVQER TIFFKDDGNYKTRAEVKFEGDTLVNRIELK GIDFKEDGNILGHKLEYNYNSHNVYIMADK QKNGIKVNFKIRHNIEDGS VQLADHYQQNTPIGDGPVLLPDNHYLSTQSALSKDPNEKRD HMVLLEFVTAAG ITLGMDELYKGHMSAPMAEGGGQNHHEVVKFMDVYQRSYCHPIETLVDIFQEYP DEIEYIFKPSCVPLMRCGG CCNDEGLECVPTEESNITMQIMRIKPHQ GQHIGEMSFLQHNKCECRPKKDRARQENPCGP CSERRKHLFVQDPQT CKCSCKNTDSRCKARQLELNERTCRCDKPRRNHM NSYFEQASG FYGHPHQATGMAMGSGGHHD QTASAAAAAY RGFPLSLGMS PYANHHLQRT TQDSPYDASI TAACNKIYGD GAGAYKQDCL NIKADAVNGY KDIWNTGGSN GGGGGGGGGG GGGAGGTGGA GNANGGNAAN ANGQNNPAGG MPVRPSACTP DSRVGGYLDT SGGSPVSHRG GSAGGNVSVS GGNGNAGGVQ SGVGVAGAGT AWNANCTISG AAAQTAAASSLHQASNHTFY PWMAIAGKIR SDLTQYGGIS TDMGKRYSES LAGSLLPDWL GTNGLRRRGR QTYTRYQTLE LEKEFHTNHY LTRRRRIEMA HALCLTERQI KIWFQNRRMK LKKEIQAIKE LNEQEKQAQA QKAAAAAAAA AAVQGGHLDQ |
| Fibronectin domain8-10-Ubx | MGHHHHHHHH HHSSGHIDDD DKHMAVPPPT DLRFTNIGPD TMRVTWAPPP SIDLTNFLVR YSPVKNEEDV AELSISPSDN AVVLTNLLPG TEYVVSVSSV YEQHESTPLR GRQKTGLDSP TGIDFSDITA NSFTVHWIAP RATITGYRIR HHPEHFSGRP REDRVPHSRN SITLTNLTPG TEYVVSIVAL NGREESPLLI GQQSTVSDVP RDLEVVAATP TSLLISWDAP AVTVRYYRIT YGETGGNSPV QEFTVPGSKS TATISGLKPG VDYTITVYAV TGRGDSPASS KPISISSGSG GHMNSYFEQA SGFYGHPHQA TGMAMGSGGH HDQTASAAAA AYRGFPLSLG MSPYANHHLQ RTTQDSPYDA SITAACNKIY GDGAGAYKQD CLNIKADAVN GYKDIWNTGG SNGGGGGGGG GGGGGAGGTG GAGNANGGNA ANANGQNNPA GGMPVRPSAC TPDSRVGGYL DTSGGSPVSH RGGSAGGNVS VSGGNGNAGG VQSGVGVAGA GTAWNANCTI SGAAAQTAAA SSLHQASNHT FYPWMAIAGK IRSDLTQYGG ISTDMGKRYS ESLAGSLLPD WLGTNGLRRR GRQTYTRYQT LELEKEFHTN HYLTRRRRIE MAHALCLTER QIKIWFQNRR MKLKKEIQAI KELNEQEKQA QAQKAAAAAA AAAAVQGGHL DQ |

### 3.2.2 Protein expression and purification

All Ubx-fusion expressing plasmids were transformed individually into Rosetta(DE3)pLysS competent cells. For each growth, a single colony was inoculated into l00 ml of Luria broth plus 100 mg/L carbenicillin and 34 mg/L chloroamphenicol and incubated with shaking overnight. The overnight culture (5 ml) was then sub-cultivated into 1 L Luria broth plus the same antibiotics at 37 °C. Once the absorbance at 600 nm reached 0.6-0.65, 1 mM IPTG was added to induce protein expression. For protein expression, all cultures were grown for 16 hours at 25 °C. Cells were harvested by centrifugation at 3500 RCF for 30 minutes at 4 ˚C and stored as frozen pellet at -20 °C. For purification, all procedures were performed carefully on ice to prevent protease degradation. In order to compare final protein yield of all fusions, a more complete lysis protocol was performed. Each aliquot was thawed and lysed in 10 mL of lysis buffer (50 mM sodium phosphate buffer, pH 8.0, 5 % glucose w/v, 500 mM NaCl, 1 protease inhibitor tablet (Roche), 0.8 mg/L DNase I, 5 mg Lysozyme, and 2 mM DTT). Thawed lysate was frozen again at -80°C. The freeze and thaw procedure was performed twice more, followed by ultrasound sonication (Branson digital sonicator, Model S250) at 25 % intensity in 10 second intervals for 5 minutes. Cell lysates were centrifuged at 37000 RCF for 30 minutes. The supernatant was loaded on a gravity column with 3-5 ml nickel-nitrilotriacetic acid (Ni-NTA) agarose resin (Qiagen), which was pre-equilibrated with equilibration buffer (5% glucose w/v, 500 mM NaCl, 50 mM sodium phosphate buffer, 1 mM DTT, pH 8.0). The column was then washed with 10 column volumes of W1 buffer, 10 column volumes of W2 buffer, and 5 column volumes of W3 buffer (W1, W2, W3 buffers are equilibration buffer containing 20 mM, 40 mM, and 80 mM imidazole,

respectively). Protein was eluted with 10 mL of elution buffer (equilibration buffer plus 200 mM imidazole). Concentrations of the purified Ubx samples were determined using the BioRad protein assay (BioRad).

### 3.2.3 Quantification of total (soluble + insoluble) protein

For all fusion proteins, a single colony containing transformed cells was inoculated into 250 ml flask containing 50 ml Luria broth with 100 mg/L carbenicillin and 34 mg/L chloroamphenicol and grown at 37 $^{0}$C at 250 r.p.m. When the absorbance at 600 nm reached 0.6 to 0.65, 1 mM IPTG was added to induce protein expression and the temperature was lowered to 25 °C, for an additional 16 hours. The final absorbance at 600 nm for fermentations to produce all Ubx fusion proteins ranged from 1.2-1.3. An aliquot (0.5 ml) of cell culture was collected from each flask and spun down by centrifugation at 16000 RCF for 3 minutes. Pelleted cells were lysed by 0.5 ml SDS PAGE sample buffer and heating at 95 $^{0}$C for 10 minutes. Protein sample and cell debris were then separated by centrifugation at 16000 RCF for 15 minutes. Protein sample was then resolved using 10 % SDS-PAGE followed by western blotting (Bio-Rad). Low molecular weight proteins (39.0-61.4 kD) were transferred to nitrocellulose membrane at 50 V, 150 mA for 2 hours. High molecular weight proteins (67.2-102.7 kD) were transferred at 50 V, 200 mA for 3 hours. A monoclonal mouse anti His-tag antibody (Qiagen, Cat# 34670) was used as primary antibody at a 1:5000 dilution. An antibody conjugated to a near infrared fluorescence dye, IRDye 800CW Goat anti-Mouse IgG (Li-Cor), was used as secondary antibody. Signal generated by the secondary antibody was

detected by an Odyssey Imaging System. All fusions were tested 3 times from the plasmid transformation step to final scanning step.

### 3.2.4 Solubility assays

To test solubility of all fusions, an ammonium sulfate tolerance assay was performed (Trevino et al., 2007, Trevino et al., 2008). Purified Ubx-fusions were concentrated and dialyzed into assay buffer (50 mM sodium phosphate buffer, pH 8.0, 5% glucose w/v, 500 mM NaCl, 100 mM imidazole). All measurements were performed at room temperature (25°C). The solubility of fusion proteins was measured as the quantity of 32 μM fusion protein that remains in solution in 1.1 M ammonium sulfate dissolved in assay buffer. The mixture was allowed to equilibrate for 3 minutes at room temperature. Samples were then centrifuged for 3 minutes at 18000 RCF. The protein concentrations in the supernatants were quantified by BioRad protein assay (BioRad). Assays of all fusions were replicated for 3 times, and reported as an average with standard deviation.

### 3.2.5 Assembly of Ubx fibers

All assays were performed with same protein concentration, fixed incubation time, and controlled environmental parameters (temperature at 25 ˚C and 40-60% humidity). Ubx fusion protein (30 nmol) was placed in a Teflon-coated tray filled with material forming buffer (50 mM sodium phosphate buffer, pH 8.0, 5% glucose w/v, 500 mM NaCl). The tray was then incubated for 16 hours at room temperature (approximately 25°C) and 30-40 % humidity. Fibers were pulled using a 4 mm diameter inoculating loop from the air-water interface. Figure 3.4 shows the method for trays setting and fibers pulling. Only the

length of the first fiber of each tray was measured. At least 5 fibers, each pulled from an operating tray, were measured for each Ubx-fusion, and the results were evaluated by statistical analysis.

Step 1: Add 590 ml buffer G into tray

Step 2: Spread the purified Ubx protein into the tray equally

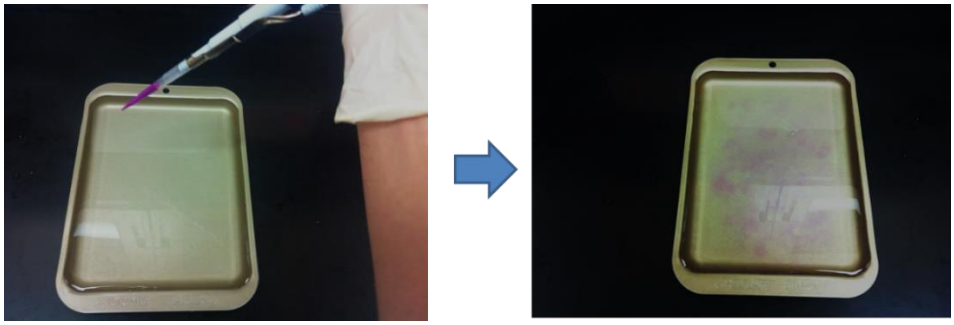

Step 3: Cover the tray and incubate for 4 hours- 2days (longer time allows more material formation, which means stronger fiber/film)

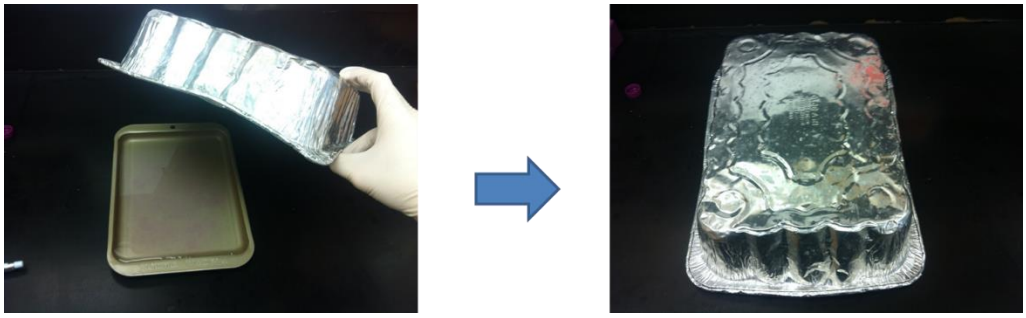

**Figure 3.4 Assembly of Ubx materials.**

Step 4: Ubx forms islet on the air/ aqueous interface. Use plastic rack to collect the material.

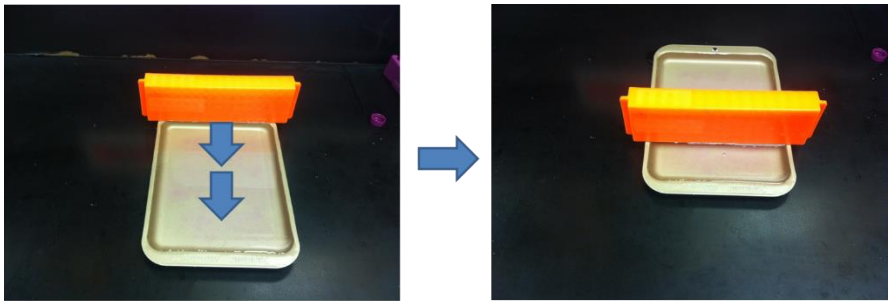


Step 5: Ubx material is now concentrated near the rack. Use plastic loop, touch the surface of the buffer. Let Ubx material stick to the loop. Then gently pull fiber /film.

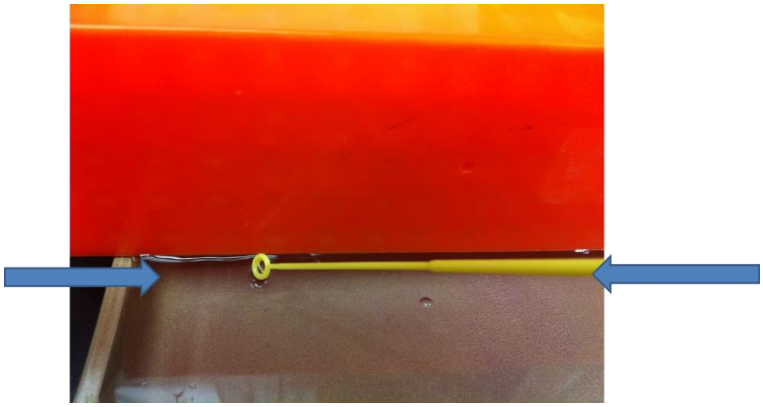

**Figure 3.4 Continued.**

### 3.2.6 Ethanol washing and autoclaving of Ubx materials

mCherry-Ubx fibers were pulled using a 4 mm diameter plastic inoculating loop (VWR) from Teflon tray and dried in air for 30 minutes as described above. Loops with mCherry fiber were either dipped into 100% ethanol solution for 30 minutes or autoclaved, the loops were sterilized in steam sterilizer for 20 minutes (121°C, 1.27 kg/cm). mCherry-Ubx fibers were then observed, and the fluorescence intensity was measured by confocal microscopy.

### 3.2.7 Mixing Ubx and EGFP-Ubx

Protein mixtures to assess the efficiency of fiber assembly were made by first purifying and quantifying pET19b-Ubx and EGFP-Ubx as previously described. The concentrations of each protein were used to create mixtures of 0, 20, 40, 60, 80, and 100% EGFP-Ubx by pipetting the appropriate amount of each protein into 6 micro centrifuge tubes and allowing them to incubate at room temperature for 15 minutes. Each mixture was added into a separate Teflon coated tray filled with material forming and incubated for 20 hours at room temperature (approximately 25°C) and 30-40 % humidity. Fibers (N=5) were pulled by a 4 mm diameter inoculating loop from the air-water interface, covered, and allowed to dry on the lab bench at room temperature for 30 minutes. The loops were then placed on a 22 mm x 55 mm coverslip, and imaged immediately using a Nikon Eclipse Ti A1R inverted confocal microscope equipped with NIS Elements AR 4.10.01 software to analyze fluorescent intensity of both the DAPI and FITC channels.

## 3.3 Results

### 3.3.1 Generating Ubx fusion proteins

Previously, we demonstrated that four proteins could be fused to Ubx and retain their function once incorporated into materials (Huang et al., 2011). However, all of these proteins were stable monomers – traits that may have facilitated their successful use. Conversely, less stable functional proteins could potentially hamper expression of the fusion protein, highly charged proteins could inhibit assembly by charge-charge repulsion, or very large/multimeric functional proteins may mis-position the self-assembling region of Ubx, creating weaker materials or possibly even preventing assembly. Our goal was to test the impact of fusing single proteins to Ubx on monomer production, materials assembly, and mechanical properties, and identify properties of the appended proteins that predict whether a specific fusion can be successfully produced and assembled into useful materials. To accomplish this, we fused 24 peptides or proteins to the N-terminus of Ubx (Figure 3.5A, Table 3.1). We also tested several fusions to the C-terminus of Ubx, but these proteins did not express well in *E. coli,* and further C-terminal fusions were not pursued. A similar effect of fusion order on protein expression and activity has been previously reported for other protein systems (Jansson et al., 2014, Christensen et al., 2009).

By carefully selecting peptides and proteins, we were able to test a wide range of physical properties: size (0.45 – 60.9 kDa), predicted charge (-47 - +8.5 at pH =8), stability (intrinsically disordered as well as thermostable proteins), secondary structure ($\alpha$, $\beta$, $\alpha+\beta$, $\alpha/\beta$), quaternary structure (monomer, dimer, and tetramer) and solubility. When

possible, groups of related proteins were selected so that as few of these properties as possible were simultaneously varied. Consequently, we focused on 6 categories of fusions: peptides, cytokines, fluorescent proteins, solubility tags, enzymes, and ligand binding proteins (Table 3.2). A series of charged peptides were generated to test the impact of charge density on the appended moiety as well as provide additional positively charged fusions. In particular, monomeric and tetrameric fluorescent proteins, which have similar charges, monomer sizes, and tertiary structures, provided a direct test of the role of quaternary structure in materials production. The series of solubility tags are collectively far more soluble and stable than the other proteins. To examine stability, we compared Ubx fused to osteopontin (Opn), an intrinsically disordered protein, with mesostable human proteins, and proteins derived from thermophilic bacteria.

Peptide linking sequences were included between the appended proteins and Ubx to ensure both proteins had sufficient space to fold and function. These sequences are rich in glycine (to provide flexibility) and serine or histidine (to provide solubility) (Table 3.2). For fusions of Ubx to peptides, we used a Gly-Ser-Gly-Ser linking sequences. For full-length proteins fused to Ubx, the sequence linking the two proteins was Gly-His. The one exception was pyruvate kinase-Ubx, in which the C-terminus of this tetrameric protein has the potential to interfere with subunit contacts. Therefore, in pyruvate kinase-Ubx we used a longer and more flexible Gly-Gly-Ser-Gly-Ser linker.

### 3.3.2 Ubx protein fusions are more stable in materials than as free monomers

Purified recombinant proteins are both expensive and labile (Chatterjee et al., 2010). Single-pot synthesis of functionalized materials would significantly lower production costs. The structure and function of protein monomers are notoriously sensitive to environmental conditions. Since the material is in an altered environment relative to bulk solvent, it is possible that the material itself could stabilize or destabilize a fused protein. Conversely, confining the functional protein within the materials could stabilize the functional protein by preventing the motions required for denaturation. To determine whether incorporation of protein fusions alters the stability of the appended protein, we examined the structure and fluorescence of mCherry-Ubx fibers under the denaturing conditions imposed by sterilization procedures: autoclaving and ethanol washing. Ubx materials are remarkably robust and can even survive boiling (Greer et al., 2009). Interestingly, mCherry-Ubx fibers remained intact and retained almost 80% of fluorescence intensity after incubation in 100% ethanol for 30 minutes (Figure 3.5 B-E). After autoclaving mCherry-Ubx fibers in steam sterilizer for 20 minutes (121°C, 1.27 $kg/cm^2$), 20% of the fluorescence intensity remained. In both cases, the fiber structure appeared undamaged by treatment. For comparison, monomeric mCherry-Ubx and mCherry unfolded, releasing their chromophores, and precipitated when treated with alcohol and precipitated when autoclaved (data not shown). These results imply that Ubx fibers remarkably stabilize proteins incorporated by gene fusion. These results are consistent with prior studies in which immobilization improved enzyme efficiency or stability (Cummings et al., 2013, Forstater et al., 2013, Ma et al., 2007).

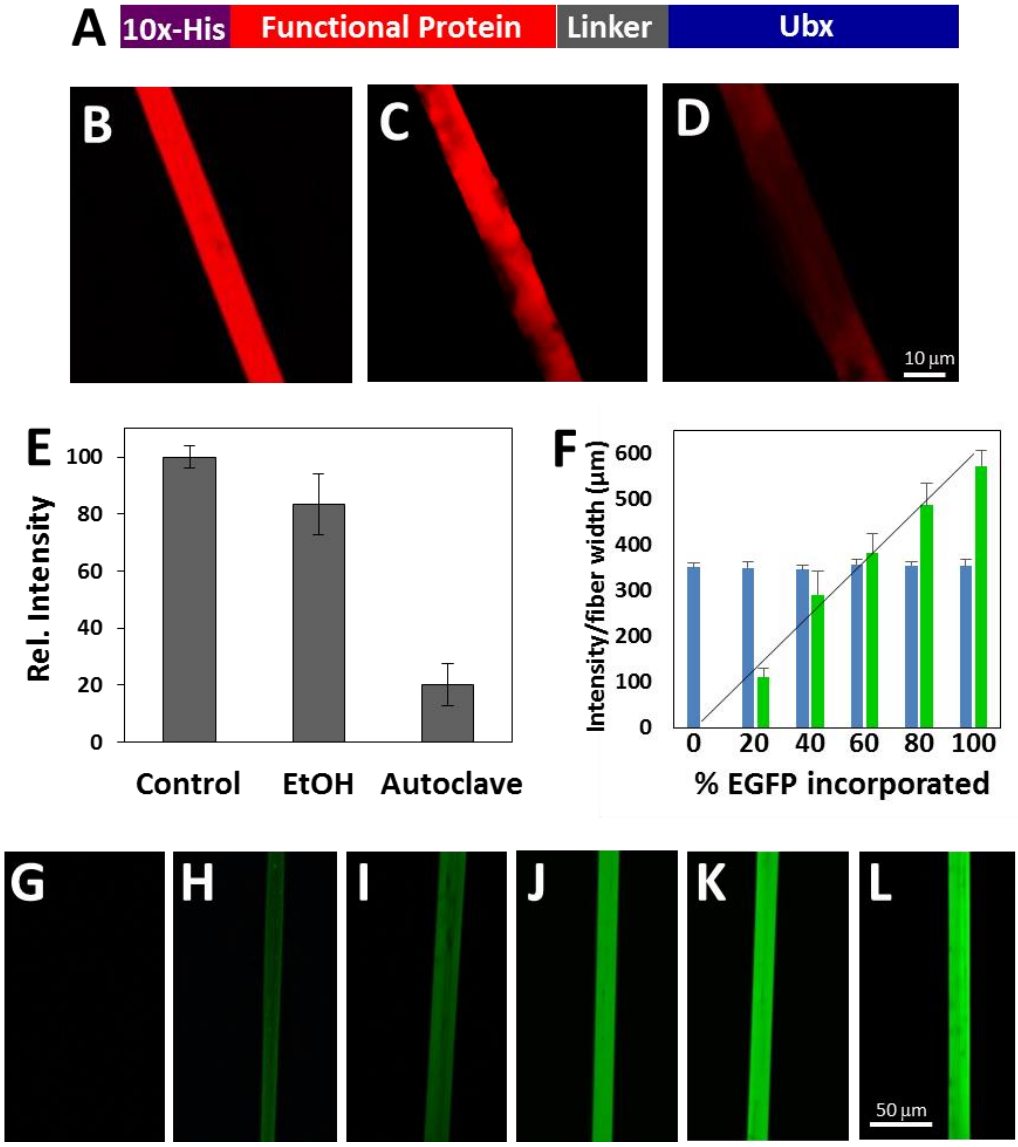


**Figure 3.5 Incorporation into materials stabilizes proteins fused to Ubx. (**A) Schematic depicting a Ubx fusion protein, in which an N-terminal histidine tag, linker, and a functional protein is linked to Ubx via a glycine-histidine linker in a single polypeptide chain. Protein assembled into Ubx material retains some activity under harsh sterilization methods. (B) Photomicrograph of mCherry-Ubx fibers. (C) Fiber that has been incubated for 30 min. in 100% EtOH. (D) An mCherry-Ubx fiber that has been autoclaved for 30 min. (E) mCherry in fibers exposed to EtOH or autoclaved retain more activity than monomeric mCherry in the same conditions. (F) Fluorescence from fibers produced from mixtures of EGFP-Ubx and Ubx correlates with the percentage of EGFP-Ubx. (G-L) Fluorescent micrographs of fibers composed of 0, 20, 40, 60, 80, and 100% EGFP-Ubx, respectively.

**Table 3.2 Properties of proteins fused to Ubx.**

| Fusion category | Fusion | Size (kDa) | Charge at pH 8 | SCOP Classification | Quaternary Structure | Linker |
|---|---|---|---|---|---|---|
| Peptides[1] | GSGSGS | 0.45 | -0.5 | Peptide | Monomer | H |
| | RGD | 0.78 | -0.5 | Peptide | Monomer | GSGSH |
| | WRW | 0.98 | 0.5 | Peptide | Monomer | GSGSH |
| | YKLKYY | 1.3 | 1.5 | Peptide | Monomer | GSGSH |
| Cytokines | SDF-1α[2] | 8.2 | 7.5 | α+β | Dimer | GH |
| | bFGF | 17.4 | 8.5 | β | Dimer | GH |
| | VEGF | 19.6 | -3.2 | β | Dimer | GH |
| | Osteopontin | 35.6 | -46.9 | N/A[3] | Monomer | GH |
| Fluorescent protein | AmCyan | 25.5 | -2.6 | α+β | Tetramer | GH |
| | mCherry | 26.9 | -6.6 | α+β | Monomer | GH |
| | EBFP | 27.1 | -8.9 | α+β | Monomer | GH |
| | EGFP | 27.1 | -9.0 | α+β | Monomer | GH |
| Fusion tags | SUMO | 12.2 | -6.5 | α+β | Monomer | GSGSH |
| | Thioredoxin | 12.8 | -6.0 | α/β | Dimer | GSGSH |
| | GST | 26.5 | -4.6 | α | Dimer | GSGSH |
| | MBP | 41.3 | -10.9 | α/β | Monomer | GSGSH |
| | NusA | 55.8 | -41.4 | α | Monomer | GSGSH |
| Enzymes | PFK | 34.6 | -4.1 | α/β | Tetramer | GSGSH |
| | L-PYK | 58.9 | -4.1 | β | Tetramer | GGSGSH |
| | Luciferase | 60.9 | -5.6 | α+β, α/β, β | Monomer | GH |
| Ligand Binding Protein | TneSSB | 16.7 | -7.5 | β | Tetramer | GSGSH |
| | TmaSSB | 16.7 | -7.5 | β | Tetramer | GSGSH |
| | Myoglobin | 17.6 | 2.7 | α | Monomer | GH |
| | FN | 30.0 | -6.4 | β | Monomer | GH |

[1]The sequences of appended peptides are listed

[2]Abbreviations: SDF-1a, Stromal cell-derived factor-1; bFGF, basic Fibroblast growth factor; VEGF, vascular endothelial growth factor; EBFP, Enhanced blue fluorescent protein; EGFP, Enhanced green fluorescent protein; SUMO, Small ubiquitin-like modifier protein; GST, Glutathione S-transferase; MBP, Maltose binding protein; PFK, phosphofructokinase; L-PYK, liver pyruvate kinase; TneSSB, *Thermotoga neapolitana* Single-stranded DNA binding protein; TmaSSB, *Thermatoga maritime* Single-stranded DNA binding protein; FN, type III domain 8-10 of Fibronectin.

[3]Not Applicable

### 3.3.3 The appended proteins determine Ubx fusion protein expression levels

In addition to the fibers altering the fused protein, the fused protein could impact Ubx materials. In particular, proteins fused to Ubx could impact various aspects of materials production: expression, solubility, purification yield, and assembly (Table 3.3). Materials assembly is strongly dependent on protein concentration (Figure 3.6), and therefore any factors that alter protein production or assembly will also impact the amount of materials that can be produced. In general, high levels of protein expression are desirable because they increase the yield of purified protein and ultimately the amount of materials produced. However, robust expression of a polymer-forming protein, such as Ubx, in bacteria may lead to aggregation / inclusion body formation and thus lower the total yield. It is well established that protein fusions can dramatically alter the expression of proteins (Bondos, 2006, Davis et al., 2000, Forrer and Jaussi, 1998, Zhang et al., 2004). To determine how fusions alter Ubx expression in *E. coli*, we used Western blots to compare the expression of Ubx and its variants 16 hrs after induction with IPTG. This method measures total (soluble and insoluble) protein produced by the bacteria (Figure 3.7, Figure 3.8). We found the results varied significantly among the Ubx fusion proteins, ranging from more than tripling protein expression to reducing expression to nearly undetectable levels.

We also measured the expression of a subset of the functional proteins not fused to Ubx. Proteins were selected to test the range of productive expression levels observed. The expression of the isolated functional protein and the corresponding Ubx fusion protein correlate very well, suggesting that the protein appended to Ubx determines the

expression level (Figure 3.7). We examined whether properties of the fused protein could predict expression levels. Expression does not appear to correlate with the molecular weight, the predicted charge density, or the quaternary structure of the appended proteins (Figure 3.9).

Protein solubility is another factor that influences the production of recombinant proteins (Bondos, 2006, Davis et al., 2000, Forrer and Jaussi, 1998, Zhang et al., 2004). Protein solubility was determined by measuring the resistance of each protein to ammonium sulfate precipitation. In the presence of ammonium sulfate, solubility determines the concentration of protein that remains in solution (Trevino et al., 2007, Trevino et al., 2008). Our measurements were performed at 1.1 M ammonium sulfate, at which concentration differences in the solubility of Ubx fusions are most pronounced (Figure 3.10). This observation is consistent with data from other proteins. The solubility varies > 3-fold among Ubx fusion proteins (Figure 3.11), and fusions can either increase or decrease solubility relative to Ubx. The measured solubilities roughly correlate with the yield from the protein purification ($r = 0.83$). Monomeric proteins were more soluble, on average, when fused with Ubx than dimeric or tetrameric proteins. The reduced solubility of dimeric and tetrameric Ubx fusions is not an artifact of protein selection; the corresponding isolated proteins have solubilties similar to the monomeric proteins tested (Figure 3.12). Because fusions solubility is related to the solubility of the appended protein, the solubility and quaternary structure of the appended protein can be used to estimate the relative purification yield of the Ubx fusion. Neither the size nor the charge density of the appended proteins correlated with the solubility (Figure 3.13).

Furthermore, the expression level of the fusion protein also did not correlate with the solubility of the appended protein (Figure 3.13).

**Table 3.3 Definition of terms.**

| Term | Definition |
|---|---|
| Expression | The amount of soluble and insoluble Ubx or fusion protein generated in *E. coli.* |
| Yield | The amount of soluble protein purified from *E. coli*. |
| Solubility | The maximum amount of protein that be dissolved in 1.1 M ammonium sulfate. |
| Assembly | The ability of a protein to self-assemble into materials. |

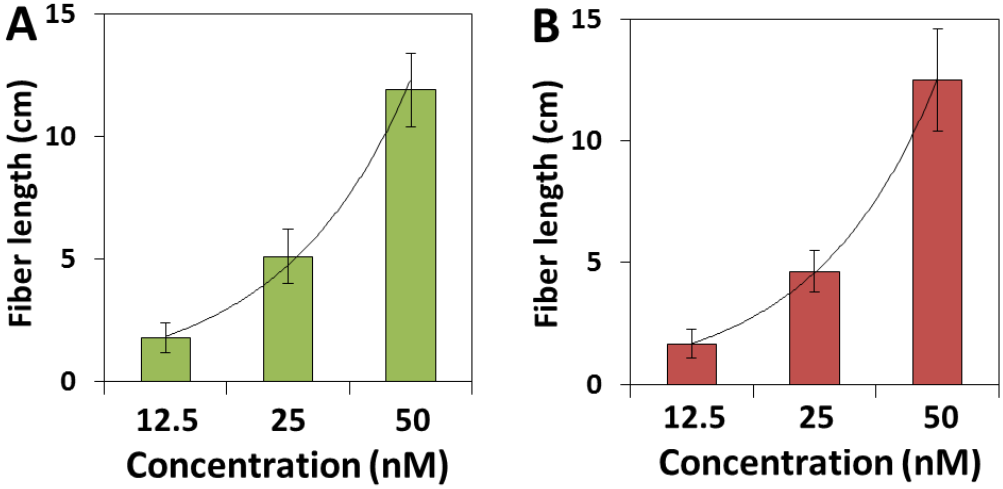


**Figure 3.6 Protein concentration is a determinative factor in materials assembly.** The length of fiber that can be drawn from solution is dependent on the ability of the Ubx variant to self-assemble into materials. Fiber assembly is strongly dependent on protein concentration for (A) bFGF-Ubx and (B) mCherry-Ubx, even though these proteins have a different charge (20 kDa vs. 30 kDa), fold as defined by SCOP (loops/strands vs b barrel), and quaternary structure (dimer vs. monomer).

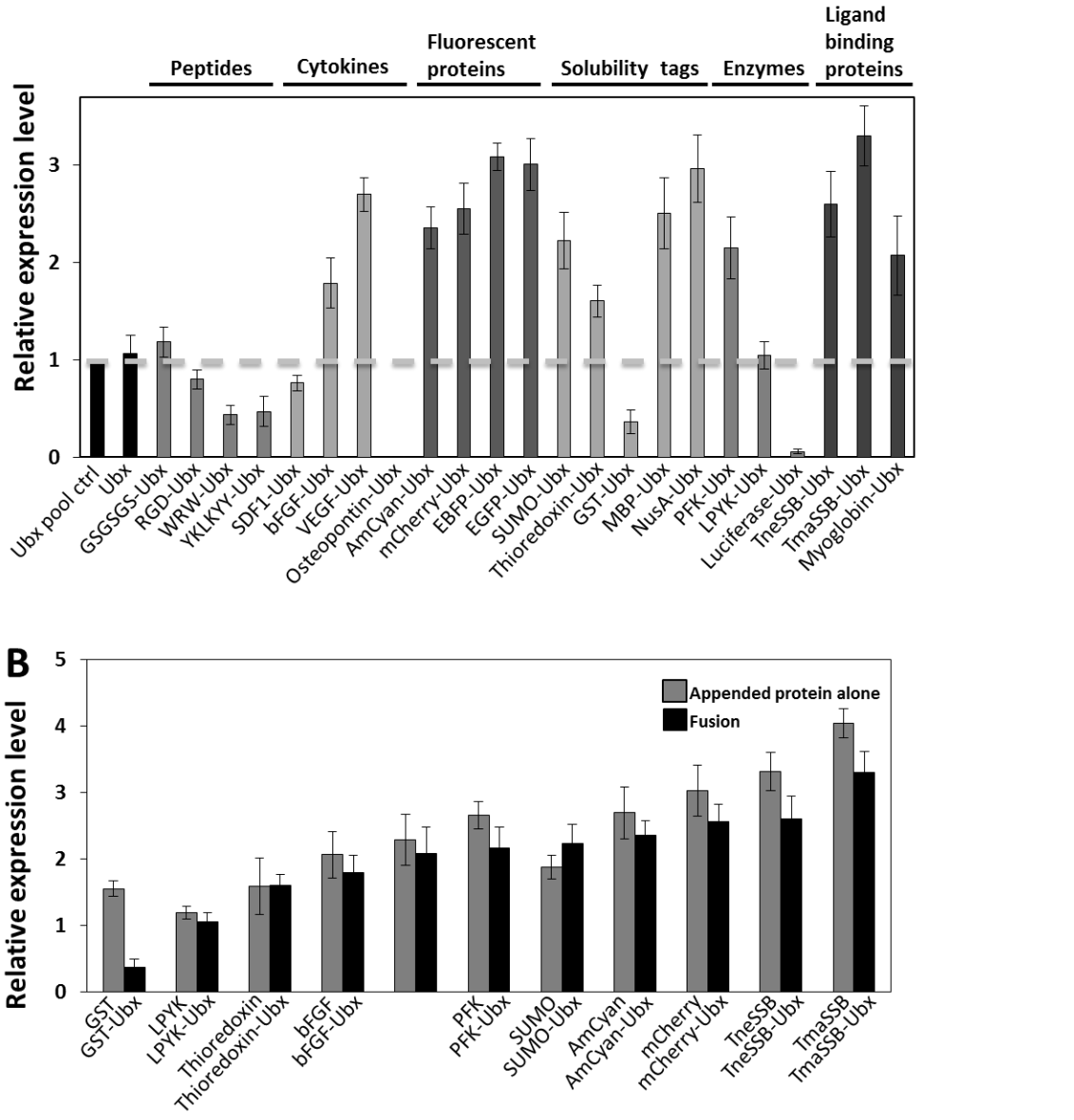


**Figure 3.7 Expression of Ubx fusion proteins varies significantly with the identity of the appended protein.** **(**A) Expression of all tested Ubx fusion proteins. (B) Comparison of the expression Ubx fusions proteins (black bars) with the isolated functional proteins. Expression was measured by Western blot of whole-cell lysates, and representative results are shown.

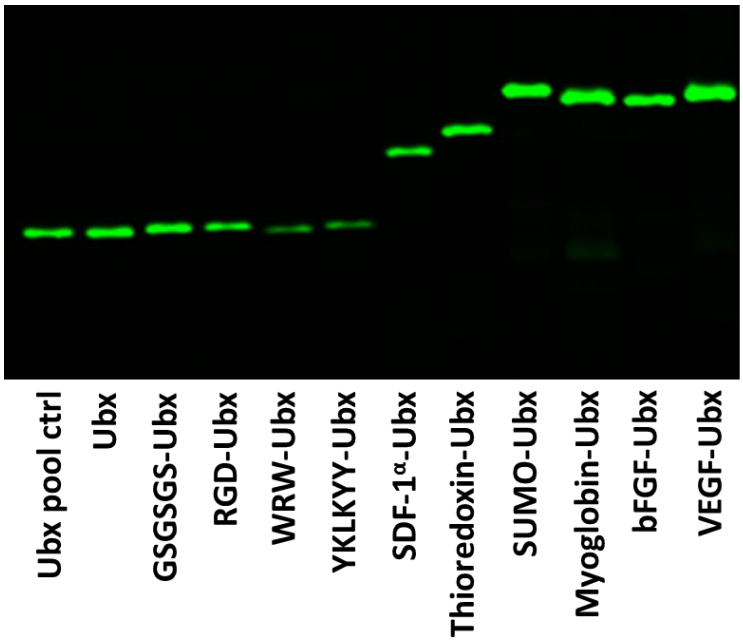


**Figure 3.8 Western blot showing the relative expression levels of plain Ubx and a subset of Ubx fusion proteins.**

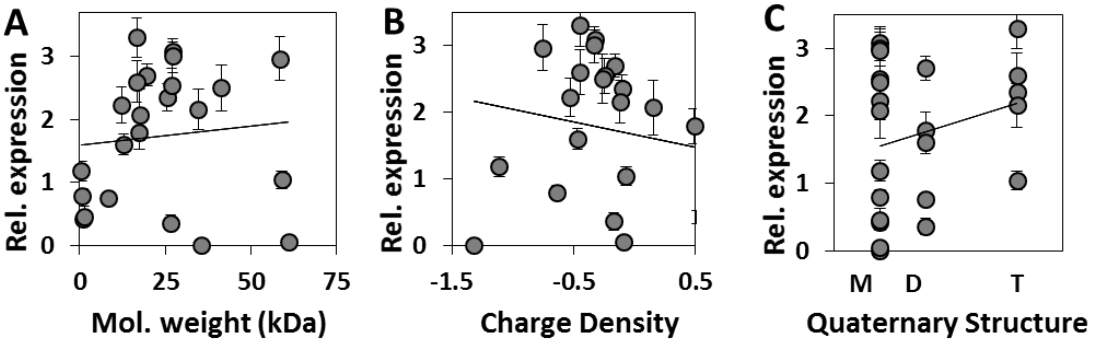


**Figure 3.9 The expression of Ubx fusion proteins relative to Ubx does not correlate with the size, charge, or quaternary structure.** Theoretical charge density was calculated as Charge*1000/Molecular weight. M, monomer. D, dimer, T, tetramer.

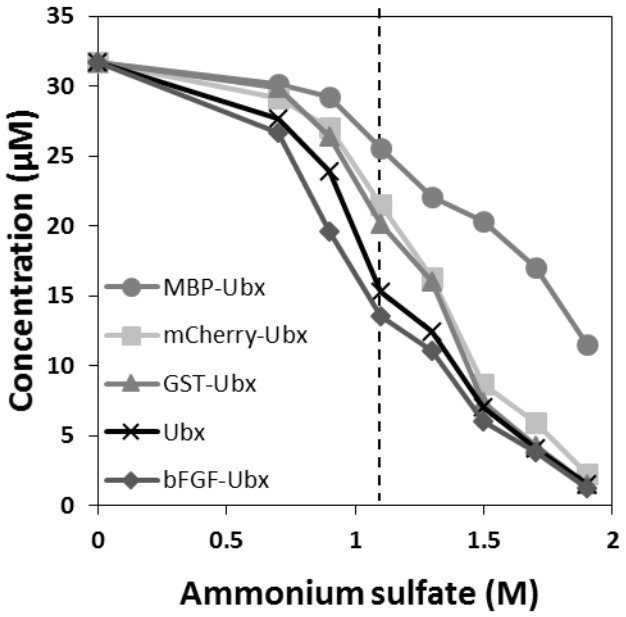


**Figure 3.10 Measuring the solubility of Ubx fusions by their resistance to ammonium sulfate precipitation.** Differences in protein solubility are reflected in the differences in the concentration of protein that remain in solution at each ammonium sulfate concentration. Ubx and representative Ubx fusion proteins are shown. Because the rank order of protein solubility persists at every concentration of ammonium sulfate, all proteins were analyzed based on the concentration of each proteins' soluble fraction at 1.1 M ammonium sulfate, where the differences between proteins are largest. This approach has been used previously (Trevino 2007, Trevino 2008).

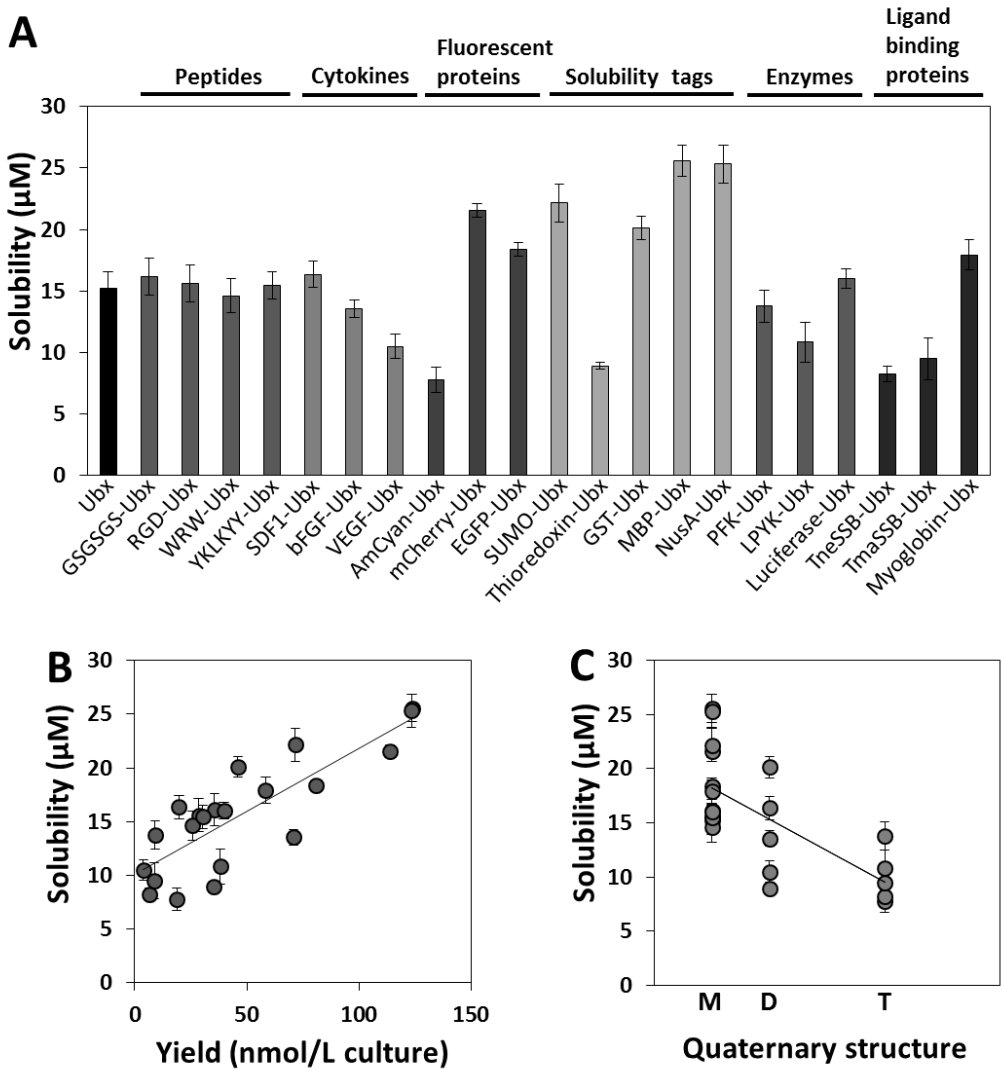


**Figure 3.11 Assessing the solubility of Ubx and Ubx fusion proteins. (**A) Relative solubility of Ubx-fusions measured by ammonium sulfate precipitation. (B) Solubility correlates with protein yield (r=0.83). (C) Formation of quaternary structure correlates with reduced protein solubility (r= 0.69). M, monomer. D, dimer, T, tetramer.

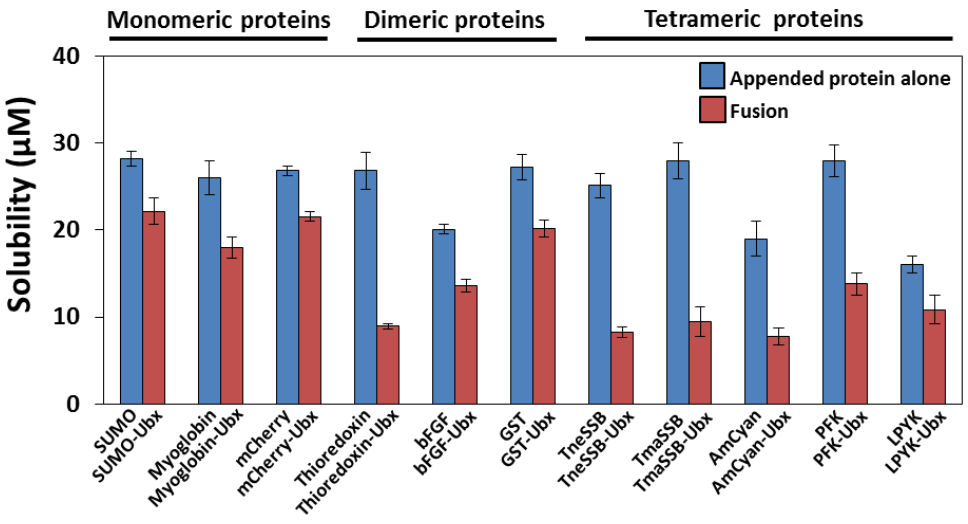


**Figure 3.12 The observation of low solubility in fusions that form quaternary structure is not an artifact that caused by the selection of less soluble appended proteins.** The solubility of selected functional proteins (blue) and fusion proteins (red) in 1.1 M ammonium sulfate is shown.

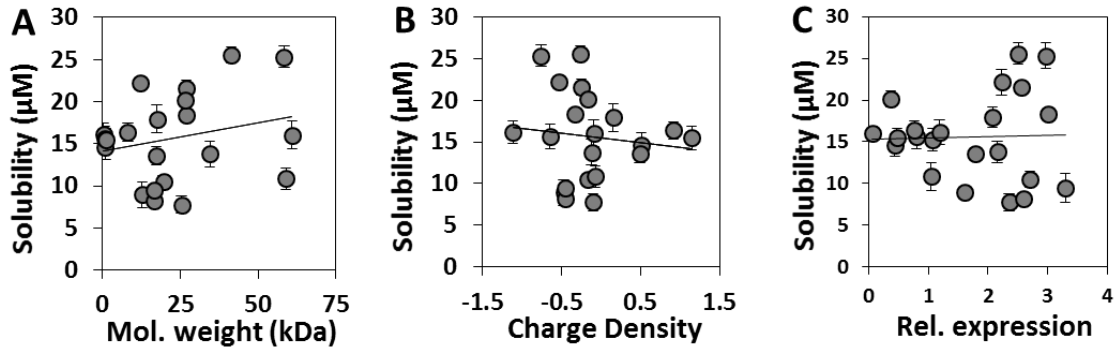


**Figure 3.13 The solubility of Ubx fusion proteins relative to Ubx does not correlate with the size, or the charge of the appended protein.** (C) Furthermore, protein expression and solubility also do not correlate (r = 0.03). Theoretical charge density was calculated as Charge*1000/Molecular weight.

### 3.3.4 The appended proteins have no significant effect on materials assembly

Solubility and stability tags are widely used to prevent aggregation, assist folding, and improve protein yield (Bondos, 2006, Davis et al., 2000, Forrer and Jaussi, 1998, Zhang et al., 2004). Thus, they have the potential to positively contribute to the production of protein-based materials. On the other hand, very soluble proteins may also impede protein polymerization and thus reduce materials production. For example, fusing GST to a Huntington protein fragment can prevent aggregation to amyloid (Scherzinger et al., 1997). In contrast, GST improves Ubx solubility without impacting self-assembly (Figure 3.11 and 3.14). Although the reason for this difference is not known, one reasonable hypothesis is that the GST protein (26.5 kDa) is more easily accommodated in the extensible Ubx materials than in rigid amyloid fibrils. Furthermore, the density of GSTs would be lower in Ubx materials because Ubx is a much larger protein (13.7 kDa Huntingtin fragment vs. 40 kDa Ubx). Nevertheless, proteins appended to Ubx can potentially impede self-assembly by many additional mechanisms. If the appended protein carries a large charge, then charge-charge repulsion could inhibit the intermolecular interactions required for self-assembly. The appended protein could bind Ubx and block the assembly interface. This mechanism is especially concerning for Ubx, since, like many transcription factors, it has a net positive charge, whereas many cytosolic or secreted proteins have a negative charge. Finally, fusing large or multimeric proteins could mis-position the self-assembling protein such that it cannot form the necessary intermolecular interactions.

To determine whether the presence of the functional proteins compromises material assembly, we compared the ability of Ubx fusions to assemble under constant conditions. Ubx fusions were incubated at a fixed protein concentration (50 nM), temperature (25˚C) and humidity (40-60%) to form a film at the air-water interface. This film was subsequently drawn into fibers. The length of fiber produced depends, in part, on the ability of Ubx variants to assemble; proteins that assemble poorly produce less film and thus shorter fibers (Greer et al., 2009). Surprisingly, despite the variations in size, charge, stability, and quaternary structure, all Ubx-fusions formed materials equally well (Figure 3.14). This similarity was not an artifact of the selected conditions, since the similarities persist at different protein concentrations (Figure 3.6). Given we observed no significant variation, there was of course no correlation with molecular weight, charge density, or quaternary structure (Figure 3.15). Confocal microscopy confirms that fibers produced by all Ubx-fusions have nearly identical morphology (Figure 3.14, Figure 3.16).

If Ubx and Ubx fusion proteins form materials equally well, then a mixture of the two proteins should produce fibers containing the same ratio of the two proteins. However, if one protein assembles more efficiently than the other, then the protein content in the fiber should be biased toward the protein that assembles more efficiently. We generated a series of assembly trays containing the same total concentration of protein, but different ratios of Ubx to EGFP-Ubx. The EGFP content of fibers drawn from these trays was measured by fluorescence microscopy (Figure 3.5). The intensity of the natural blue fluorescence of Ubx fibers were used to gauge the reproducibility of these measurements.

We found the EGFP-Ubx content in fibers linearly correlates with percentage of EGFP-Ubx in the original protein mixture, indicating that these two proteins are equally able to self-assemble into materials (Figure 3.5). Together, these results indicate that the strong tendency of Ubx protein to self-assemble is not altered by the use of fusion proteins.

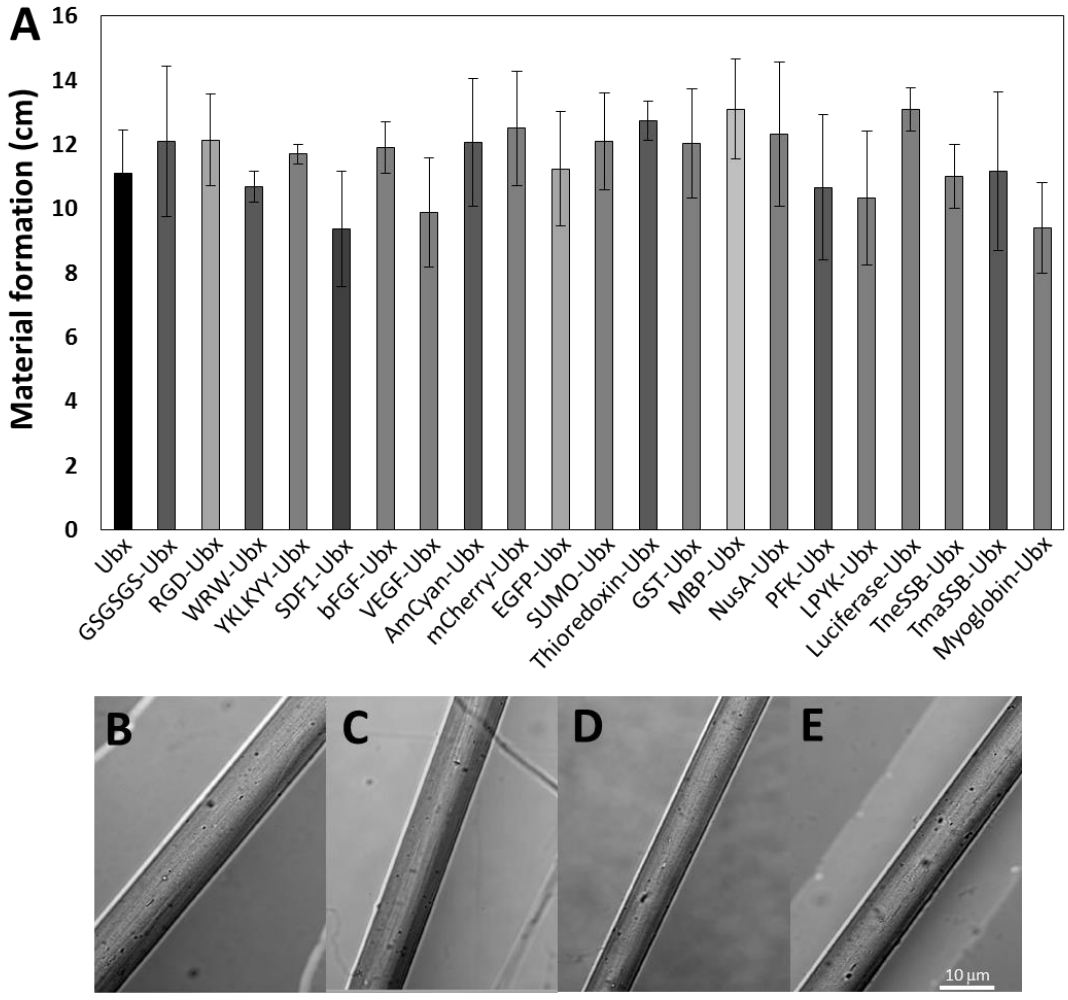


**Figure 3.14 Materials assembly is not significantly impacted by protein fusion.** (A) For all experiments, 50 nM of the Ubx variants were incubated at room temperature for 16 hrs. Materials formation was measured as length of fiber that can be drawn from the surface of the assembly solution. (B-E) Differential interference contrast microscopy of Ubx, VEGF-Ubx, MBP-Ubx, and Phosphofructokinase-Ubx, respectively. Images of the remaining Ubx fusions are in Figure 3.16.

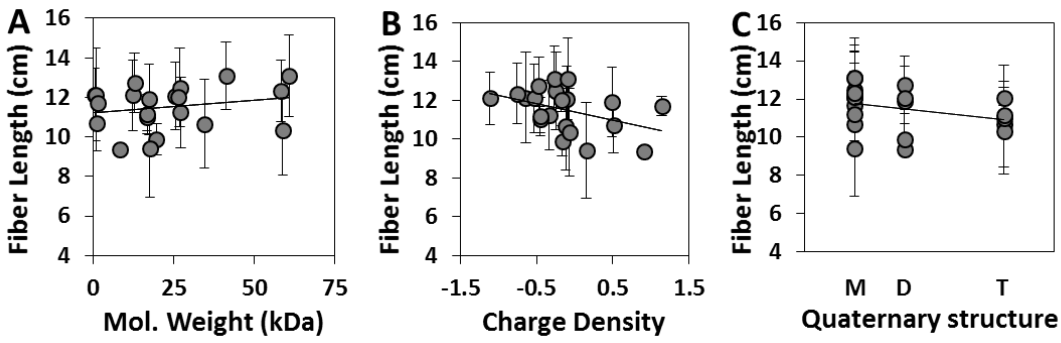


**Figure 3.15 Fiber length of the Ubx fusion fibers does not correlate with size and charge.** Theoretical charge density was calculated as Charge*1000/Molecular weight. M, monomer; D, dimer; T, tetramer.

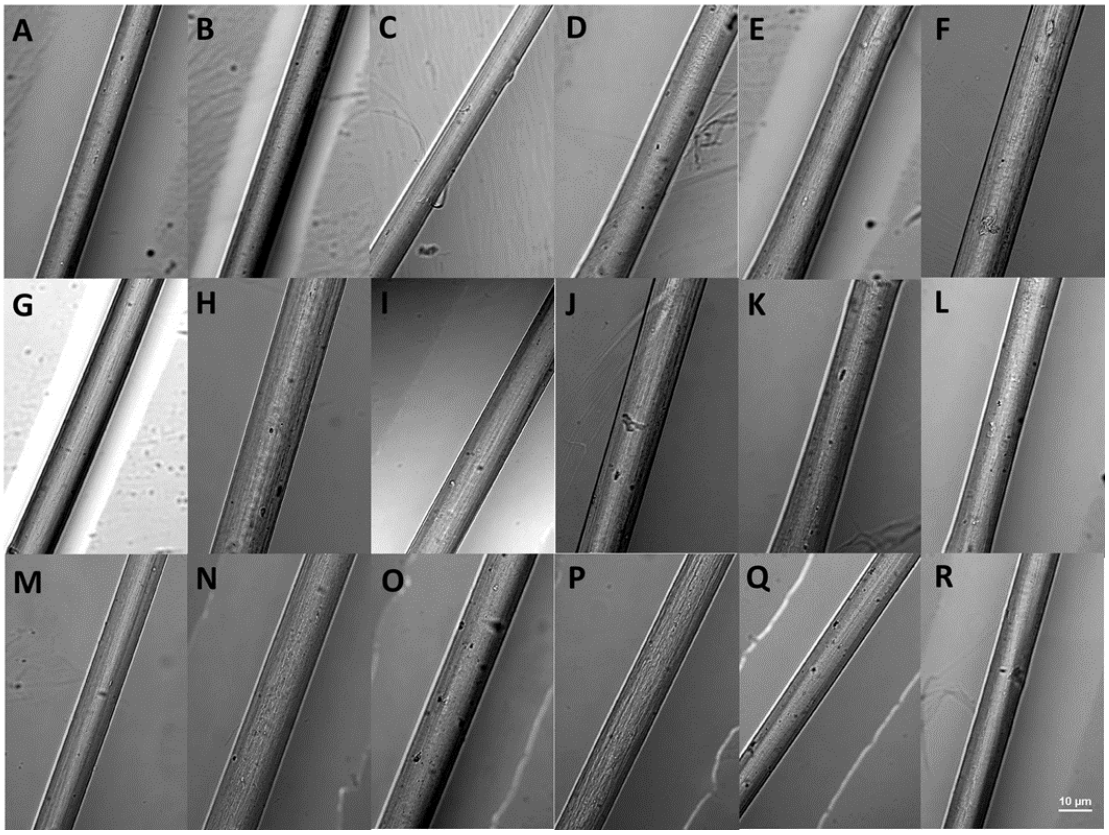


**Figure 3.16 Confocal differential interference contrast (DIC) microscopy images of fibers composed of Ubx and Ubx fusions are similar.** Panel (A) GSGSGS-Ubx, (B) RGD-Ubx, (C) WRW-Ubx, (D) YKLKYY-Ubx, (E) SDF1a-Ubx, (F) bFGF-Ubx, (G) AmCyan-Ubx, (H) mCherry-Ubx, (I) EGFP-Ubx, (J) SUMO-Ubx, (K) Thioredoxin-Ubx, (L) GST-Ubx, (M) NusAUbx, (N) Myoglobin-Ubx, (O) Luciferase-Ubx, (P) TmaSSB-Ubx, (Q) TneSSB-Ubx, (R) L-PYK-Ubx.

### 3.3.5 Double Ubx fusion proteins self-assemble

Despite the differences in the properties of the appended proteins, the possibility exists that all Ubx variants only appear to self-assemble equally well because we did not select proteins that produce a difference. In particular, the size and charge of the appended proteins were expected to have a large impact on Ubx self-assembly. To push both of these boundaries, we fused two NusA proteins to Ubx. Thus, the appended portion adds 110.6 Da, which is approximately 3 times the size of Ubx. Furthermore, the triple fusion has a theoretical charge of -82.2 at pH = 8.0. To our surprise, the NusA-NusA-Ubx protein still self-assembled into materials (Figure 3.17).

The fact that double fusion proteins can be successfully produced and incorporated into materials creates two additional advantages. First, by using double fusions, two proteins can be simultaneously incorporated into Ubx at stoichiometric ratios, increasing the functional capacity of the materials. Second, the solubility or purification yield of difficult fusions can be potentially enhanced by adding a well-behaved protein. To test this possibility, we created EGFP-VEGF-Ubx. Both the solubility and purification yield of the double fusion was improved relative to VEGF-Ubx (Figure 3.17). In a second test, we fused NusA to the N-terminus of Opn-Ubx, which does not express in *E. coli*. In contrast, the NusA-Opn-Ubx double fusion does express **(**Figure 3.18). Finally, a fusion of domains 8-10 of fibronectin type III to Ubx could not be reliably expressed in *E. coli* due to severe proteolysis. Additional fusion of GST to the N-terminus reduces this proteolysis, allowing production of the full-length fusion protein (Figure 3.18). Thus, double fusions can facilitate the production of many problem proteins. Notably, this

solution requires a self-assembling protein, like Ubx, that can accommodate large fusions.

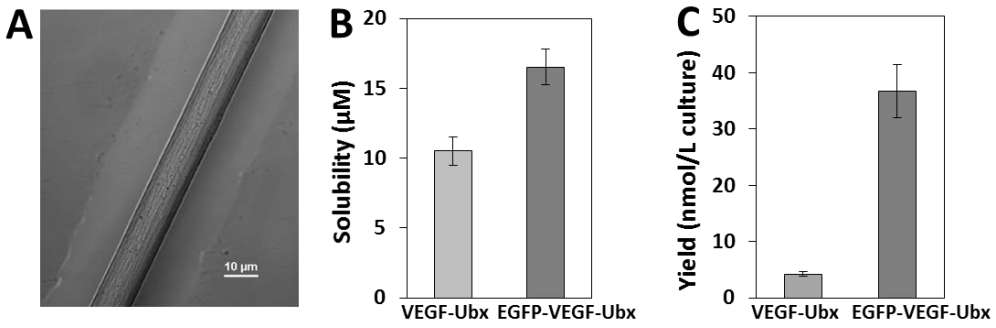


**Figure 3.17 Double fusions solve low solubility / yield problems.** (A) Ubx can assemble large, highly charged triple fusion proteins, i.e. NusA-NusA-Ubx (110.6kD, -82.2 charge at pH=8) into material. (B-C) Fusion with soluble protein increases solubility and boosts the yield of VEGF-Ubx.

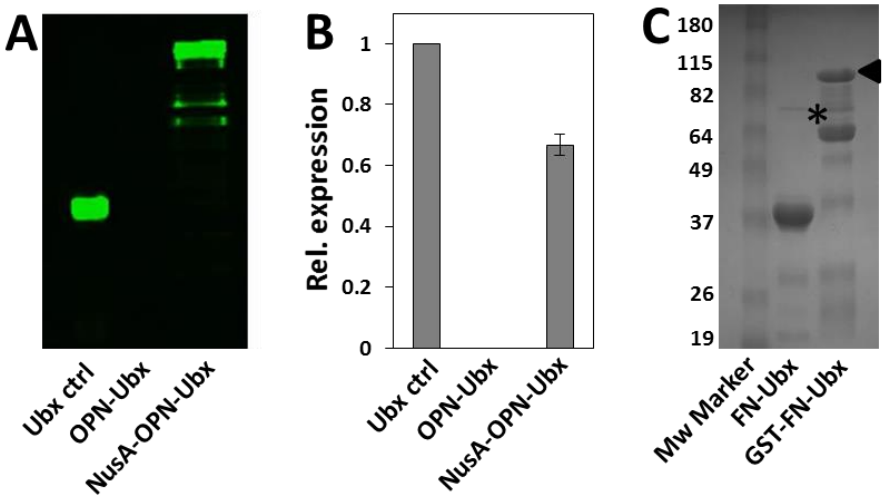


**Figure 3.18 Double fusion solves problems in different steps of producing Ubx materials.** (A) Western blot with infra-red dye showed that fusion with NusA protein increases the expression of Osteopontin-Ubx. (B) Relative expression level of Ubx, OPN-Ubx and NusA-OPN-Ubx. (C) Fusion with GST stabilizes Fibronectin domains-Ubx (*:FN-Ubx, ◀ :GST-FN-Ubx)

### 3.3.6 A comparison of the mechanical properties of Ubx and EGFP-Ubx

In addition to altering monomer production and materials assembly, fusing proteins to Ubx may also impact the mechanical properties of the resulting materials. Fiber diameter dictates the mechanical properties of unmodified Ubx materials: small diameter (5-10 μm) Ubx fibers have high breaking stress and low breaking strain and undergo elastic deformation, whereas larger Ubx fibers exhibit a combination of elastic and plastic deformation, are highly extensible, and rupture at lower stress. To test whether protein fusions impact the mechanical properties of Ubx fibers, we examined EGFP-Ubx fibers. Similar to Ubx fibers, the mechanical properties of EGFP-Ubx fibers were strongly dependent on fiber diameter (Figure 3.19). In addition, EGFP-Ubx fibers wrinkle, similar to Ubx fibers, upon unloading, to an extent that depends on both strain and fiber diameter (Figure 3.20) (Huang et al., 2010). Compared to Ubx fibers of the same diameter, the breaking strain is reduced in the EGFP-Ubx fusion fibers. Indeed, a 20 μm Ubx fiber is ~120% extensible, whereas a 20 μm EGFP-Ubx fiber is only 40% extensible. Since the mechanical properties of all fibers are diameter-dependent, a specific breaking strain can still be achieved by generating fibers with the appropriate diameter. Even with these alterations, it is important to note that the mechanical properties of EGFP-Ubx fibers are still in a biologically relevant range.

At any given fiber diameter, the breaking stress of the EGFP-Ubx chimera fibers is slightly higher than that for the Ubx fibers, suggesting that the presence of EGFP may contribute to the tensile strength of the fibers. This increased strength may be due to intermolecular interactions in the materials between the negatively charged EGFP and the

positively charged DNA binding domain in the Ubx protein (Majithia et al., 2011). From these data, we conclude that the chimeric partner for Ubx is capable of influencing the mechanical properties of the fiber. Consequently, mechanical properties should be considered when engineering a novel chimeric monomer for materials assembly.

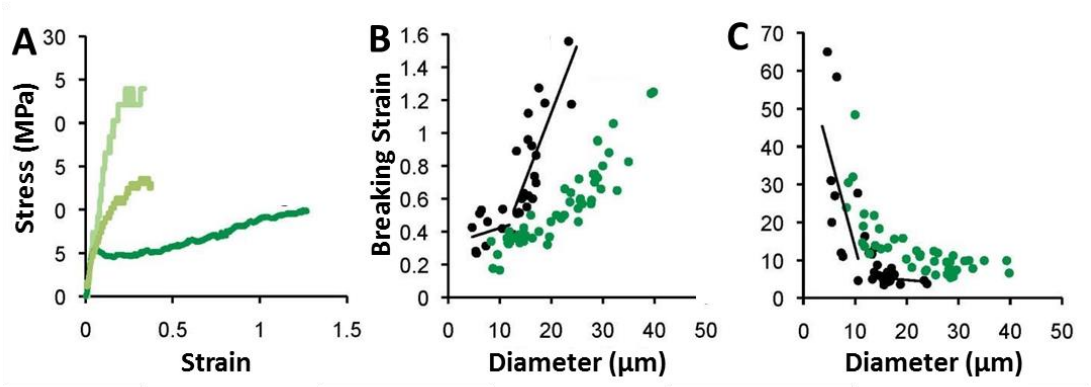


**Figure 3.19 Although fusions don't impact fiber morphology, the mechanical properties of fibers are altered. (**A) Stress-strain curves for small (x-y um) medium (a-b um) and wide (>z um) EGFP-Ubx fibers. (B-C) Comparing engineering stress and engineering strain for Ubx (grey) and EGFP-Ubx (green) fibers as a function of fiber diameter.

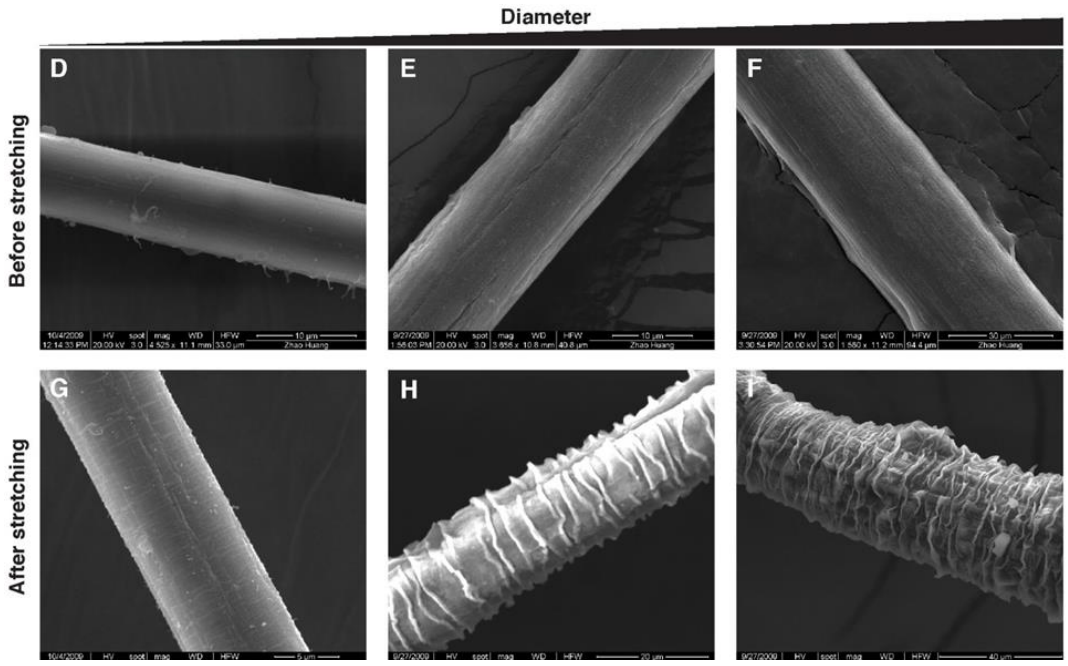


**Figure 3.20 SEM images of EGFP-Ubx fibers of different diameters before and after stretching.** Plastic deformation is more pronounced as the diameters of EGFP-Ubx fibers increase, as observed for Ubx fibers.

### 3.4. Conclusions

Protein fusions provide a facile mechanism to incorporate a broad array of chemical functions into protein-based materials. Not only can proteins be safely incorporated by this method, incorporation into materials can also enhance their stability. However, the presence of the appended protein has the potential to compromise production of the fusion protein monomers, assembly of the monomers into materials, and the mechanical properties of the functionalized materials. We created >20 fusion proteins to determine to what extent the appended proteins impact the production and properties of the final materials. Proteins were selected with a range of sizes, structures, stabilities, solubilities, and charges. We found that the appended protein had a large effect on production of the monomer protein, with solubility and quaternary structure of the appended protein being the best predictors for success. In contrast, the ability to self-assemble into materials was

dominated by Ubx, and the presence or identity of a fused protein had little impact on materials assembly. Although the appended protein can alter the mechanical properties of the materials as demonstrated by the EGFP-Ubx fusion, these properties, like those of Ubx fibers, (i) can be adjusted by varying fiber diameter and (ii) lie in a biologically relevant range (Greer et al.,2009, Huang et el., 2010).

Generating materials from fusion proteins and from a mixture of protein monomers allows easy control of the concentration of the functional protein and enables incorporation of multiple functionalities. Because all Ubx-based materials self-assemble equally well, mixing Ubx fusions with each other or with plain Ubx precisely and predictably determines the concentration of the functional proteins in the resulting materials. This ability allows specific mixtures of functionalities to be incorporated into materials. The potential to functionalize Ubx materials is further enhanced by creating double fusion proteins, in which two functional proteins are present at stoichiometric levels. Double fusion proteins can also ameliorate the low expression levels or poor solubility associated with some single fusion proteins by appending a highly soluble protein to the sequence. In summary, the range of functional proteins that can be incorporated into elastomeric protein-based materials is far greater than previously established.

# CHAPTER IV

# USING FUNCTIONALIZED UBX BIOMATERIAL TO MAKE BIOCOMPATIBLE MATERIALS FOR STENT USE

## 4.1 Introduction

Previous collaborations between Bondos, Bayless and Rice-Ficht laboratories in Texas A&M University have already shown that Ubx materials are biocompatible and exhibits low immunogenicity (Patterson et al., 2014, Patterson et al. 2015) (Figure 1.3). In addition, Ubx materials adhere to plastic and metal, and thus can be used to coat to a variety of shapes and textures of tools for different purposes. By circular dichroism, fluorescence spectrometry, and enzymatic experiments, our laboratory has shown that proteins still retain their structures and functions when fused to Ubx and assembled into materials (Figure 1.4) (Huang et al., 2011). VEGF-Ubx materials show strong ability to stimulate migration and survival of ECs *in vitro* and promote angiogenesis *in vivo*. (Appendix) Together, Ubx materials demonstrate great potential to be used in a variety of biomedical applications. Our laboratory first aimed to use Ubx biomaterials to make biocompatible and functional stent for deployment during angioplasty surgery.

Cardiovascular disease is the leading cause of death globally (Go et al., 2004). Atherosclerosis, one of the major causes of cardiovascular disease, occur when an artery wall thickens as a result of accumulation of lipids, cell debris and a mixture of cells (foam cells, smooth muscle cells, platelets, etc.)(Hansson and Libby, 2006)

Atherosclerosis can narrow coronary arteries and reduce the blood flow to heart, leading to heart attack or sudden cardiac death.

Treatments of atherosclerosis include drugs inhibiting the synthesis of cholesterol, diet management and angioplasty procedures that include stents and bypass surgery. In angioplasty surgery, stents are often inserted into and physically hold/open the artery after clearance of plaque (Howard-Alpe et al., 2007, Iqbal et al., 2003). However, the stents are inserted into the damaged part of artery, where inflammation and plaque formation are already highly active (Farooq et al., 2011). The insertion of stent also causes damage to the artery during surgery and recruit more platelets to the damaged area. In addition, the stent may induce immune responses due to the use of materials which are not biocompatible. Damage of arterial walls not only induce the recruitment of platelet cells, but also monocytes, macrophages, and neutrophils to the site of injury. (Shah, 2003) Macrophages in particular express many growth factors, cytokines, and enzymes that facilitate vascular smooth muscle cell migration and proliferation from in the tunica intima, which causes the thickening of arterial walls and decreased arterial lumen space (Danenberg et al., 2002). Together, plaque formation, recurrence of atherosclerosis and re-narrowing of artery often happens within 3-6 months after the surgery (Fischman, et al., 1994) (Serruys, et al., 1994), resulting in the need of more angioplasty surgeries. Therefore, a biocompatible stent that can: i) prevent platelet and smooth muscle cells binding ii) induce the area to heal without further constricting blood flow is needed to improve this treatment and the quality of lives of patients (Avci-Adali et al., 2010). Rapid and selective capture of endothelial cells (ECs) and endothelial

progenitor cells (EPCs) on the stent could prevent platelet and smooth muscle cells binding and avoid plaque formation and reduce restenosis. ECs can stimulate re-endothelialization of injured blood vessels and induce the formation of new blood vessels in areas with a low supply of oxygen (Avci-Adali et al., 2010, Shu et al., 2013). Because endothelial progenitor cells are present in the blood at very low concentrations, the stent needs to be coated with molecules that will not only attract and bind endothelial cells, but also subsequently induce them to repair the artery by forming a new inner lining on the surface of the implanted stent. Many different molecular strategies have been devised to attract and retain ECs at the stent surface, but most rely on coating the surface in a protein or peptide that specifically binds ECs. Different strategies to attach these proteins or peptides to the stent include adsorption of protein to the stent surface, trapping the molecules in the stent plastic, and chemically tethering the molecules to the stent surface.

However, each of these approaches can inactivates many of the protein molecules (Avci-Adali et al., 2010). Furthermore, proteins are eventually lost from the stent during the adsorption and trapping steps because they are not covalently bound to the stent. The resulting low density of active proteins or peptides on the stent surface limits the utility of this approach. A second problem is that other studies only captured ECs without providing any instructions to stimulate ECs to divide and migrate, which are required to rapidly reform the inner lining of the artery. Our goal is to design Ubx materials that can specifically attract endothelial cells (ECs), but not smooth muscle cells (SMCs) or platelets. After implantation into an artery, the nearby endothelial cells and the progenitor endothelial cells in blood flow can be recruited by the active molecules on the Ubx

material on the coated stent surface. To achieve this goal, we aim to create multiple Ubx fusions that have different functions on regulating the cell behaviors of ECs, SMCs and platelet cells. The fusions we planned to make and test are: VEGF (Appendix), SDF-1α, bFGF, YIGSR peptide. Our ultimate goal is to mix these fusions and make a multi-functional Ubx material that has synergistic effects on inducing in stent-re-endothelialization and can prevent thrombosis and in-stent restenosis. The functions of each fusions and the signal transduction pathways regulated by them are described below.

### 4.1.1 SDF-1α (CXCL12)

The stromal cell-derived factor 1α (SDF-1α), also known as C-X-C motif chemokine 12 (CXCL12), is a chemokine protein. The receptor for this chemokine is CXCR4, a GPCR which was previously called LESTR or fusin (Bleul et al., 1996). The SDF-1α-CXCR4 interaction used to be considered exclusive (unlike other chemokines and their receptors), but recently it was suggested that SDF-1α may also bind the CXCR7 receptor (Burns et al., 2006). Binding of SDF-1α to CXCR4 induces the dimerization of the receptor and activation of inhibitory G proteins. Several signal transduction pathways downstream of CXCR4 have now been identified, including activation of tyrosine kinases, focal adhesion kinase, paxilin, extracellular-signal-regulated kinases, protein kinase C (PKC), phospholipase C-γ, and phosphoinositol 3-kinase. Previous studies suggest that SDF-1α has strong effect on endothelial cells. For example, SDF-1α regulates angiogenesis by recruiting endothelial progenitor cells (EPCs) from the bone marrow through a CXCR4 dependent PI3K/Akt/eNOS pathway (Zheng et al., 2007). SDF-1α also decrease the apoptosis of endothelial progenitor cells, which is also through PI3K/Akt/eNOS pathway

(Zheng et al., 2008). SDF-1α also has been shown to promote ECs migration through activating ERK signaling (Pi et al. 2009, Beverly et al., 2010). SDF-1α can induce angiogenesis by promote endothelial cell chemotaxis and tube formation. Therefore, SDF-1α may be very potent for the stent project because it has the desired effects on endothelial cells (ECs), as described above. However, SDF-1α expresses in most organs and is believed to control other physiological responses, for example, it may stimulate the mobilization and adhesion of smooth muscle progenitor cells (Andreas et al., 2006). Although there is no clear and direct evidence, but the effects of SDF-1α on SMC migration may also through PI3K/AKT pathway (Andreas et al., 2006). Therefore, when conduct experiments on the SDF-1α-Ubx fusion, the effects on smooth muscle cells also needs to be taken into consideration. Although SDF-1α -Ubx material may also stimulate the migration and proliferation of SMCs and induce restenosis, we hope to see that the SDF-1α -Ubx material triggers stronger responses on endothelial cells, for example, higher adhesion, migration or survival. Heparin is a similar example. Heparin coated stent is widely studied and there are already many clinical trials on it. Although heparin also induce the proliferation of SMC, but it triggers much higher proliferation rate on ECs and therefore compromises its effects on SMCs.

### 4.1.2 bFGF

bFGF, the basic fibroblast growth factor, also known as FGF2 or FGF-β, is a member of the fibroblast growth factor family (Kim et al., 1998). bFGF signals through binding with FGFR1 and FGFR2 (El-Husseini et al., 1994). FGF is known to be very important for new blood vessel growth at the wound site (Werner et al., 2003). Endothelial cells

express high levels of FGFR1 and FGFR2 (Turner et al., 2010). FGFs stimulates both endothelial cell proliferation and migration mainly through MAPK activation (Turner et al., 2010). PKC activation is also required for FGF-induced endothelial cell proliferation and migration (Daviet et al., 1990). Blocking of PI3K signaling is also shown to inhibit the motility of endothelial cells. (Landgren et al., 1998). Although bFGF also stimulates the migration and proliferation of SMCs, some studies have shown that bFGF has strong effects on in stent-re-endothelialization that may overwhelm its effects on SMCs (Kitamura et al., 2014).

### 4.1.3 YIGSR peptide

YIGSR increase the adhesion and migration of ECs, but not SMCs or platelet (Fittkaua et al., 2005, Jun et al., 2004, Ruoslahti et al., 1996). YIGSR is a peptide derived from the laminin B1 chain. Unlike RGD and PHSRN, the other two common cell binding peptides, YIGSR does not interact with the integrin family of cell receptors but with the 67 kDa laminin binding protein (LBP) (Avci-Adali et al., 2010). Although YIGSR is derived from laminin and facilitate identical cellular adhesion as laminin, YIGSR is unable to promote the same signaling triggered by laminin B1 chain (Boateng et al., 2005). Therefore, it is difficult to examine the signaling change by YIGSR peptide. Since we want to use YIGSR to promote cell binding of ECs, we will focus on the adhesion affinity and migration ability of ECs and SMCs with YIGSR-Ubx fiber.

## 4.2 Materials and methods

### 4.2.1 Ubx materials

Monomers of his-tagged Ultrabithorax splicing isoform Ia, along with SDF-1α, bFGF, Ghlerin-Ubx and YIGSR-Ubx (Tsai et al., 2015), were produced in *E. coli* from the pET19b-UbxIa vector and purified as previously described. Ubx fibers were produced by the buffer reservoir system, also as previously described (Tsai et al., 2015).

### 4.2.2 Cell culture

Primary human umbilical vein endothelial cells (HUVEC) (Lonza, C2517A) were cultured and used at passages 3-6. Cells were grown on gelatin-coated tissue culture flasks, passaged once per week in M199 growth medium supplemented with heparin, bovine hypothalamic extract, fetal bovine serum, antibiotics and gentamycin as described.

### 4.2.3 Migration assay

HUVECs or GFP-transfected HUVECs were seeded onto gelatin-coated 24-wells plate with 300 µl supermedia and allowed to reach confluency (around 24 hours). Supermedia was then removed and wells were washed by 300 µl M199 media. Cells were cultured in 300 µl M199 without serum for 2 hours. M199 media was then replaced by 225 µl M199 + 1.5 % fetal bovine serum prior to placement of inoculation loops wrapped with SDF-1α-Ubx or plain Ubx fibers (4 fibers on each side) onto cell monolayers. After a 16 hour incubation in M199 with 1.5% serum, the cells on Ubx fibers were fixed and stained by DAPI and imaged using confocal microscopy.

### 4.2.4 Testing signaling triggered by Ubx materials

Loops wrapped around by SDF-1α-Ubx or plain-Ubx fibers (4 fibers on each side) were pulled and rehydrated in a sealed Styrofoam box with wet paper towels for 2 hours. Loops with rehydrated fibers were then placed in 24-well tissue culture plate. One T75 flask with confluent HUVECs was trypsinized and re-suspended by 6.5 ml of supermedia. Suspended cells (125 µl) was seeded directly onto the fibers. Cells were allowed to attach to fibers for 5-10 minutes before an extra 125 µl of supermedia was added into each well. HUVECs were cultured with fibers for 16 hours and the cultured media was removed, following by 300 µl of M199 wash to starve the cells. 225 µl of M199 and cells were incubated for varying amounts of time as indicated. Loops were collected and cells were directly lysed in 1X sample buffer.

### 4.2.5 Western blot

Four loops containing attached cells were collected in 125 µl of 1X sample buffer and boiled in microcentrifuge tubes for 10 minutes at 95°C. Protein lysates were separated by SDS-PAGE and transferred to polyvinylidene fluoride membranes (Fisher Scientific). After blocking in 5% nonfat dry milk or BSA ( for pERK) at room temperature for 1 hour, the membranes were incubated with monoclonal antibody against ERK (1:500 in TBST; p44/42 MAPK (Erk1/2) (137F5) Rabbit mAb, #4695S, Cell Signaling Technology), pERK (1:500 in TBST; Phospho-p44/42 MAPK (Erk1/2)(Thr202/Tyr204) Antibody #9101 Cell Signaling Technology), PECAM or GAPDH (1:10,000 in TBST; Abcam) at 4 °C for 16 hours. The membranes were washed five times before incubation with goat anti-rabbit secondary antibody (1:5,000; DAKO) for 2 hours. Immunoreactive

proteins were visualized using enhanced chemiluminescence (Millipore) and followed by film (Denville Scientific) exposure.

## 4.3 Results

### 4.3.1 SDF-1α-Ubx material promotes endothelial cell migration and attachment *in vitro*

SDF-1α has been shown to promote ECs migration through activating ERK signaling and PI3K/Akt signaling (Pi et al. 2009, Teicher et al., 2010). Therefore, we first asked whether SDF-1α-Ubx materials can induce the same effects on ECs. In the migration assays, HUVECs or GFP-transfected HUVECs were cultured as a confluent monolayer prior to incubation at low serum (1.5%) for 2 hours. Ubx materials were then placed into the culture wells and incubated with the cells for 16 hours in media containing low level (1.5%) of serum. The cells were then fixed and stained with DAPI to identify cells that migrated onto Ubx materials (Figure 5.1 A-B). Although the effect is not as strong as VEGF-Ubx material (Figure 4.5), significantly more HUVECs migrated onto SDF-1α-Ubx fibers when compared to control Ubx fibers (Figure 5.1C; $p<0.01$), indicating that VEGF-Ubx materials stimulated migration of ECs in low serum conditions.

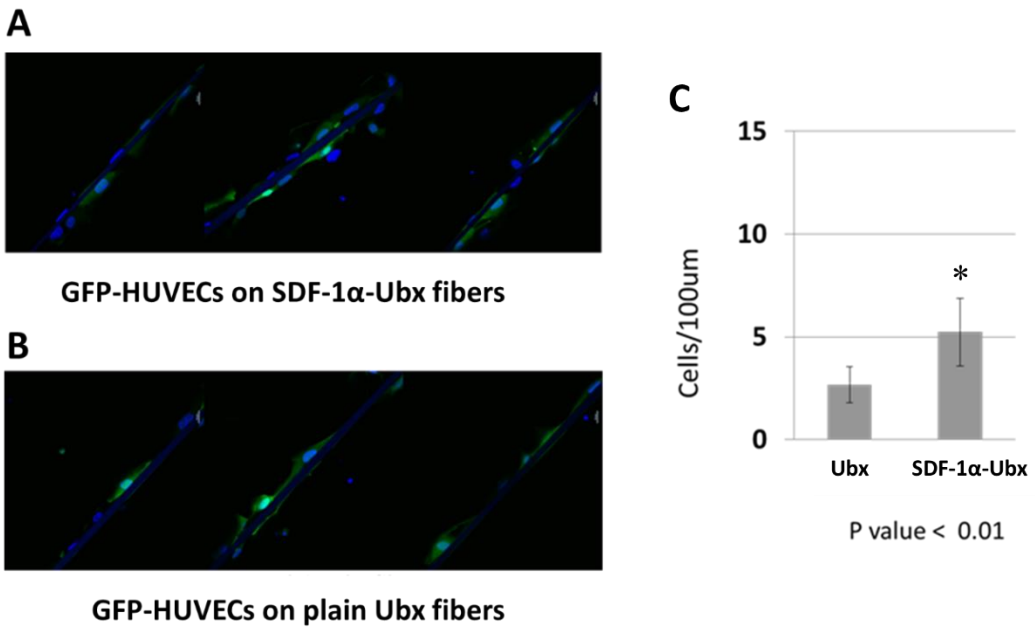


**Figure 4.1 SDF-1α -Ubx fiber promotes enhanced recruitment and migration of endothelial cells.** SDF-1α-Ubx (A) and plain Ubx (B) fibers were cultured overnight with an established monolayer of GFP-transfected HUVECs in low (1.5%) serum. Cells were fixed, stained with DAPI (blue), and imaged using confocal microscopy. (C) Quantification of the number of cells/100 μm distance attached to plain Ubx vs. SDF-1α-Ubx fibers. Data were averaged from 10 independent fields in each group from 3 experiments. Data were analyzed for significance using univariate analysis of variance (ANOVA) with * indicating $p < 0.01$.

### 4.3.2 SDF-1α–Ubx fiber does not induce the ERK signaling in HUVECs

SDF-1α-Ubx material promotes endothelial cell migration and attachment *in vitro,* suggesting that SDF-1α protein in Ubx material may induce the down steam signaling of SDF-1α in HUVECs. The major signaling pathways involved in the SDF-1α induced EC migration signal through PI3K/Akt or ERK signaling (Pi et al. 2009, Teicher et al., 2010). We tested the signaling changes by seeding HUVECs onto SDF-1α-Ubx fibers and culturing the HUVECs / fibers overnight prior to serum starvation. HUVECs were then collected and lysed at specific time points after serum starvation (1, 2, 3, 4 hours) and

analyzed by western blot. We were not able to detect the signal of phosphorylated AKT. This could be due to the fact that the only available anti-pAkt antibody is of poor quality. Therefore, we tested whether signaling could be detected via pERK, because the anti-pERK and Anti-ERK antibodies work well. However, we didn't observe significant difference between the HUVECs, when cultured with SDF-1α–Ubx fibers and plain-Ubx fibers (Figure 4.2).

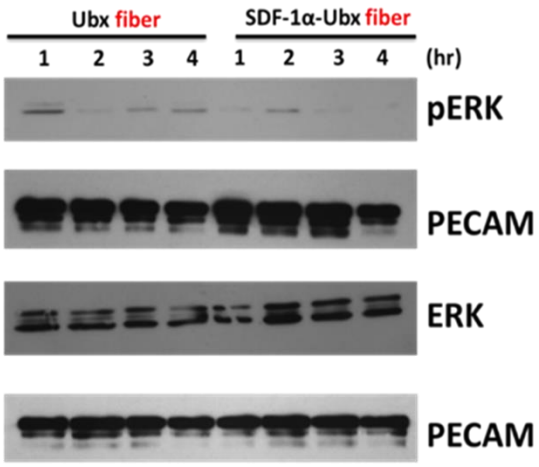


**Figure 4.2 SDF-1α–Ubx fiber does not induce ERK signaling in HUVECs.** HUVECs cultured with SDF-1α Ubx fibers and plain Ubx fibers in serum starved environment were collected at the specified time, and western blot analyses were used to probe for pERK (Thr 202/Tyr 204), ERK and PECAM.

### 4.3.3 Soluble SDF-1α–Ubx stimulates ERK signaling in HUVECs in the same pattern as soluble SDF-1α protein

Although SDF-1α-Ubx material promotes endothelial cell migration and attachment *in vitro*, we were not able to detect the ERK signaling accordingly. To ensure SDF-1α-Ubx fusion is not causing misfolding or loss-of function of SDF-1α protein in the fusion with Ubx, we compared the efficacy of soluble SDF-1α–Ubx protein with commercially

acquired SDF-1α protein (R&D system, #P48061). HUVECs were cultured until confluency and then serum starved for 2 hours to completely eliminate the signaling induced by old serum added media. Soluble SDF-1α–Ubx (25 μM) and SDF-1α protein (12.5μM) were then added to stimulate the HUVECs. Because SDF-1α–Ubx is purified by one affinity column and the estimated purity is 50-60 % by SDS-PAGE, double the SDF-1α–Ubx protein concentration was used to compare with commercial SDF-1α protein. Soluble SDF-1α–Ubx is able to stimulate ERK signaling in HUVECs. pERK was detected soon after SDF-1α-Ubx addition (5 minutes), which is comparable to commercial SDF-1α protein control and similar to the time course reported previously (Pi et al., 2009) (Figure 4.3). We conclude that SDF-1α protein is correctly folded and functional in the fusion protein with Ubx.

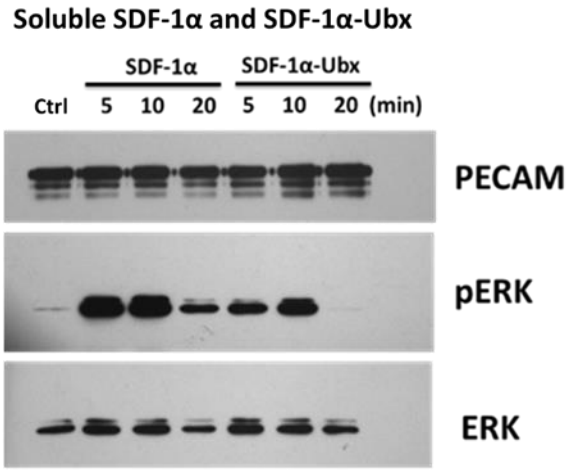


**Figure 4.3 Soluble SDF-1α–Ubx stimulates ERK signaling in HUVECs.**
Soluble SDF-1α–Ubx trigger ERK signaling in HUVECs in the same pattern as soluble SDF-1α protein (R&D system, #P48061). Ctrl: Control, HUVECs without treatment.

### 4.3.4 Adding linker between growth factors and Ubx does not improve the delivery of growth factors to cells

Soluble SDF-1α-Ubx protein stimulates ERK signaling in HUVECs, which is comparable to soluble SDF-1α protein acquired commercially, suggesting that the folding and function of SDF-1α protein within this fusion is intact in the monomers. However, SDF-1α-Ubx material is not able to trigger ERK signaling when cultured with HUVECs, presumably because Ubx : Ubx or SDF-1α : Ubx contacts formed in the materials unfold SDF-1α or sequester the SDF-1α interface for receptor binding. To test this hypothesis, we lengthened the linker from Glycine to Glycine-Serine-Glycine-Serine between SDF-1α protein and Ubx. We also made the same modification in bFGF-Ubx, another potent ERK signaling activator of HUVECs. However, we were not able to see any improvement by this modification (Figure 4.4).

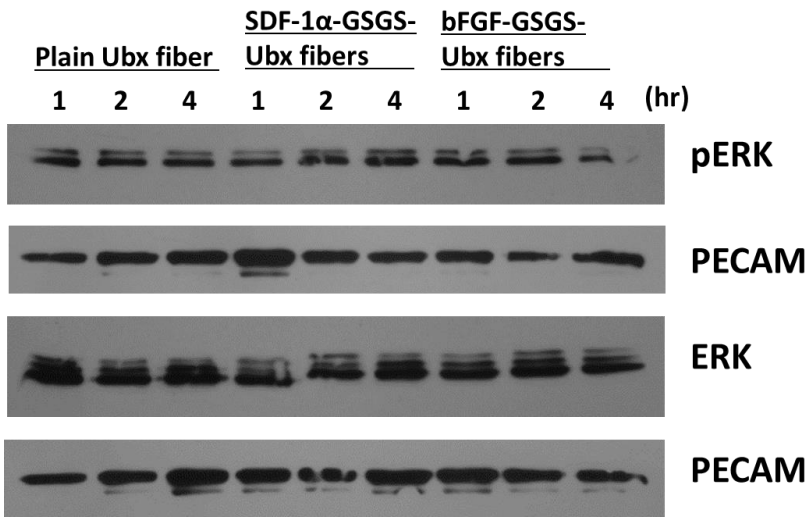


**Figure 4.4 Adding linker between growth factors and Ubx does not improve delivery of growth factors to cells.** HUVECs cultured with plain Ubx fibers, SDF-1α-GSGS-Ubx fibers and bFGF-GSGS-Ubx fibers in serum starved environment were collected at the specified time, and western blot analyses were used to probe for pERK (Thr 202/Tyr 204), ERK and PECAM. GSGS: Glycine-Serine-Glycine-Serine peptide

## 4.4 Conclusions

In this chapter, we aimed to make biocompatible and multi-functional Ubx materials for stent uses. To achieve this goal, we planned to make a variety of Ubx fusions with growth factor or cell-binding peptide that have specific functions for recruiting ECs or preventing the binding of platelet and smooth muscle cells. We first tested the SDF-1α-Ubx, both in the forms of soluble protein or in materials. SDF-1α-Ubx material promotes the migration of HUVECs. In addition, soluble SDF-1α-Ubx protein shows similar efficacy as SDF-1α protein, suggesting the SDF-1α protein is correctly folded and functional when produced with Ubx as a fusion protein. However, we were not able to detect the ERK signaling triggered by SDF-1α-Ubx material. Here we propose three possible explanations:

1. We looked at the wrong pathway. Although SDF-1α is known to promote HUVECs migration by inducing PI3K/AKT and ERK signaling, in Ubx material, it may induce different pathways because the physical interaction between HUVECs and material is quite different from the conventional interaction between soluble SDF-1α and HUVECs in tissue culture dishes.
2. SDF-1α-Ubx material indeed triggers the ERK signaling, but we looked at the wrong timing. According to the result of Figure 4.3, soluble SDF-1α induces the signaling only at a very early time points when the HUVECs has been serum starved for 2 hours. In our experiments, HUVECs were directly added onto the SDF-1α-Ubx fibers and incubated for overnight prior to serum starvation. The signaling induced by SDF-1α protein in HUVECs may be weakened since the

cells have been exposed to SDF-1α protein for more than 16 hours, which may result in the difficulty of detecting the changes in signaling.

3. SDF-1α protein is embedded in the material and its binding site is not accessible for the receptors on cells. The observation that the SDF-1α-Ubx material promotes more HUVECs migration than plain Ubx-material, may be caused by the physicochemical properties of SDF-1α protein rather than specific interaction with the receptors. For example, SDF-1α protein has a predicted +9.0 charge at pH 7.2, which may help the attachment of HUVECs.

To test these explanations, in the future, we first plan to look at different pathways that may be induced by SDF-1α-Ubx material. We may also need to modify the experiment protocol, in order to maximize the signals and detect the changes in signaling at the right timing.

# CHAPTER V

# OVERALL CONCLUSION AND FUTURE DIRECTION

## 5.1 Research summary

In this study, we have made several discoveries. First of all, we discovered the formation of dityrosine bonds in Ubx materials, which is correlated to the physical strength of Ubx materials. Most importantly, we identified the specific tyrosine residues involved in the bond formation, allowing us to manipulate the mechanical properties of Ubx materials in the future. Secondly, we have systematically tested the physicochemical effects of the fusion proteins on the production and assembly of functional Ubx materials. We found that the appended proteins dominate the expression and solubility of the entire fusions. Interesting, Ubx fusions show strong and consistent ability to assemble into materials despite the physicochemical effects of the appended proteins. We concluded that a far wider range of proteins can be successfully incorporated into Ubx materials than originally anticipated. Finally, we demonstrated that functional molecules, such like VEGF, can be incorporated into Ubx-materials and induce corresponding signaling pathway to instruct ECs behaviors *in vitro* and *in vivo*. However, successful incorporation of proteins into materials is no guarantee that the proteins will remain active within the materials, as exemplified by SDF-1α and bFGF. In conclusion, we see Ubx material has great potential as a novel protein-based material. In the future, we hope to use this material for a variety of biomedical applications.

### 5.2 Compare Ubx material with other protein-based materials

In Chapter III, we demonstrated that Ubx protein possesses a very strong and consistent ability to incorporate appended proteins into materials. Successful Ubx fusions cover a much wider range of physicochemical properties than current protein-based materials (Huang et al., 2007, Jansson et al., 2014). This unique feature makes Ubx material a very attractive system for functionalizing protein-based materials. Many potential biomedical applications could be implemented by the functionalized Ubx materials. A representative example in my studies is the multifunctional tissue engineering scaffold intended to stimulate multiple desired cell behaviors (attachment, survival, proliferation) of HUVEC at the same time (Appendix and Chapter IV). This unique advantage of Ubx material is likely because Ubx protein not only has elastin-like motifs and spider silk-like motifs that promote non-covalent protein-protein interaction (Greer et al., 2009), but also has intermolecular dityrosine bonds that crosslink Ubx molecules in materials.

Compared to other protein-based materials, Ubx material also has some challenges need to be overcame in the future. First, although Ubx materials can be digested by trypsin (Hsiao et al., manuscript in preparation), we have not designed a successful programmable hydrolysis or a specific degradation for Ubx material yet, which limits Ubx materials' applications as a biodegradable drug delivery vehicle or a subcutaneous biosensor. Another technique needs to be developed for Ubx materials is the method/equipment for making more complex structures of Ubx materials. At present, we are able to make Ubx materials into different morphologies such like film, sheet, fiber and bundle. However, some biomedical applications need more complex 3D structures,

for example, a sponge-like scaffold for cartilage tissue engineering (Aoki et al., 2003, Morita et al, 2002). Currently, the most common method to make complex protein-based structures is electrospinning (Rockwood et al., 2011, Hu et al., 2012). A typical electrospinning device is composed of a Gama High Voltage DC power and a syringe pump. Briefly, the material-forming protein solutions form a droplet at the orifice of a stainless steel needle. The droplet is then stretched and splayed into a series of fine filaments under a high-voltage electric field. The generated nanofibers are collected on aluminum foil, silicon die, or glass slides (Qiu et al., 2010). Recently, 3D-printing technique has also been used for making tissue engineering scaffolds (Schacht et al., 2015). In the Bio-3D printer system, before printing, the protein solution (spider silk protein) was pre-gelled overnight at 37 °C and 95 % relative humidity to form hydrogel, a robotic bioplotter is then used to dispense the protein gel into different structures. The two techniques described above may be useful for Ubx materials to create more complex structures, but both need to be further tested and adjusted.

### 5.3 Suture functional proteins with Ubx material by DiY bonds

In Chapter V, we discussed that SDF-1α protein may be embedded in the material, therefore its binding site is not accessible for the receptors on cells. To solve this problem, we planned to employ the finding we discovered in Chapter II, the dityrosine bonds in Ubx-materials. We first tested the Y167-Y240 bond, the strongest bond found in Ubx materials. The Y240 and Y167 and their surrounding amino acids (around 12-24 amino acids) were cloned and inserted into the N-terminus of growth factors and Ubx protein, respectively. Y167 peptide inserted Ubx protein will be made as material first.

Y240 peptide inserted growth factors will then be incubated with the Y167 inserted-Ubx material to allow the Y167-Y240 bond to form and link the growth factor to the surface of Ubx material. (Figure 5.1)

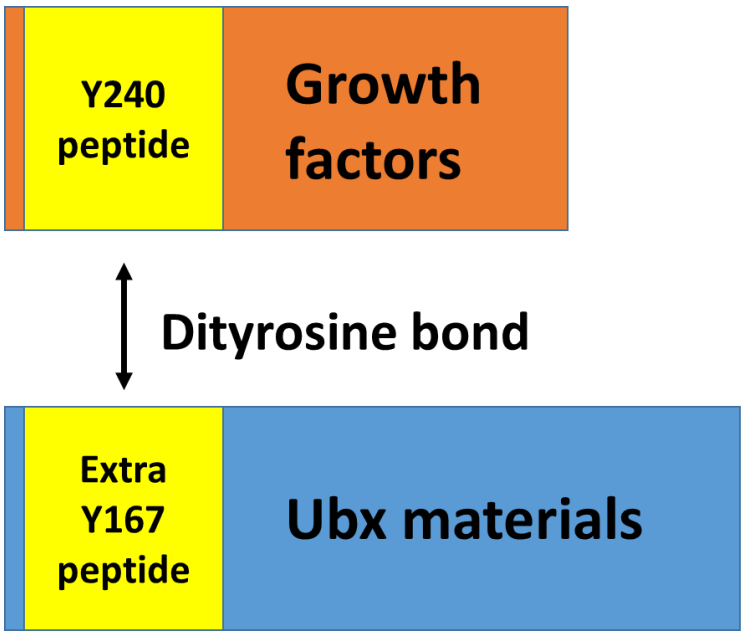


**Figure 5.1 Growth factors or other functional molecules can be potentially linked to Ubx-materials by the formation of dityrosine bonds.**

### 5.4 Micro-beads for therapeutic protein production

In 1986, human tissue plasminogen activator (tPA, Genentech) became the first recombinant protein therapeutics available on market (Wurm, 2004). Since then, protein therapeutics keeps growing with a compound annual growth rate of 12-13% and the market is likely to grow and to reach $141.5 billion in 2017 (according to the report: Global Protein Therapeutics Market Forecast to 2015 - Research and Markets, 2012). Most recombinant protein pharmaceuticals are produced in mammalian cells, including some typical high yield cell lines such as CHO cells or HEK-293 Cells. Although the

production yield of mammalian cell lines cannot compete with the high production yield in bacteria or yeast systems, mammalian cell lines are irreplaceable therapeutic protein producing factories because most proteins require proper posttranslational modifications such as glycosylation to gain full functions (Kim et al., 2012). Early stages of protein therapeutics studies are usually conducted in academia or industrial laboratories. Once the protein therapeutics candidates are selected, many rounds of protein engineering, modifications and optimization will be performed to pursue the highest specificity, lowest side effects and the most optimized efficacy of the lead molecules. In each round, scientists need to produce enough amount of the engineered product for a variety of tests, such as affinity assays by surface plasmon resonance, ADCC/CDC assays, pharmacokinetic/pharmacodynamic modeling and experiments in animal models (Tuntland et al., 2014). To produce enough amount proteins for these assays is always challenging in the laboratory, particularly due to the limited space for mammalian cell culture. There are several ways to overcome this problem, for example, using multilayer cell culture flasks or a rolling bottle cell culture system. Both methods are designed to increase the surface area for cell attachment in the flasks and therefore increase cell number and protein yield (Figure 5.2). An alternative method is using micro-carrier beads for cell attachment. The micro-carrier beads can be suspended by the impellers in spinning flask. This 3-dimensional culture system fully utilizes the medium in the flask and dramatically increases the cell density and protein production in the flask (Figure 5.3). However, cells can only attach and survive on the micro-carrier beads for 1-2 weeks, and the preparation of these beads is time-consuming and costly. To solve this disadvantage of conventional micro-carrier beads, we can use functionalized Ubx

materials. There are at least three advantages of Ubx materials as the next generation of micro-carrier. 1. Ubx materials are cytocompatible. A variety of cell types attach to Ubx materials well. We also can design specific binding sites for different cell types to maximize cell attachment. 2. We can fuse growth factors (such as EGF or IGF-1) to Ubx and make functional materials that promote cell proliferation and inhibit apoptosis, which can greatly prolog the production period. 3. Functional molecules are stable and protected in the Ubx materials (Figure 3.5A). Ideally, functional molecules will not be digested by proteases in the culture media or engulfed by endocytosis. Therefore we can reduce the cost of extra supplements, compared to conventional culture systems.

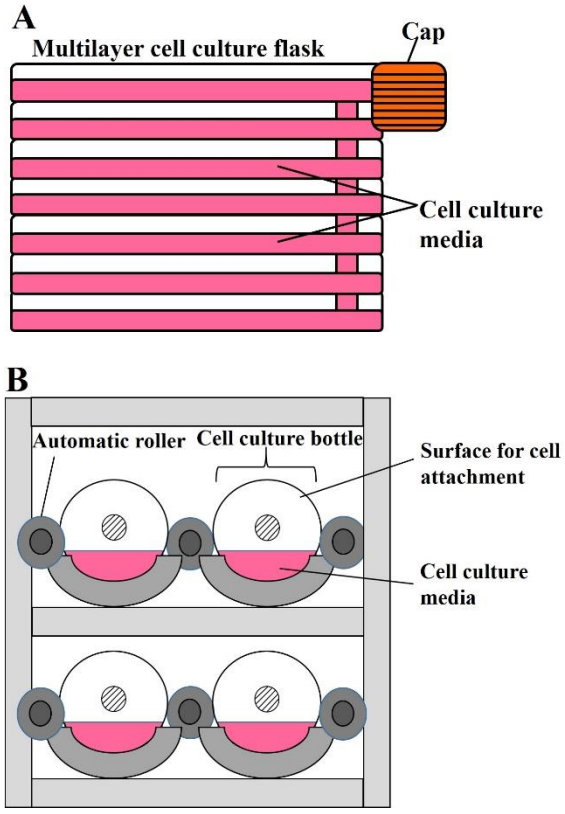


**Figure 5.2 High cell density cell culture systems.** (A) Multi-layer cell culture flask. (B) Rolling bottle cell culture system.

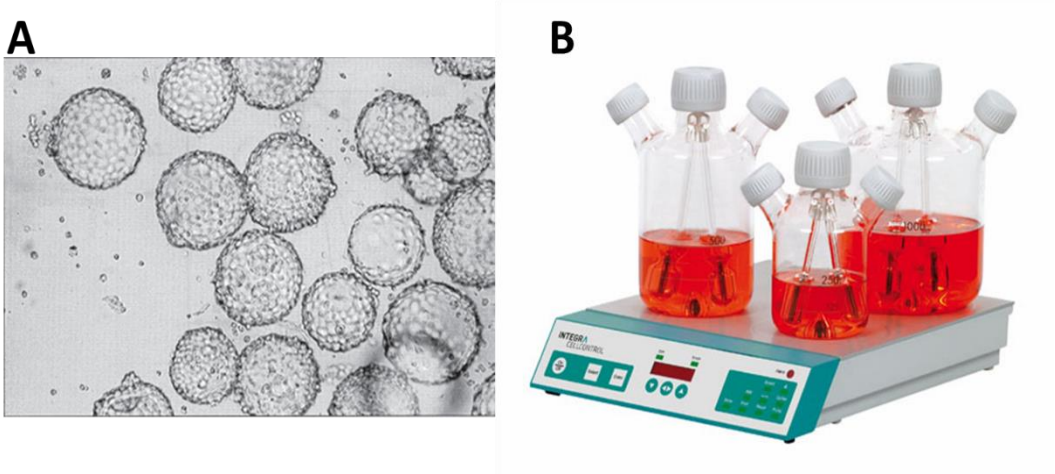


**Figure 5.3 Micro-carrier cell culture systems. (**A) Cells are attaching to the micro-carrier beads. (B) Micro-carrier beads can be suspended by the impellers in spinning flask. (Merten, 2015)

### 5.5 Using Ubx-materials as drug delivery vector

Treatments of rheumatoid arthritis, polyarticular juvenile idiopathic arthritis and psoriatic arthritis include surgery, physical therapy, nonsteroidal anti-inflammatory drugs (NSAIDs), and injection of protein therapeutics. Etanercept is an example of protein therapeutics for these diseases. Etanercept is a dimeric human tumor necrosis factor receptor (TNFR) p75-Fc fusion protein made of 2 extra-cellular domains of the human 75 kD (p75) TNFR that captures the free TNF-α in body fluid (Garrison et al., 1999, Murray et al., 1997). To decrease the injection frequency and improve the quality of lives of patients, these types of protein therapeutics are usually modified by fusing with Fc domain or BSA to increase half-life (Hutt et al., 2012). However, standard treatment still requires an injection every two weeks to one month. To improve this, we can apply Ubx material as a drug delivery system. We can first fuse TNF-α receptor with Ubx and make a hydrogel or a small sponge-like material. The material can then be implanted or

injected into the knees or other joints of mice to test the biocompatibility. Ideally, the TNF-α Receptor-Ubx will be gradually released and absorb free TNF-α in synovial fluid and inhibit local inflammation in knees or other joints.

REFERENCES

Adak AK, Li BY, Huang LD, Lin TW, Chang TC, Hwang KC, Lin CC. ACS Appl. Mater. Interfaces 2014, 6, 10452.

Aeschbach R, Amado E, Neukom H. Biochim. Biophys. Acta.1976, 439, 292.

Altman GH, Diaz F, Jakuba C, Calabro T, Horan RL, Chen J, Lu H, Richmond J, Kaplan DL. Biomaterials 2003, 24. 401.

Anderson SM, Shergill B, Barry ZT, Manousiouthakis E, Chen TT, Botvinick E, Platt MO, Iruela-Arispe ML, Segura T. Integr. Biol. 2011, 9, 887.

Andreas S, Karshovska E, Zernecke A, Weber C. Trends in Cardio. Med. 2006, 16, 103.

Aoki H, Tomita N, Morita Y, Hattori K, Harada Y, Sonobe M, Wakitani S, Tamada Y. Biomed. Mater. Eng. 2003, 13, 309.

Aparecido dos Santos-Pinto JR, Lamprecht G, Chen WQ, Heo S, Hardy JG, Priewalder H, Scheibel TR, Palma MS, Lubec G. J. Proteomics 2014, 105, 174.

Appelmann I, Liersch R, Kessler T, Mesters R, Berdel W. Cancer Res. 2010, 180, 51.

Asai D, Xu D, Liu W, Garcia QF, Callahan DJ, Zalutsky MR, Craig SL, Chilkoti A. Biomaterials 2012, 33, 5451.

Asti A, Gioglio L. Int. J. Artif. Organs. 2014, 37, 187.

Avci-Adali M, Ziemer G, Wendel HP. Biotechnol. Adv. 2010, 28, 119.

Baker M, Robinson SD, Lechertier T, Barber PR, Tavora B, D'Amico G, Jones DT, Vojnovic B, Hodivala-Dilke K. Nat. Protoc. 2012, 1, 89.

Baneyx F, Schwartz DT. Curr. Opin. Biotechnol. 2007, 18, 312.

Bayless KJ, Davis GE. Biochem. Biophys. Res. Commun. 2003, 4, 903.

Bayless KJ, Davis GE. J. Biol. Chem. 2004, 12, 11686.

Bayless KJ, Kwak HI, Su SC. Nat. Protoc. 2009, 12, 1888.

Beachy PA, Varkey J, Young KE, von Kessler DP, Sun BI, Ekker SC. Mol. Cell Biol. 1993, 13, 6941.

Bleul CC, Farzan M, Choe H, Parolin C, Clack-Lewis I, Sodroski J, Springer TA. Nature 1996, 382, 829.

Bondos SE. Curr. Anal. Chem. 2006, 2, 157.

Boateng SY, Lateef SS, Mosley W, Hartman TJ, Hanley L, Russell B. Am. J. Physiol. Cell Physiol. 2005, 288, 30.

Brooks AE, Strickler SM, Joshi SB, Kamersell TJ, Middaugh CR, Lewis RV. Biomacromolecules 2008, 9, 1506.

Bryant SJ, Anseth KS. Biomaterials 2001, 6, 619.

Burns JM, Summers BC, Wang Y, Melikian A, Berahovich R, Miao Z, Penfold ME, Sunshine MJ, Littman DR, Kuo CJ, Wei K, McMaster BE, Wright K, Howard MC, Schall TJ. J. Exp. Med. 2006, 203, 2201.

Bursac N, Papadaki M, Cohen RJ, Schoen FJ, Eisenberg SR, Carrier R, Vunjak-Novakovic G, Freed LE. Am. J. Physiol. 1999, 2, H433.

Carmeliet P, Ferreira V, Breier G, Pollefeyt S, Kieckens L, Gertsenstein M, Fahrig M, Vandenhoeck A, Harpal K, Eberhardt C, Declercq C, Pawling J, Moons L, Collen D, Risau W, Nagy A. Nature 1996, 6573, 435.

Chatterjee K, Lin-Gibson S, Wallace WE, Parekh SH, Lee YJ, Cicerone MT, Young MF, Simon Jr. CJ. Biomaterials 2010, 31, 5051.

Chen WQ, Priewalder H, John JP, Lubec G. Proteomics 2010, 10, 369.

Chilkoti A, Christensen T, MacKay JA. Curr. Opin. Chem. Biol. 2006, 10, 652.

Christenson LK, Stouffer RL. Biol. Reprod. 1996, 6, 1397.

Christensen T, Amiram M, Dagher S, Trabbic-Carlson K, Shamji M, Setton LA, Chikloti A. Potein Sci. 2009, 18, 1377.

Crawford A, Hatton PV. Biomed. Pharmacother. 2008, 62, 493.

Churion K, Howell DW, Ramasamy S, Catanese DJ, Tsai SP, Northern K, Zechiedrich L, Matthews KS, Bondos SE. Nat. Mater. 2015, unpublished.

Cummings C, Murata H, Koepsel R, Russell AJ. Biomaterials 2013, 34, 7437.

Cunningham SA, Waxham MN, Arrate PM, Brock TA. J. Biol. Chem. 1995, 35, 20254.

Daviet I, Herbert JM, Maffrand JP. FEBS Letters 1990, 259, 315.

Davis GD, Elisee C, Newham DM, Harrison RG. Biotechnol. Bioeng. 2000, 65, 382.

Danenberg HD, Fishbein I, Gao J, Mönkkönen J, Reich R, Gati I, Moerman E, Golomb G. Circulation. 2002, 30, 599.

Delcour A, Verpoest I, Plummer CJ. Biomacromolecules 2004, 5, 1262.

Deming TJ. Prog. Polym. Sci. 2007, 32, 858.

Dent P. Cancer Biol. Ther. 2014, 3, 245.

Ding Y, Li Y, Qin M, Cao Y, Wang W. Langmuir 2013, 29, 13299.

Dougher M, Terman BI. Oncogene 1999, 8, 1619.

Dohle DS, Pasa SD, Gustmann S, Laub M, Wissler JH, Jennissen HP, Dünker N. J. Visualized Exp. 2009, 33, 1620.

Dosztányi Z, Mészáros B, Simon I. Bioinformatics 2009, 25, 2745.

Elvin CM, Carr AG, Huson, MG, Maxwell JM, Pearson RD, Vuocolo T, Liyou NE, Wong DC, Merritt DJ, Dixon NE. Nature 2005, 437, 999.

Endrizzi BJ, Huang G, Kiser PF, Stewart RJ. Langmuir 2006, 22, 11305.

Ellis LM, Hicklin DJ. Nat. Rev. Cancer 2008, 8, 579.

Elvin CM, Brownlee AG, Huson MG, Tebb TA, Kim M, Lyons RE, Vuocolo TN, Liyou NE, Hughes TC, Ramshaw JA, Werkmeister JA. Biomaterials 2009, 30, 2059.

Engler AJ, Sen S, Sweeney HL, Discher DE. Cell 2006, 126, 677.

Fang J, Li H. Langmuir 2012, 28, 8260.

Fang J, Mehlich A, Koga N, Huang J, Koga R, Gao X, Hu C, Jin C, Rief M, Kast J, Baker D, Li H. Nat. Commun. 2013, 4, 2974.

Farahani M, Treweeke AT, Toh CH, Till KJ, Harris RJ, Cawley JC, Zuzel M, Chen H. Leukemia 2005, 19, 524.

Farooq V, Gogas BD, Serruys PW. Circulation, 2011, 4, 195.

Faury G. Pathologie Biologie 2001, 49, 310.

Folkman J, Klagsbrun M. Science 1987, 235, 442.

Fischman DL, Leon MB, Baim DS, Schatz RA, Savage MP, Penn I, Detre K, Veltri L, Ricci D, Nobuyoshi M, Cleman M, Heuser R, Almond D, Teirstein PS, Fish RD, Colombo A, Brinker J, Moses J, Shaknovich A, Hirshfeld J, Bailey S, Ellis S, Rake R, Goldberg S. N. Engl. J. Med. 1994, 331,496.

Fittkau MH, Zilla P, Bezuidenhout D, Lutolf MP, Human P, Hubbell JA, Davies N. Biomaterials 2005, 26, 167.

Forrer P, Jaussi R. Gene 1998, 224, 45.

Forstater JH, Kleinhammes A, Wu Y. Langmuir 2013, 29, 15013.

Galas RJ, Liu JC. J. Cell. Biochem. 2014, 115, 111.

Garlotta D, Doane W, Shogren R, Lawton J, Willett JL. J. Appl. Polymer Sci. 2003, 88, 1775.

Garrison LW. Ann. Intern. Med. 1999,130, 478.

Gazit E. FEBS J. 2007, 274, 317.

Gerber HP, McMurtrey A, Kowalski J, Yan M, Keyt BA, Dixit V, Ferrara N. J. Biol. Chem. 1998, 46, 30336.

Gentile P, Chiono V, Carmagnola I, Hatton PV. Int. J. Mol. Sci. 2014, 15, 3640.

Gnavi S, di Blasio L, Tonda-Turo C, Mancardi A, Primo L, Ciardelli G, Gambarotta G, Geuna S, Perroteau I. Tissue Eng. Regener. Med. 2014. DOI: 10.1002/term.1936.

Go AS, Chertow GM, Fan D, McCulloch CE, Hsu CY, N. Engl. J. Med. 2004, 351, 1296.

Gosline JM, Guerette PA, Ortlepp CS, Savage KN. J. Exp. Biol. 1999, 202, 3295.

Greer AM, Huang Z, Oriakhi A, Lu Y, Lou J, Matthews KS, Bondos SE. Biomacromolecules 2009, 10, 829.

Grip S, Johansson J, Hedhammar M. Protein Sci. 2009, 18, 1012.

Georges PC, Hui J, Gombos Z, McCormick ME, Wang AY, Uemura M, Mick R, Janmey PA, Furth EE, Wells RG. Am. J. Physiol. Gastrointest. Liver Physiol. 2007, 293, G1147.

Gomes S, Leonor IB, Mano JF, Reis RL, Kaplan DL. Prog. Polym. Sci. 2012, 37, 1.

Grevellec J, Marquie C, Ferry L, Crespy A, Vialettes V. Biomacromolecules 2001, 2, 1104.

Hahn MS, Miller JS, West JL. Adv. Mater. 2005, 17, 2939.

Hansson GK, Libby P. Nat. Rev. Immunol. 2006, 6, 508.

Harms GS, Pauls SW, Hedstrom JF, Johnson CK. J. Fluoresc. 1997, 7, 283.

Hermann DM, Zechariah A. J. Cereb. Blood Flow Metab. 2009, 10, 1620.

Hershel U, Dahmen C, Kessler H. Biomaterials 2003, 24, 4385.

Hollister SJ, Maddox RD, Taboas JM. Biomaterials 2002, 23, 4095.

Huang L, McMillan RA, Apkarin RP, Pourdeyhimi B, Conticello VP, Chaikof EL, Macromolecules 2000, 33, 2989.

Howard-Alpe GM, Bono JD, Hudsmith L, Orr WP, Foex P, Sear JW. Br. J. Anaesth. 2007, 5, 560.

Howell DW, Tsai SP, Churion K, Patterson JL, Abbey CA, Atkinson JT, Porterpan D, You YH, Meissner KE, Bayless KJ, Bondos SE. Adv. Funct. Mater. 2015, 37, 5988.

Hu C, Cui W. Adv. Healt. Mater. 2012, 1, 809.

Huang J, Wong C, Geroge A, Kaplan DL. Biomaterials 2007, 28, 2358.

Huang Z, Lu Y, Majithia R, Shah J, Meissner K, Matthews KS, Bondos SE, Lou J. Biomacromolecules 2010, 11, 3644.

Huang Z, Salim T, Brawley A, Patterson J, Matthews KS, Bondos SE. Adv. Funct. Mater. 2011, 21, 2633.

Hutt M, Färber-Schwarz A, Unverdorben F, Richter F, Kontermann RE. J. Biol. Chem. 2012, 287, 4462.

Iqbal J, Gunn J, Serruys PW. Br. Med. Bull. 2013 doi: 10.1093/bmb/ldt009

Jakeman L, Armanini M, Phillips H, Ferrara N. Endocrinology 1993, 2, 848.

Landgren E, Klint P, Yokote K, Claesson-Welsh L. Oncogene 1998, 7, 283.

Jansson R, Thatikonda N, Lindberg D, Rising A, Johansson J, Nygren PA, Hedhammar M. Biomacromolecules 2014, 15, 1696.

Jun HW, West J. J. Biomater. Sci. Polym. 2004, 15, 73.

Kelley FW. Fed. Proc. 1968, 27, 773.

Kendall RL, Rutledge RZ, Mao X, Tebben AJ, Hungate RW, Thomas KA. J. Biol. Chem. 1999, 10, 6453.

Kharlampieva E, Kozlovskaya V, Gunawidjaja R, Shevchenko VV, Vaia R, Naik RR, Kaplan DL, Tsukruk VV. Adv. Funct. Mater. 2010, 20, 840.

Kim HS. Cell Genetics 1998, 83, 73.

Kim SH, Kiick KL. Macromol. Rapid Commun. 2010, 31, 1231.

Kim JY, Kim YG, Lee GM. Appl. Microbiol. Biotechnol. 2012, 93, 917.

Kitamura N. J. Atheroscler. Thromb. 2014, 21, 477.

Knowles TP, Buehler MJ. Nat. Nanotechnol. 2011, 6, 469.

Kroll J, Waltenberger J. J. Biol. Chem. 1997, 51, 32521.

M. Kumar, K. J. Sanford, W. A. Cuevas, M. Du, K. D. Collier, N. Chow, Biomacromolecules 2006, 7, 2543.

Kyte J, Doolittle RF. J. Mol. Biol. 1982, 157, 105.

Lagziel-Simis S, Cohen-Hadar N, Moscovich-Dagan H, Wine Y, Freeman A. Curr. Opin. Biotechnol. 2006, 17, 569.

Lazaris A, Arcidiacono S, Huang Y, Zhou JF, Duguay F, Chretien N, Welsh EA, Soares JW, Karatzas CN. Science 2002, 295, 472.

Leal-Egaña A, Scheibel T. Biotechnol. Appl. Biochem. 2010, 55, 155.

Li RK, Yau TM, Weisel RD, Mickle DAG, Sakai T, Choi A, Jia ZQ. J. Thorac. Cardiovasc. Surg. 2000, 2, 368.

Liivak O, Blye A, Shah N, Jelinski WL. Macromolecules 1998, 31, 2947.

Lee KY, Peters MC, Mooney DJ. J. Control. Release 2003, 1–3, 49.

Lee SM, Pippel E, GƟsele U, Dresbach C, Qin Y, Chandran CV, Bräuniger T, Hause G, Knez M. Science 2009, 324, 488.

Lin Y, Wang S, Chen Y, Wang Q, Burke KA, Spedden EM, Stall C, Weiss AS, Kaplan DL. Nanomedicine 2015, 10, 803.

Liu Y, Matthews KS, Bondos SE. J. Biol. Chem. 2008, 283, 20874.

Liu Y, Matthews KS, Bondos SE. J. Mol. Biol. 2009, 390, 760.

Ma J, Zhang L, Liang Z, Zhang W, Zhang Y. J. Sep. Sci. 2007, 30, 3050.

Majithia R, Patterson J, Bondos SE, Meissner KE. Biomacromolecules 2011, 12, 3629.

Makadia HK, Siegel J. Polymers (Basel). 2011, 3, 1377.

Marler JJ, Upton J, Langer R, Vacanti JP. Adv. Drug Delivery Rev. 1998, 1–2, 165.

Marquez LA, Dunford HB. J. Biol. Chem. 1995, 270, 30434.

Martin I, Vunjak-Novakovic G, Yang J, Langer R, Freed LE. Exp. Cell Res. 1999, 2, 681.

Martino MM, Brkic S, Bovo E, Burger M, Schaefer DJ, Wolff T, Gürke L, Briquez PS, Larsson HM, Gianni-Barrera R, Hubbell JA, Banfi A. Front. Bioeng. Biotechnol. 2015, 3, 45.

Maskarinec SA, Tirrell DA. Curr. Opin. Biotechnol. 2005, 16, 422.

Masson V, Devy L, Grignet-Debrus C, Bernt S, Bajou K, Blacher S, Roland G, Chang Y, Fong T, Carmeliet P, Foidart JM, Noël A. Biol. Proced. Online 2002, 4, 24.

Matsumoto T, Claesson-Welsh L. Sci. STKE 2001, 112, 21.

Matsumoto T, Bohman S, Dixelius J, Berge T, Dimberg A, Magnusson P, Wang L, Wikner C, Qi JH, Wernstedt C, Wu J, Bruheim S, Mugishima H, Mukhopadhyay D, Spurkland A, Claesson-Welsh L, EMBO J. 2005, 13, 2342.

Meng F, Hennink WE, Zhong Z. Biomaterials 2009, 30, 2180.

Merten OW. Philos. Trans. R. Soc. Lond. B. Biol. Sci. 2015, 5, 1661.

Mészáros B, Simon I, Dosztányi Z. PLoS Comput. Biol. 2009, 5, e1000376.

MiJung K, Takaoka A, Hoang QV, Trokel SL, Paik DC. Invest. Ophthalmol. Visual Sci. 2014, 55, 3247.

Moon JJ, Saik JE, Poché RA, Leslie-Barbick JE, Lee SH, Smith AA, Dickinson ME, West JL, Biomaterials 2010, 14, 3840.

Moran JM, Pazzano D, Bonassar LJ. Tissue Eng. 2003, 9, 63.

Morita Y, Tomita N, Aoki H, Wakitani S, Tamada Y, Suguro T, Ikeuchi K. Biomed. Mater. Eng. 2002, 12, 291.

Mullerova AM, Michlik I, Blazej A. Leder 1974, 5, 85.

Murray KM. Ann Pharmacother. 1997, 11, 1335.

Nagaoka M, Jiang HL, Hoshiba T, Akaike T, Cho CS. Ann. Biomed. Eng. 2010, 38, 683.

Nairn KM, Lyons RE, Mulder RJ, Mudie ST, Cookson DJ, Lesieur E, Kim M, Lau D, Scholes FH, Elvin CM. Biophys. J. 2008, 95, 3358.

Nerem R. Ann. Biomed. Eng. 1991, 5, 529.

Obradovic B, Carrier RL, Vunjak-Novakovic G, Freed LE. Biotechnol. Bioeng. 1999, 2, 197.

Olsson AK, Dimberg A, Kreuger J, Claesson-Welsh L. Nat. Rev. Mol. Cell Biol. 2006, 5, 359.

Ong SR, Trabbic-Carlson KA, Nettles DL, Lim DW, Chilkoti A, Setton LA, Biomaterials 2006, 27, 1930.

Ozawa CR, Banfi A, Glazer NL, Thurston G, Springer ML, Kraft PE, McDonald DM, Blau HM. J. Clin. Invest. 2004, 4, 516.

Pace CN, Scholtz JM, Grimsley GR. FEBS Lett. 2014, 588, 2177.

Papadaki M, Bursac N, Langer R, Merok J, Vunjak-Novakovic G, Freed LE. Am. J. Physiol. 2001, 1, H168.

Park JY, Shim JH, Choi SA, Jang J, Kim M, Lee SH, Cho DW. J. Mater. Chem. B 2015, 3, 5415.

Pasquali-Ronchetti I. Microsc. Res. Tecniq. 1997, 38, 428.

Passner JM, Ryoo HD, Shen L, Mann RS, Aggarwal AK. Nature 1999, 397, 714.

Patel AS, Smith A, Attia RQ, Mattock K, Humphries J, Lyons O, Saha P, Modarai B, Jayasinghe SN. Integr. Biol. 2012, 4, 628.

Patterson JL, Abbey CA, Bayless KJ, Bondos SE. J. Biomed. Mater. Res. A 2014, 102, 97.

Patterson JL, Arenas-Gamboa AM, Wang TY, Hsiao HC, Howell DW, Pellois JP, Rice-Ficht A, Bondos SE. J. Biomed. Mater. Res. A 2015, DOI: 1002/jbm.a.35295.

Phelps EA, García AJ. Curr. Opin. Biotechnol. 2010, 5, 704.

Pi X, Wu Y, Ferguson JE 3rd, Portbury AL, Patterson C. PNAS, 2009, 106, 5675.

Plouët J, Moukadiri H. J. Biol. Chem. 1990, 36, 22071.

Pownall ME, Isaacs HV. Colloq. Ser. Dev. Biol. 2010, 1, 1.

Qin G, Lapidot S, Numata K, Hu X, Meirovitch S, Dekel M, Podoler I, Shosyov O, Kaplan DL. Biomacromolecules 2009, 10, 3227.

Qiu W, Teng W, Cappello J, Wu X. Biomacromolecules 2009, 10, 602.

Qiu W, Huang Y, Teng W, Cohn CM, Cappello J, Wu X. Biomacromolecules 2010, 11, 3219.

Richardson TP, Peters MC, Ennett AB, Mooney DJ. Nat. Biotechnol. 2001, 11, 1029.

Rincón AC, Molina-Martinez IT, de Las Heras B, Alonso M, Baílez C, Rodríguez-Cabello JC, Herrero-Vanrell R.J. Biomed. Mater. Res. A. 2006, 78, 343.

Roberts JR, Perkins GD, Fujisawa T, Pettigrew KA, Gao F, Ahmed A, Thickett DR. Crit. Care Med. 2007, 35, 2164.

Rockwood DN, Preda RC, Yücel T, Wang X, Lovett ML, Kaplan DL. Nat. Protoc. 2011, 6, 1612.

Rodríguez-Cabello JC, Prieto S, Requera J, Arias FJ, Ribeiro A. J. Biomater. Sci. Polym. Ed. 2007, 18, 269.

Ruoslahti E. Annu. Rev. Cell Dev. Biol. 1996, 12, 697.

Sackewitz M, von Einem S, Hause G, Wunderlich M, Schmid FX, Schwartz E, Protein Sci. 2008, 17, 1044.

Sando L, Kim M, Colgrave ML, Ramshaw JA, Werkmeister JA, Elvin CM. J. Biomed. Mater. Res. A 2010, 95, 901.

Schacht K, Jüngst T, Schweinlin M, Ewald A, Groll J, Scheibel T. Angew Chem Int. Ed Engl. 2015, 54, 2816.

Scheibel T. Microbial Cell Factories 2004, 3, 14.

Scherzinger E, Lurz R, Turmaine M, Mangiarini L, Hollenbach B, Hasenbank R, Bates GP, Davies SW, Lehrach H, Wanker EE. Cell 1997, 90, 549.

Serruys PW, Jaegere P, Kiemeneij F, Macaya C, Rutsch W, Heyndrickx G, Emanuelsson H, Marco J, Legrand V, Materne P, Belardi J, Sigwart U, Colombo A, Goy JJ, van den Heuvel P, Delcan J, Morel M. N. Engl. J. Med. 1994, 331, 489.

Shah PK. Circulation 2003, 107, 2175.

Shen YH, Shoichet MS, Radisic M. Acta Biomater. 2008, 3, 477.

Shogrena RL, Doaneb WM, Garlottaa D, Lawtona JW, Willetta JL. Polym. Degrad. Stab. 2003, 79, 405.

Shu X, Wu W, Mosteller RD, Broek D. Mol. Cell. Biol. 2002, 22, 7758.

Shweiki D, Itin A, Neufeld G, Gitay-Goren H, Keshet E. J. Clin. Invest. 1993, 5, 2235.

Silva EA, Mooney DJ. Biomaterials 2010, 6, 1235.

Souza JM, Giasson BI, Chen Q, Lee VM, Ischiropoulos H. J. Biol. Chem. 2000, 275, 18344.

Sun G, Shen YI, Kusuma S, Fox-Talbot K, Steenbergen CJ, Gerecht S. Biomaterials 2011, 1, 95.

Tabara H, Kohno H, Dhar DK, Kotoh T, Yoshimura H, Masunaga R, Tachibana M, Kubota H, Nagasue N. Acta Oncol. 2001, 40, 622.

Teicher BA, Fricker SP. Clin. Cancer Res. 2010, 16, 2927.

Teng W, Cappello J, Wu X. Biomacromolecules 2009, 10, 3028.

Terman BI, Carrion ME, Kovacs E, Rasmussen BA, Eddy RL, Shows TB. Oncogene 1991, 9, 1677.

Tian L, George SC. J. Cardiovasc. Transl. Res. 2011, 5, 685.

Tour E, Hittinger CT, McGinnis W. Development 2005, 132, 5271.

Trevino SR, Schotlz JM, Pace CN. J. Mol. Biol. 2007, 16, 449.

Trevino SR, Scholtz JM, Pace CN. J. Pharm. Sci. 2008, 97, 4155.

Tsai SP, Howell DW, Huang Z, Hsiao HC, Lu Y, Matthews KS, Lou J, Bondos SE. Adv. Funct. Mater. 2015, 25, 1442.

Tuntland T, Ethell B, Kosaka T, Blasco F, Zang RX, Jain M, Gould T, Hoffmaster K. Front Pharmacol. 2014, 28, 174.

N. Turner. Nat. Rev. Cancer 2010, 10, 116.

Vacanti JP, Langer R. Lancet 1999, S32.

Vaccaro E, Waite JH. Biomacromolecules 2001, 2, 906.

Vaisman N, Gospodarowicz D, Neufeld G. J. Biol. Chem. 1990, 32, 19461.

Vashi AV, Wekmeister JA, Vuocolo T, Elvin CM, Ramshaw JAM. J. Biomed. Mater. Res. Part A 2012, 100A, 2239.

Velema J, Kaplan DL. Adv. Biochem. Eng. Biotechnol. 2006, 102, 187.

Vivian JT, Callis PR. Biophys. J. 2001, 80, 2093.

Waffenschmidt S, Woessner JP, Beer K, Goodenough UW. Plant Cell 1993, 5, 809.

Waltenberger J, Claesson-Welsh L, Siegbahn A, Shibuya M, Heldin CH. J. Biol. Chem. 1994, 43, 26988.

Werner S, Grose R. Physiol. Rev. 2003, 83, 835.

Williams DF. Biomaterials 2009, 30, 5897.

Woerdeman DL, Veraverbeke WS, Parnas RS, Johnson D, Delcour JA, Verpoest I, Plummer CJ. Biomacromolecules 2004, 5, 1262.

Woolfson DN, Mahmoud ZN. Chem. Soc. Rev. 2010, 39, 3464.

Wurm FM. Nat. Biotech. 2004, 22, 1393.

Yamaguchi N, Zhang L, Chae BS, Palla CS, Furst EM, Kiick KL. J. Am. Chem. Soc. 2007, 129, 3040.

Yang Z, Mo X, Gong Q, Pan Q, Yang X, Cai W, Li C, Ma JX, He Y, Gao G. Apoptosis 2008, 13, 1331.

Yang J, Li W, He X, Zhang G, Yue L, Chai Y. Dis. Markers 2015, DOI: 10.1155/2015/786790.

Zachary I. Biochem. Soc. Trans. 2003, 6, 1171.

Zhang YB, Howitt J, McCorkle S, Lawrence P, Springer K, Freimuth P. Protein Expr. Purif. 2004, 36, 207.

Zheng H, Fu G, Dai T, Huang H.J. Cardiovasc. Pharmacol. 2007, 50, 274.

Zheng H, Dai T, Zhou B, Zhu J, Huang H, Wang M, Fu G. Atherosclerosis 2008, 201, 36.

# APPENDIX

# FUNCTIONALIZATION OF ULTRABITHORAX MATERIALS WITH VASCULAR ENDOTHELIAL GROWTH FACTOR ENHANCES ANGIOGENIC ACTIVITY*

## 1. Introduction

The field of tissue engineering (Marler e al., 1998, Nerem et al., 1991, Vacanti et al., 1999) strives to develop new therapies that replace, restore, or enhance function in damaged tissues. Due to the limited diffusion of metabolites and oxygen, cell viability in sizeable scaffolds is confined to within a few hundred micrometers of the tissue periphery (Bryant et al., 2001, Bursac et al., 1999, Li et al., 2000, Martin et al., 1999, Obradovic et al., 1999, Papadaki et al., 2001, Tian and George 2011). Rapid formation of blood vessels, via neovascularization or angiogenesis, is critical to maintain cell viability within tissue engineered scaffolds. Consequently, successful scaffold design must include a strategy to vascularize the tissue.

Scaffold perfusion can be achieved by administering angiogenic proteins, which drive neovascularization *in vivo* (Folkman and Klagsbrun 1987, Tabara et al., 2001, Martino et al., 2015, Park et al., 2015, Jansson et al., 2014). In particular, vascular endothelial growth factor (VEGF) promotes the formation of new blood vessels and can trigger endothelial cell (EC) proliferation, migration, and survival through activation of multiple signaling pathways (Bayless and Davis, 2003, Carmeliet et al,. 1996, Jakeman et al.,

* Reprinted with permission from "Functionalization of Ultrabithorax Materials with Vascular Endothelial Growth Factor Enhances Angiogenic Activity" by Howell DW, Duran CL, Tsai SP, Bondos SE, Bayless KJ, 2016. Manuscript submitted to Advanced Functional Materials. DOI 10.1002/adfm.201505365

1993, Pownall et al., 2010, Shweiki et al., 1993).

Although various strategies have been devised to deliver pro-angiogenic growth factors, an effective system to vascularize thick scaffolds is still needed. Methods such as microsphere encapsulation (Richardson et al., 2001), hydrogel entrapment (Lee et al., 2003, Sun et al., 2011, Gnavi et al., 2014, Kim et al., 2010, Yamaguchi et al., 2007), and bio-spraying technologies (Patel et al., 2012) provide ECs with pro-angiogenic factors to stimulate formation of capillary networks.

An alternate approach is to covalently crosslink the functional proteins to the materials. However, the crosslinking process can also inactivate the tethered protein or leave chemical residues in the materials, rendering them toxic to cells (MiJung et al., 2014, Woolfson et al., 2010). Additionally, the crosslinking strategy can orient some portion of the protein such that ligand binding, and hence protein function, is blocked (Hahn, et al., 2005, Galas et al., 2014). All of these methods result in random distribution of factors throughout the scaffold, which may alter the behavior of non-vascular cells. Thus, successfully engineered scaffolds must not only present and pattern active stimulatory factors, but also do so using non-toxic methods.

Therefore, we propose a new method of delivering growth factors for successfully engineering blood vessels in tissue engineered scaffolds. Our lab has developed materials composed of the *Drosophila melanogaster* Hox protein Ultrabithorax (Ubx), which self-assembles rapidly in mild, aqueous buffers. Ubx materials can be readily functionalized

with VEGF via gene fusion (Huang et al., 2011, Tsai et al., 2015). In this approach, the gene encoding a functional protein is fused to the ubx gene without intervening stop codons. As a result, a single polypeptide is produced containing the sequence of both the functional protein and Ubx. We have previously fused small, stable monomeric proteins to Ubx that retain activity in the resulting materials (Huang et al., 2011). For Ubx materials to be useful as vascular scaffolds, proteins for which incorporation is more challenging, due to instability or quaternary structure, must retain activity in Ubx materials. Previously, we demonstrated that the VEGF-Ubx and EGFP-VEGF-Ubx fusions both self-assemble to form materials (Tsai et al., 2015). In this study, we created VEGF-Ubx and EGFP-VEGF-Ubx fusion fibers to test the activity of complex proteins in Ubx fibers using *in vitro, ex vivo, and in vivo* assays. This approach provides a novel method for delivering VEGF to activate and promote survival of ECs in a dose-dependent manner. Furthermore, when VEGF-Ubx fibers are embedded in collagen, only cells interacting with the fiber are influenced by VEGF. Thus, Ubx is a unique material able to incorporate active growth factors in a biocompatible material (Patterson et al., 2014, Patterson et al., 2015) with tunable mechanical properties (Greer et al., 2011, Howell et al., 2015, Huang et al., 2010). To our knowledge, we are the first to append VEGF to biomaterials via gene fusion.

## 2. Material and methods

### 2.1 Ubx materials

Monomers of his-tagged Ultrabithorax splicing isoform Ia, along with EGFP, VEGF, and EGFP-VEGF Ubx (Tsai et al., 2015), were produced in *E. coli* from the pET19b-UbxIa vector and purified as previously described (Patterson et al., 2014). Ubx fibers were

produced by the buffer reservoir system, also as previously described (Tsai et al., 2015, Huang et al., 2010, Greer et al., 2009). EGFP-Ubx and EGFP-VEGF-Ubx were used when possible due to i) increased expression of the monomers in *E. coli* and ii) ability to visualize the fibers using green fluorescence. The EGFP-fused constructs could not be used in immunoassays in which green fluorescence is one of the reporters.

### 2.2 Cell culture

Primary human umbilical vein endothelial cells (HUVEC) (Lonza, C2517A) were cultured and used at passages 3-6. Cells were grown on gelatin-coated tissue culture flasks, passaged once per week in M199 growth medium supplemented with heparin, bovine hypothalamic extract, fetal bovine serum, antibiotics and gentamycin as described (Bayless et al., 2009).

### 2.3 Immunofluorescence

Cell suspensions were incubated with Ubx fibers wrapped around inoculation loops to allow cells to attach to fibers and cultured as previously described (Patterson et al., 2014, Patterson et al., 2015). For time course experiments, cells cultured on Ubx were transferred to new wells containing M199 without serum for 0 to 4 hours. While ECs seeded on VEGF-Ubx were untreated, 40 ng/ml of soluble VEGF was added to ECs seeded on Ubx alone to compare cell responses to immobilized versus soluble VEGF. In all immunofluorescence experiments, a freshly made 10% paraformaldehyde stock in PBS (500 μL) was added to the existing culture media at a final concentration of 4%, and samples were fixed prior to two 15 minute washes with a 25 mM Tris, 200 mM glycine solution. Samples were then permeabilized with 500 μL of 0.5% Triton X-100 solution in PBS for 20 minutes. Wells were aspirated and samples were blocked overnight in 500 μL 0.1% Triton X-100, 1% BSA, 0.2% sodium azide, and 5% goat serum at 4°C. Primary antibodies raised against ERK (1:100; Cell Signaling Technology), pERK (phosphorylated at T202/Y204) (1:1000; Cell Signaling Technology), and pVEGFR2 (phosphorylated at Y1214) (1:300;Cell Signaling Technology) were diluted in blocking solution and incubated in the wells for 3 hours. Loops were washed three times for 10 minutes each in 0.1% Triton X-100 in PBS

(500 µl) and incubated with (1:200 dilution) goat anti-rabbit Alexa Fluor 488 and goat anti-mouse Alexa Fluor 594 conjugated secondary antibodies (Molecular Probes) in blocking solution for 1 hour. Loops were washed three times and counterstained with 10 mM 4',6-diamidino-2-phenylindole (DAPI; Molecular Probes), placed on a 22 mm X 55 mm coverslip and imaged immediately using confocal microscopy on a Nikon Eclipse ti equipped with NIS Elements AR 4.10.01 software.

### 2.4 Migration Assay

DiI-labeled HUVECs were seeded onto gelatin-coated wells and allowed to reach confluency. Cells were then cultured in M199 without serum for 6 hours prior to placement of inoculation loops wrapped with EGFP-Ubx or EGFP-VEGF-Ubx fibers onto cell monolayers. After a 16 hour incubation in M199 with 1.5% serum the cells on Ubx fibers were fixed and immunofluorescence was conducted as described above.

### 2.5 Terminal deoxynucleotidyl transferase dUTP nick end labeling (TUNEL) assay

Fiber wrapped loops, directly seeded with 35,000 cells suspended in 250 µl of growth media, were cultured overnight so that cells could attach to Ubx fibers. Growth media was aspirated and cells cultured on Ubx fibers were starved for 8 hours in M199 without serum and then fixed using paraformaldehyde. A TUNEL assay kit from Abcam was used per manufacturers' protocol and imaged using confocal microscopy as described above.

### 2.6 Western Blot

Loops containing attached cells were collected in 60 µl of preheated Laemmli sample buffer and boiled in microcentrifuge tubes for 10 minutes at 95°C. Protein lysates were separated by SDS-PAGE and transferred to polyvinylidene fluoride membranes (Fisher Scientific). After blocking in 5% nonfat dry milk or BSA at room temperature for 1 hour, the membranes were incubated with monoclonal antisera directed against PECAM (1:1000 in TBST; Cell Signaling Technology), ERK (1:1000 in TBST; Cell Signaling Technology), pERK (1:1000 in TBST; Cell Signaling Technology), PECAM or GAPDH (1:10,000 in TBST; Abcam) at room temperature for 3 hours. The membranes were

washed three times before incubation with rabbit anti-mouse secondary antibody or goat anti-rabbit secondary antibody (1:5,000; DAKO) for 1 hour. Immunoreactive proteins were visualized using enhanced chemiluminescence (Millipore) and followed by film (Denville Scientific) exposure. For image quantification, images were scanned with a FluorChem 8900 digital imaging system (Alpha Innotech, San Leandro, CA). Band intensities were measured using NIH ImageJ image analysis software.

### 2.7 Aortic Ring Assay

Aortae were harvested from Sv129-Pas mice between 6-10 weeks of age, and prepared as described (Baker et al., 2012). Aortae were cut into 0.5 mm segments along the length of the vessel, creating rings. Collagen type I was prepared at a concentration of 1.5 mg/ml as previously described (Bayless et al., 2009), substituting Opti-MEM for M199. Collagen (150 µL) was added per well of a 48-well, glass bottom plates (MatTek) on ice. One aortic ring per well was embedded in the collagen, and loops wrapped with EGFP-Ubx or EGFP-VEGF-Ubx fibers were placed in the collagen so that the fibers were in close proximity to the aortic rings. After the collagen polymerized, 500 µl of Opti-MEM containing 2.5% FBS, gentamycin, and 40 ng/mL VEGF was added. Rings were incubated at 37 °C with 5% $CO_2$. After 24 hours, VEGF-containing media was removed and replaced with media lacking VEGF. After six total days of incubation, samples were fixed with 4% paraformaldehyde in PBS for 30 minutes. Wells were rinsed two times for 30 minutes with Tris-Glycine buffer (0.3% Tris and 1.5% Glycine). After rinsing, samples were permeabilized with 500 µl 0.5% Triton X-100 in PBS by rocking for 2 hours at room temperature and then blocked overnight with 1 ml 0.1% Triton X-100, 1% BSA and 1% goat serum in Tris-buffered saline at room temperature. Solutions were added containing primary antibodies directed against PECAM-1 (BD Transduction, 550274) diluted 1:100 in blocking buffer at room temperature with gentle agitation for 3 hours. After rinsing rings four times for 30 minutes with 1 ml 0.1% Triton X-100 in PBS at room temperature, samples were incubated with Alexa Fluor 595-conjugated secondary antibodies (Molecular Probes) diluted 1:200 in blocking buffer at 4 °C overnight. The samples were then washed overnight at room temperature with 1 ml 0.1% Triton X-100 in PBS. Nuclei were stained with 1 µM DAPI (Molecular Probes) for 30

minutes at room temperature with gentle agitation and imaged as described above. Z-stack images (5-25 μm) were taken using 0.5 μm steps, compressed, and analyzed using Nikon Elements Software.

### 2.8 Chorioallantoic membrane assay (CAM)

Fertilized eggs were obtained from the Texas A&M University Poultry Science Center (College Station, TX). Eggs were incubated at 37 $^{0}$C, rotating continuously for 3 days before *ex ovo* culture (Dohle et al., 2009). Eggs were wiped with betadine and cracked into sterile weigh boats (VWR) containing appropriate dilutions of penstrep (Gibco), fungizone (Sigma), niacin (Sigma), and gentamycin (Gibco). Embryos were covered and placed in a humidified incubator (37 °C) for 4 days. Ubx materials wrapped around sterile rings of blot paper were placed with fibers perpendicular to established vessels. Micrographs were captured the same day Ubx materials were added on a National dissection scope (Model DC5-420TH) and then cultured for 48 hours. The embryos were then sacrificed and the same field was imaged to assess development of new vessels along Ubx fibers. To visualize fibers, images were also captured using illumination with UV light. Quantification of vessel growth was determined by comparing the images before and after addition of Ubx materials and counting the number of new vessels established along fibers.

## 3. Results

### 3.1 Human endothelial cells signal through the ERK pathway when presented with VEGF on Ubx materials

A challenge in creating functionalized materials from protein chimeras has been assembling the materials while maintaining the structure and activity of the appended functional protein. We have created several active, functionalized materials using Ubx as a platform to introduce new activities via formation of protein fusions (Tsai et al., 2015). However, thus far only stable, monomeric proteins have been shown to retain activity in Ubx materials. To use Ubx as a vascular scaffold, more complex proteins, such as VEGF, must be appended that can interact with and direct vascular cells. During angiogenesis,

VEGF signaling stimulates ERK phosphorylation (Thr 202/Tyr 204) downstream of VEGFR2 (Dougher et al., 1999, Kendall et al., 1999, Matsumote et al., 2005, Plouet and Moukadiri, 1990, Terman et al., 1991, Vaisman et al., 1990, Dent, 2014, Shu et al., 2002, Zachary, 2003). To test if VEGF immobilized in Ubx fiber is active, endothelial cells were seeded onto Ubx or VEGF-Ubx fibers and cultured overnight. Cells were cultured in basal media without serum for 2 hours to remove any non-specific signals from the growth media, and probed for ERK and pERK using immunofluorescence (Figure 1 A,B). While total ERK levels are unchanged, pERK is significantly greater for cells cultured on VEGF-Ubx fibers than for cells cultured on Ubx fibers (Figure 1C; $p<0.01$). This indicates that ERK is activated in endothelial cells when presented with VEGF appended to Ubx materials.

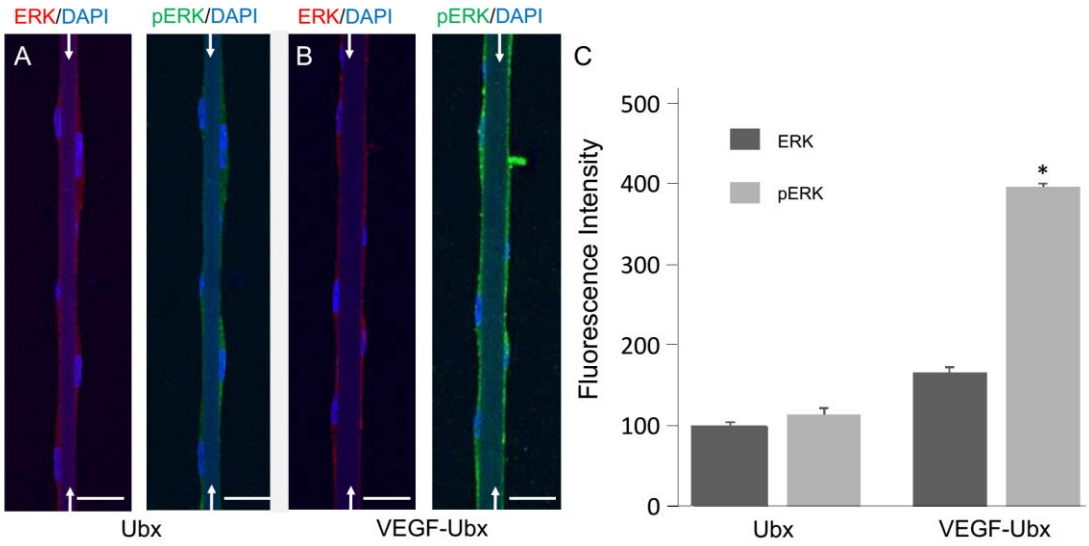


**Figure 1. Endothelial cells cultured on VEGF-Ubx fibers show significant phosphorylation of ERK.** ECs seeded on (A) Ubx fibers and (B) VEGF-Ubx fibers were cultured overnight and then starved for 2 hours prior to fixation in 4% para. Fibers in all panels are indicated by white arrows. Cells were stained for ERK, pERK (T202/Y204), and counter stained with DAPI for immunofluorescence imaging using confocal microscopy. Scale bars equal 20 µm. (C) Quantification of fluorescence intensity of ERK and pERK shows that cells cultured on VEGF-Ubx fibers show a significant increase in pERK compared to cells on Ubx fibers ($p<0.01$, indicated by *). Data are representative of 3 experiments and averaged from 25 independent fields in each group (+/- SEM) with analysis for significance using univariate analysis of variance (ANOVA) with Tukey's honest significant differences (HSD) test posthoc.

### 3.2 Signaling through VEGFR2 by VEGF-Ubx fibers is sustained for longer times relative to soluble VEGF

To verify that VEGF fused to Ubx fibers is signaling through the correct pathway, we also tested whether the VEGF receptor VEGFR2 is activated, and thus phosphorylated. At the cellular level, VEGF binding to VEGFR2 results in $Ca^{2+}$ mobilization, prostacyclin production, nitric oxide production, and phosphatidylinositol-3-kinase (PI3K)/Akt activation in addition to ERK activation (Cunninghan et al., 1995, Gerber et al., 1998, Kroll and Waltenberger, 1997, Waltenberger etal., 1994). These events cumulatively stimulate endothelial cell proliferation and migration, behaviors required for an angiogenic response (Cunninghan et al., 1995, Gerber et al., 1998, Kroll and Waltenberger, 1997, Waltenberger etal., 1994). We first verified that VEGF-Ubx leads to VEGFR2 activation and thus has the potential to instigate all of these events, ECs were seeded onto Ubx and VEGF-Ubx fibers and cultured overnight in growth media prior to serum starvation. To compare the effects of soluble VEGF stimulation on VEGF-Ubx versus Ubx fibers, ECs cultured on control Ubx fibers were treated with 40 ng/ml soluble VEGF at the onset of serum starvation. To examine VEGFR2 presentation on the cell surface, cells were fixed, but not permeablized, at 0, 2, and 4 hours and stained for VEGFR2. Figure 2A,B shows that VEGFR2 surface presentation is unchanged and therefore any changes in receptor phosphorylation during the course of these experiments are not a result of VEGFR2 internalization or downregulation. In addition to immunofluorescence, western blot analyses were performed to examine VEGFR2 phosphorylation (pVEGFR2) (Figure 2C). Quantification of pVEGFR2 normalized to VEGFR2, shows that VEGFR2 phosphorylation occurs in response to VEGF-Ubx. Furthermore, VEGFR2 phosphorylation is sustained at a significantly higher level when cells are cultured on VEGF-Ubx fibers compared to plain Ubx in the presence of soluble VEGF (Figure 2D; $^{\#}p<0.02$ vs EGFP-Ubx at 2 Hours, $*p<0.01$ vs EGFP-Ubx at 4 Hours).

Because VEGF is immobilized on Ubx, we tested whether VEGF-Ubx might sustain EC activation in the absence of serum. ECs were seeded onto EGFP-Ubx and EGFP-VEGF-Ubx fibers, cultured overnight in growth media, and then placed under starvation

conditions. EGFP-Ubx and EGFP-VEGF-Ubx were used in these experiments due to i) increased expression of the monomers in *E. coli* (Tsai et al., 2015) and ii) an ability to visualize the fibers using green fluorescence. Cell lysates from each group were collected every hour for western blot analysis of ERK phosphorylation (Figure 3A,B). Quantification of pERK normalized to ERK, with PECAM as a loading control, shows that ERK activation in ECs cultured on EGFP-VEGF-Ubx fibers can be sustained for 4 hours, while ERK activation almost completely disappears on EGFP-Ubx materials treated with soluble VEGF after an hour (Figure 3C; *$p<0.01$ vs EGFP-Ubx at 0 Hours; $^{\#}p<0.03$ vs EGFP-VEGF-Ubx at 0 Hours; $^{\$}p<0.04$ vs EGFP-VEGF-Ubx at 1 Hour; $^{\lozenge}p<0.05$ vs EGFP-VEGF-Ubx at 2 Hours; and $^{\bullet}p<0.01$ vs EGFP-VEGF-Ubx at 3 Hours). Thus EC interactions with VEGF-Ubx results in sustained ERK signaling when compared to cells cultured on EGFP-Ubx materials treated with soluble VEGF. Rapid, yet transient increases in ERK and VEGFR2 phosphorylation in response to soluble VEGF are in agreement with other studies. The results from VEGF-Ubx materials are similar to other studies in which VEGF is covalently attached to materials (Phelps and Garcia, 2010, Shen et al., 2008). However, no study reports signal duration of longer than 1 hour, while VEGF appended to Ubx sustains signaling for over 4 hours.

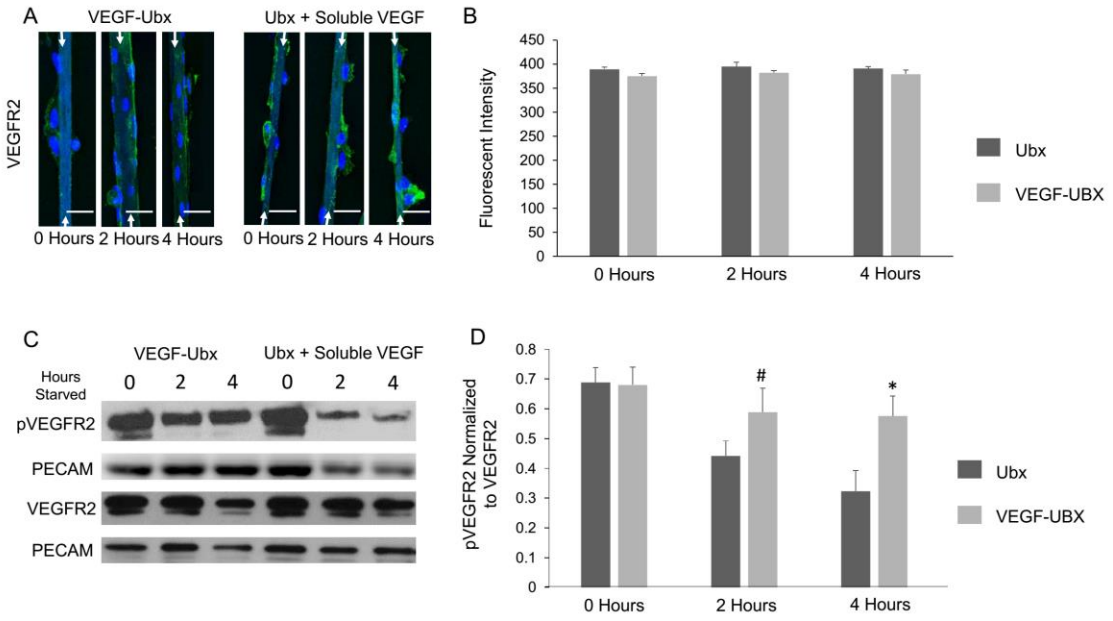


**Figure 2. VEGFR2 cell surface expression is unchanged, while phosphorylation is sustained by VEGF-Ubx. (**A) Immunofluorescence staining for VEGFR2 surface expression in ECs (green) counter stained with DAPI (blue) on Ubx or VEGF-Ubx fibers (white arrows). Cells were seeded on materials indicated overnight. Growth medium was removed and replaced with M199 alone (VEGF-Ubx) or M199 + 40 ng/ml soluble VEGF (Ubx). Cells were fixed at 0, 2, and 4 hours and stained. (B) Quantification of VEGFR2 fluorescence in the absence of permeabilization using antibodies against the extracellular motif in VEGFR2. (C) ECs seeded onto GFP-Ubx and GFP-VEGF-Ubx fibers were cultured overnight and then serum starved for up to 4 hours. ECs cultured on Ubx were treated with 40 ng/ml soluble VEGF at onset of starvation. Cells were collected, lysed, and analyzed using western blot analysis. Membranes were probed for pVEGFR2 (Tyr 1214), VEGFR2 and PECAM. (D) Quantification of pVEGFR2 normalized to VEGFR2, with PECAM as a loading control, shows that VEGFR2 is phosphorylated by VEGF-Ubx and can be sustained at a significantly high level. Data were averaged from 5 experiments and analyzed for significance using univariate analysis of variance (ANOVA) with Tukey's honest significant differences (HSD) test posthoc with # indicating $p<0.02$ vs GFP-Ubx at 2 Hours, * indicating $p<0.01$ vs GFP-Ubx at 4 Hours.

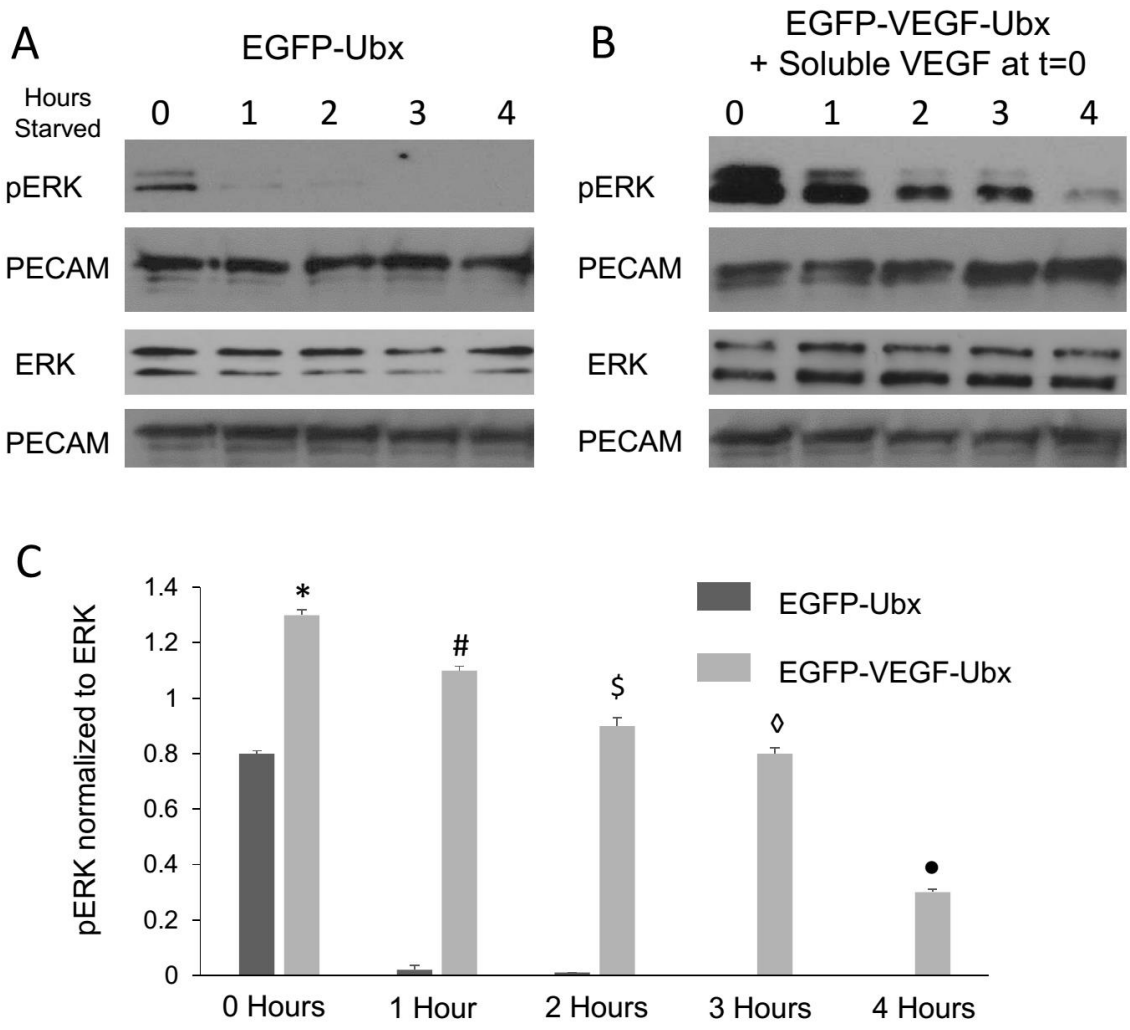


**Figure 3. VEGF-Ubx materials sustain ERK signaling in ECs.** ECs seeded onto (A) EGFP-Ubx and (B) EGFP-VEGF-Ubx fibers were cultured overnight and then starved for 4 hours. ECs cultured on EGFP-Ubx were treated with 40 ng/ml soluble VEGF at the onset of starvation. Cells were collected at the specified time, and western blot analyses were used to probe for pERK (Thr 202/Tyr 204), ERK and PECAM. (C) Quantification of pERK band intensities normalized to ERK, with PECAM as a loading control, shows that VEGF signaling on Ubx fibers can be sustained for up to 4 hours. Data were averaged from 4 experiments and analyzed for significance using univariate analysis of variance (ANOVA) with Tukey's honest significant differences (HSD) test posthoc with * indicating $p<0.01$ vs EGFP-Ubx at 0 Hours, # indicating $p<0.03$ vs EGFP-VEGF-Ubx at 1 Hours, $ indicating $p<0.04$ vs EGFP-VEGF-Ubx at 2 Hours, ◊ indicating $p<0.05$ vs EGFP-VEGF-Ubx at 3 Hours, and ● indicating $p<0.01$ vs EGFP-VEGF-Ubx at 4 Hours.

### 3.3 VEGF signaling is proportional to VEGF concentration on fibers

EC responses to VEGF *in vitro* (Cunningham et al., 1995, Gerber et al., 198) are dependent on exposure to adequate concentrations of VEGF (Silva and Mooney, 2010), while *in vivo*, overexpression of VEGF can result in aberrant angiogenesis (Ozawa et al., 2004) and enhanced angiogenic responses within tumors (Yang et al., 2015, Appelmann et al., 2010, Ellis and Hicklin et al., 2008, Olsson et al., 2006). If VEGF in Ubx materials is only partially active, the material may not reach the threshold necessary to elicit a cellular response. Alternately, a high VEGF concentration may overstimulate cells (Ozawa et al., 2004, Olsson et al., 2006). Therefore, to elicit the appropriate cellular responses for *in vivo* vascular scaffolds, it is important to present an effective concentration of active VEGF on Ubx materials. Previously, we established that a mixture of different ratios of Ubx to EGFP-Ubx produces materials in which EGFP-Ubx content in fibers linearly correlates with the percentage of EGFP-Ubx monomer in the original protein mixture (Tsai et al., 2015). We used this approach to generate fibers with varying VEGF concentrations. ECs were cultured on Ubx materials made from increasing ratios of VEGF-Ubx to Ubx, then starved for 2 hours and probed for ERK phosphorylation using western blot analysis. Expression of total ERK remained constant while levels of pERK increased proportionally with VEGF concentration, up to 75% VEGF-Ubx (Figure 4A,B). This VEGF concentration-dependent increase in ERK phosphorylation provides further evidence that immobilized VEGF is the active agent. Above 75% VEGF-Ubx, the response began to plateau as nearly all of the ERK present was phosphorylated.

Because ERK phosphorylation is linearly proportional to VEGF-Ubx concentrations, we can infer that VEGF-Ubx and Ubx assemble into materials equally well. To benchmark the extent of signaling elicited by VEGF incorporated into Ubx fibers with signaling elicited by soluble VEGF monomers, we administered increasing doses of soluble VEGF at known concentrations to ECs cultured on Ubx fibers and monitored pERK/ERK ratios (Figure 4C,D). VEGF is widely used at the physiological range of 40 to 50 ng/mL, to induce EC proliferation and migration (Bayless and Davis, 2003, Shu et al., 202, Bayless and Davis, 2004, Bayless et al., 2009, Christenson and Stouffer, 1996, Hermann and

Zechariah 2009). The level of pERK/ERK observed with 50 ng/ml soluble VEGF was similar to the pERK/ERK level induced by materials containing 25% VEGF-Ubx. Therefore, Ubx materials are useful for building *in vivo* vascular scaffolds because we are able to produce fibers with a broad range of VEGF concentrations and, more importantly, can generate VEGF levels that elicit comparable signals to physiological doses of soluble VEGF.

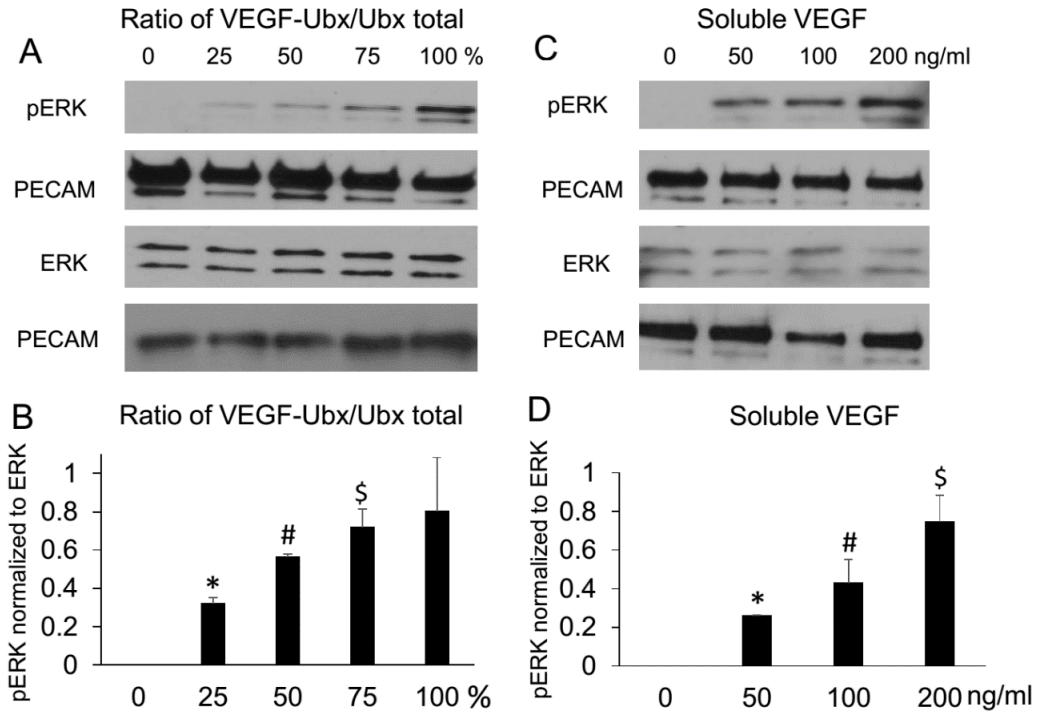


**Figure 4. ERK phosphorylation is proportional to the amount of VEGF incorporated into Ubx materials. (**A) ECs seeded onto fibers composed of an increasing ratio of VEGF-Ubx to Ubx fibers were cultured overnight and then starved for 2 hours prior to lysis in sample buffer and run on acrylamide gel for western blot analysis. Membranes were probed for pERK (Thr202/Tyr204), ERK and PECAM. (B) ERK and pERK band intensities were normalized to PECAM loading controls from respective blots. The ratio of PECAM-normalized pERk/ERK was averaged from 4 experiments and analyzed for significance using univariate analysis of variance (ANOVA) with Tukey's honest significant differences (HSD) test posthoc with * indicating $p<0.01$ vs 0, # indicating $p<0.02$ vs 25, and $ indicating $p<0.04$ vs 50. (C) ECs seeded onto Ubx fibers were cultured overnight and then starved for 2 hours prior to treatment with increasing concentrations of soluble VEGF. After 30 minutes of treatment, cell lysates were analyzed by western blotting and probed for pERK, ERK and PECAM. (D) Quantification of PECAM-normalized pERK to ERK ratios were performed as in panel B. Data were averaged from 4 experiments and analyzed for significance using univariate analysis of variance (ANOVA) with Tukey's honest significant differences (HSD) test posthoc with * indicating $p<0.02$ vs 0 ng/ml, # indicating $p<0.03$ vs 50 ng/ml, and $ indicating $p<0.01$ vs 100 ng/ml.

### 3.4 VEGF-Ubx promotes endothelial cell migration and survival *in vitro*

VEGF can impact many signaling cascades and elicit a variety of cell behaviors (Jakeman et al., 1993, Pownall et al., 2010, Shweiki et al., 1993). Although VEGF-Ubx fibers can phosphorylate ERK via VEGFR2 activation, the entire repertoire of VEGF functions are not guaranteed to be activated by immobilized VEGF. Therefore we tested whether complex cell behaviors, normally regulated by soluble VEGF, can be elicited by VEGF-Ubx fibers. In particular, we asked whether VEGF signaling can induce cells to migrate in low serum conditions or prevent cells from undergoing apoptosis in GF-depleted media. In the migration assays, primary human ECs were labeled with DiI, a red fluorescent lipophilic dye, and cultured as a confluent monolayer prior to incubation at low serum for 6 hours. Ubx materials were then added and incubated with the cells overnight in media containing low levels of serum. The cells were fixed and stained with DAPI, a blue fluorescent stain that binds DNA, to identify cells that migrated onto Ubx materials (Figure 5A,B). A significantly greater number of cells migrated onto EGFP-VEGF-Ubx fibers when compared to control EGFP-Ubx fibers (Figure 5C; $p<0.01$), indicating that VEGF-Ubx materials stimulated migration of ECs in low serum conditions.

In addition to migration, VEGF functions as a survival factor to inhibit apoptosis (Farahani et al., 2005, Yang et al., 2008, Roberts, et al., 2007). To test if Ubx materials could provide a way to sustain cell viability under stressful conditions, we cultured an equal number of ECs directly on EGFP-Ubx and EGFP-VEGF-Ubx fibers overnight to allow for cellular attachment prior to an 8 hour serum starvation. Cells were fixed, stained with DAPI, and a TUNEL assay was performed to identify cells undergoing apoptosis. While apoptotic (red) cells were detected on EGFP-Ubx fibers (Figure 6A), cells that were cultured on EGFP-VEGF-Ubx fibers showed little evidence of apoptosis (Figure 6B). Quantification shows a higher retention rate of ECs on EGFP-VEGF-Ubx materials than EGFP-Ubx (Figure 6C). Furthermore, these data indicate the majority of cells cultured on EGFP-Ubx fibers were lost and the few remaining cells were positive for TUNEL staining, while only 7% of cells remaining on EGFP-VEGF-Ubx fibers were

TUNEL positive (Figure 6A,C). Therefore, VEGF-modified Ubx fibers can influence EC behavior by promoting migration and survival.

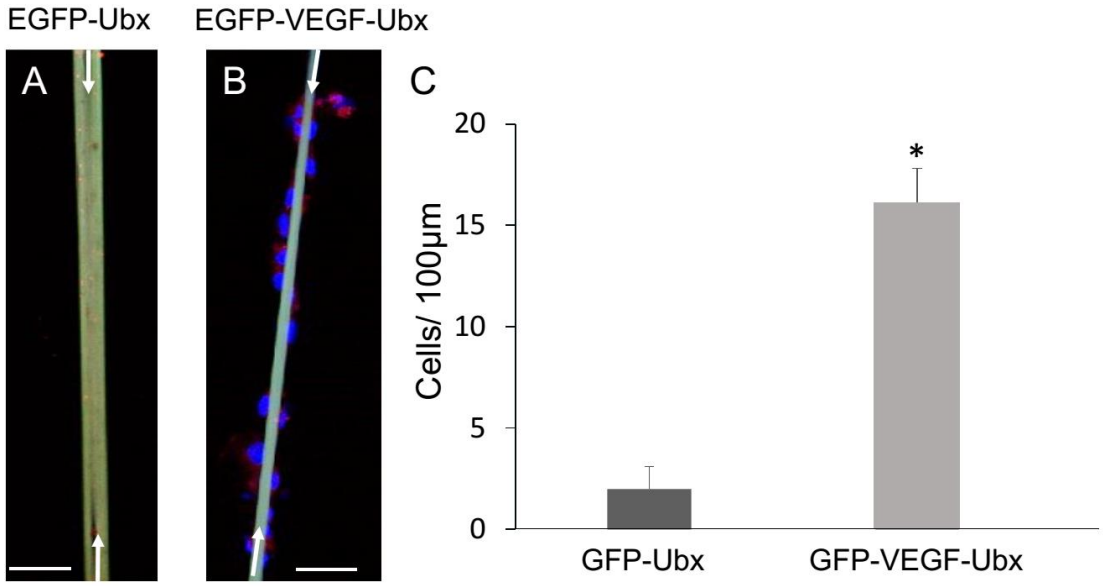


**Figure 5. EGFP-VEGF-Ubx fibers promote enhanced recruitment and migration of endothelial cells.** EGFP-Ubx (A) and EGFP-VEGF-Ubx (B) fibers (green, labeled with white arrows) were cultured overnight with an established monolayer of DiI-labeled (red) endothelial cells in low (1.5%) serum. Cells were fixed, stained with DAPI (blue), and imaged using confocal microscopy. Scale bars = 50 µm. (C) Quantification of the number of cells/100 µm distance attached to EGFP-Ubx vs. EGFP-VEGF-Ubx fibers. Data were averaged from 25 independent fields in each group (+/- SEM) from 4 experiments. Data were analyzed for significance using univariate analysis of variance (ANOVA) with Tukey's honest significant differences (HSD) test posthoc with * indicating $p<0.01$.

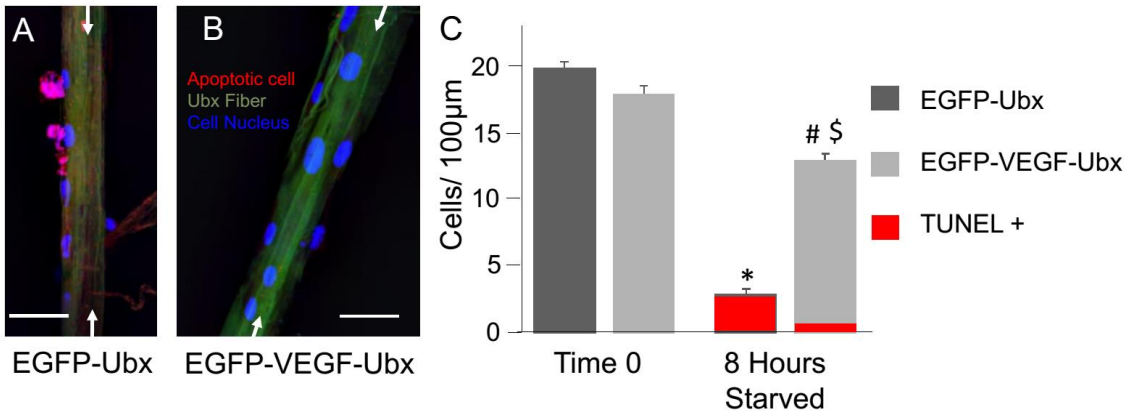


**Figure 6. EGFP-VEGF-Ubx fibers prevent endothelial cell apoptosis after starvation.** ECs seeded on EGFP-Ubx (A) and EGFP-VEGF-Ubx (B) fibers were starved for 8 hours and analyzed using TUNEL assays to detect apoptotic cells. White arrow indicates Ubx fiber. Scale bars = 10 µm. (C) Quantification of the number of viable and TUNEL-positive cells associated with EGFP-Ubx and EGFP-VEGF-Ubx fibers before (Time 0) and after 8 hours of starvation. Data shown are representative of 5 experiments and averaged from 20 independent fields in each group (+/- SEM). Statistical significance was determined using univariate analysis of variance (ANOVA) with Tukey's honest significant differences (HSD) test posthoc with * indicating $p<0.01$ vs Time 0, # indicating $p <0.04$ vs Time 0, $ indicating $p<0.03$ vs. EGFP-Ubx, 8 hour starvation. Quantification of TUNEL-positive cells (red) indicated that 95% of cells on EGFP-Ubx and only 7% of cells on EGFP-VEGF-Ubx were TUNEL positive.

### 3.5 VEGF-Ubx materials recruit endothelial sprouts in an *ex vivo* aortic ring assay

An important aspect of VEGF function is to direct or pattern angiogenic outgrowths. Therefore, we used the physiologically relevant aortic ring assay to examine how VEGF-Ubx interactions might affect vascular tissues. In this assay, angiogenic vessels sprout from freshly isolated aortic tissue that is embedded in a collagen matrix, allowing for analysis of vascular sprouting in an *ex vivo* environment. This assay is ideal for these experiments due to clearly visible, lumenized, capillary-like structures that develop at a rate similar to *in vivo* angiogenic sprouts (Baker et al., 2012, Masson et al., 2002). Importantly, supporting cells, such as pericytes, participate in the formation of microvessels, resembling events *in vivo*.

To examine Ubx interactions with angiogenic sprouts, we modified the aortic ring assay by placing Ubx fibers within the collagen gel in close proximity to embedded tissue to allow for interaction with newly formed outgrowths as sprouts develop (Figure 7). When endothelial sprouts interact with EGFP-VEGF-Ubx fibers, they alter the direction of their growth to follow and, in some cases, wrap around EGFP-VEGF-Ubx fibers (Figure 8A,B; Figure 9). This effect is rarely observed with EGFP-Ubx fibers (Figure 8C,D), suggesting that VEGF in EGFP-VEGF-Ubx fibers causes the sprouts to alter direction (Figure 8E). Because we observe comparable frequencies of initial contact between angiogenic sprouts and EGFP-VEGF-Ubx and EGFP-Ubx fibers, we conclude that angiogenic sprouts are responding to VEGF and the effect is not caused by i) durotaxis, ii) differences in the mechanical properties of fibers and collagen, or iii) differences in sprout attachment to Ubx fibers versus collagen due to the surface chemistry of these materials. Importantly, in this assay the VEGF-Ubx fibers buried in collagen form a composite material, in which VEGF-modified Ubx fibers guide angiogenic sprouts without impacting the behavior of cells within the scaffold but not in contact with the fiber. This ability to ensure and pattern sprout outgrowth by placement of angiogenic materials is required for successful tissue engineering scaffolds.

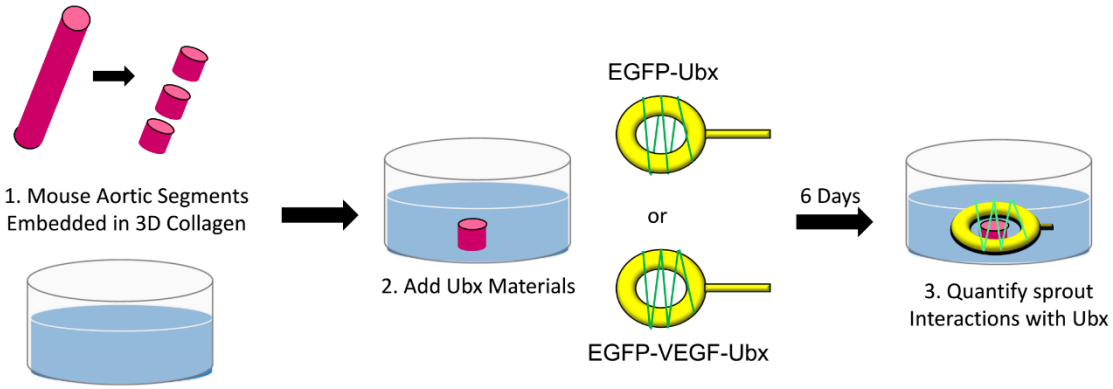


**Figure 7. Modification of mouse aortic ring assay for use with Ubx materials**

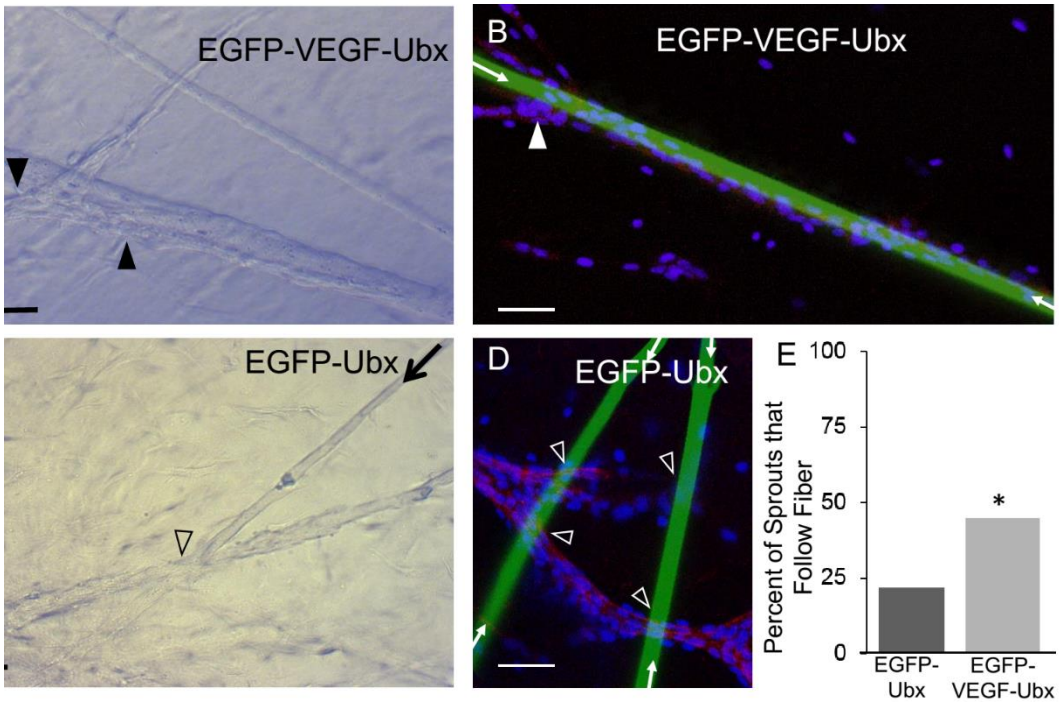


**Figure 8. EGFP-VEGF-Ubx materials redirect and attract endothelial positive outgrowths from aortic rings.** Aortic vessels excised from WT mice were divided into 0.5 mm segments and embedded in 3D collagen matrices with Ubx materials. Aortic rings were cultured for 24 hours in growth factor supplemented media to induce endothelial sprouts into the collagen. Aortic rings were cultured for an additional 5 days in media without growth factors so that EGFP-VEGF-Ubx is the only source of growth factors for endothelial sprouts. Cultures were fixed, stained for PECAM (red), and counterstained with DAPI (blue). (A) Brightfield and (B) confocal images of EGFP-VEGF-Ubx cultures show that sprouts will alter their direction to follow and in some cases envelop EGFP-VEGF-Ubx fibers (green). Images of EGFP-Ubx cultures using (C) brightfield and (D) confocal imaging. Scale bars = 50 μm. In all panels, A-D, arrows indicate EGFP-VEGF-Ubx or EGFP-Ubx materials. Solid arrowheads indicate where sprouts follow fibers while empty arrowheads indicate fibers that interact but do not follow. (E) Quantification of sprout interactions with materials. Data were collected from 50 events in 4 experiments. Values were analyzed for statistical differences using a Chi-Square test for independence with * indicating $p<0.02$.

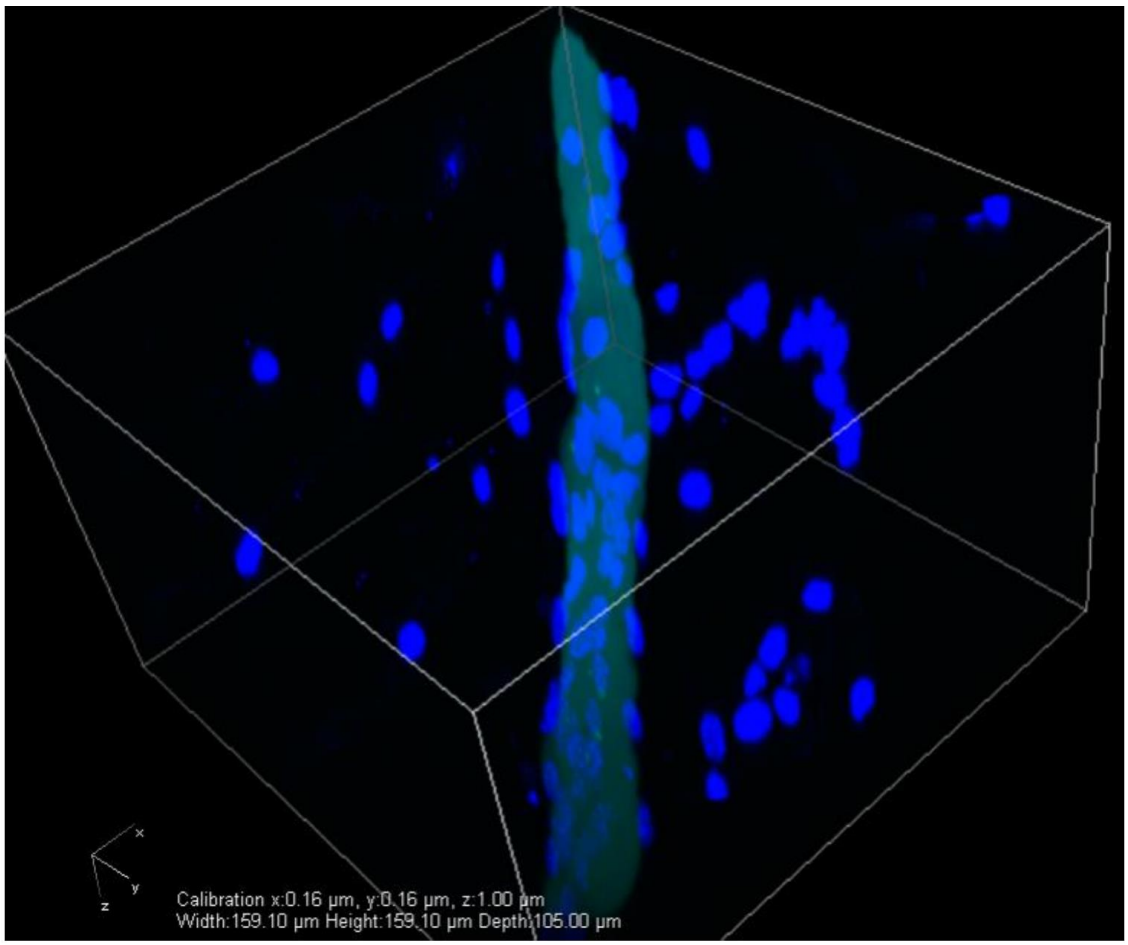


**Figure 9. 3-dimension confocal image shows endothelial sprouts wrap around the EGFP-VEGF-Ubx fiber**

### 3.6 VEGF-Ubx directs blood vessel formation *in vivo*

Thus far, we have demonstrated that VEGF-modified Ubx fibers can activate the VEGF signaling pathway in cell culture and alter the direction of growth of pre-formed angiogenic sprouts in the *ex vivo* aortic ring assay. To test whether EGFP-VEGF-Ubx fibers can *instigate* neovascularization *in vivo*, the *ex ovo* chicken embryo chorioallantoic membrane (CAM) assay (Bayless and Davis, 2004, Dohle et al., 2009) was modified for Ubx fibers. In the modified assay, chicken embryos were transferred to cell culture dishes 3 days after fertilization and incubated for an additional 4 days. EGFP-Ubx (Figure 10A) or EGFP-VEGF-Ubx (Figure 10D) fibers were then placed on the surface of the chorioallantoic membrane perpendicular to established vessels and the animals were monitored for formation of new vasculature. After 48 hours, new vessels (indicated by closed arrowheads) often formed along VEGF-Ubx fibers (Figure 10E,F) while vascular development was unaltered by plain Ubx fibers (open arrowheads, Figure 10B,C). Quantification of 50 events from 7 experiments revealed that 36% of VEGF-Ubx fibers placed on the CAM resulted in new vessel growth, while plain Ubx fibers elicited no new vessels (Figure 10G). These new vessels grew in the same direction as the VEGF-Ubx fiber axis. Therefore VEGF-modified Ubx materials can both instigate and direct vascular development *in vivo*.

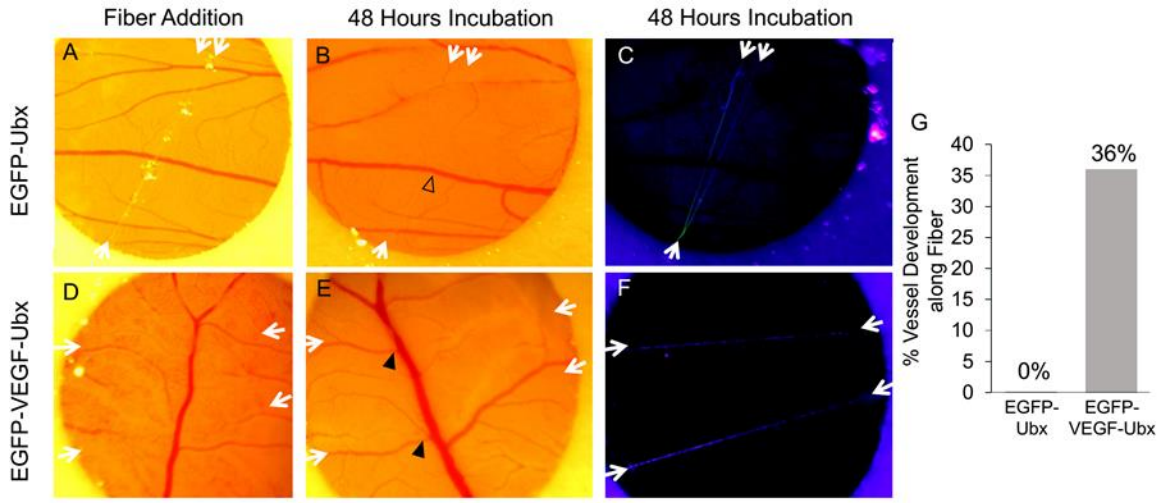


**Figure 10. EGFP-VEGF-Ubx fibers elicit more association with vasculature in chicken embryo chorioallantoic membrane (CAM) assays.** Fertilized eggs were humidified, rotating continuously for 3 days before ex ovo culture. Embryos were cultured for 4 days prior to the addition of (A-C) EGFP-Ubx and (D-F) EGFP-VEGF-Ubx materials wrapped around sterile blot paper and placed with fibers perpendicular to established vessels. (A,D) Representative brightfield images of the CAM surface captured immediately after adding materials. (B,E) Brightfield and (C,F) UV-illuminated photographs of the same fields shown in panels A and D 48 hours later. In panels A-E, fiber locations are indicated by white arrows. Open arrowhead indicates absence of vessel development, while closed arrowheads indicate development of new vessels. (G) Quantification of vessel development induced by Ubx materials. The percentage of events where vessels developed in association with materials was quantified for EGFP-Ubx (0/50 events) and EGFP-VEGF-Ubx (17/50 events).

## 4. Conclusions

The development of artificial tissues and organs requires scaffolds to physically support growth of tissue-specific cells, as well as blood vessels within the scaffold to supply those cells with oxygen and nutrients (Marler et al., 1998, Merman, 1991, Vacanti and Langer, 1999). In the absence of a functional vasculature, the largest scaffold that can be successfully implanted *in vivo* is 1-2 mm thick (Li et al., 2000, Martin et al., 1999). Thus scaffold construction requires a separate set of molecular cues to direct vascular cell adhesion, proliferation, migration, and maturation through basement membrane deposition. These specific cues must be patterned within the scaffold to elicit appropriate cell responses. However, there are currently no methods available to adequately and precisely position angiogenic factors in a scaffold.

As a first step toward this goal, we have demonstrated that VEGF, a dimeric protein, retains activity when genetically fused to Ubx and incorporated into materials. We show that ECs cultured on VEGF-Ubx fibers signal through the appropriate pathway and phosphorylate ERK and VEGFR2. In addition, VEGF signaling is extended for a longer period of time than any other current approach. Our data shows that VEGF concentration in Ubx fibers can be controlled and matched to physiologically relevant concentrations *in vitro*. Cell culture experiments show that VEGF-Ubx induces EC migration and sustains cell viability. Angiogenic sprouts change direction and can be guided by VEGF-Ubx fibers in an ex vivo aortic ring assay. Finally, in an *in vivo* CAM assay, VEGF-Ubx fibers induce formation of new vasculature when placed on the surface of the chick

chorioallantoic membrane (Huang et al., 2011, Tsai et al., 2015, Patterson et al., 2014, Greer ,et al., 2009, Huang et al., 2010, Howell et al., 2015).

It is remarkable that VEGF retains its ability to bind and activate VEGFR2 given that VEGF is covalently bound to large, solid materials and VEGFR2 is embedded in the cell membrane. This approach not only requires two large objects to be brought into close proximity, but also VEGF must be oriented correctly to bind its receptor. The fact that this approach is also effective when VEGF is fused in between EGFP and Ubx indicates the robustness of this approach. Ubx materials provide additional avenues for further optimization: the mechanical properties can be genetically tuned (Howell et al., 2015) and, because only 25% of the monomers need to be functionalized with VEGF, space is available for incorporating additional angiogenic molecules. Collectively, these data demonstrate that Ubx is a unique material able to incorporate active stimulating proteins capable of directing cell behavior *in vitro and in vivo*.